

國立交通大學

光電工程研究所

博士論文



多波長光彈調變式橢圓偏光術

Multi-wavelength Photoelastic Modulation
Ellipsometry

研究生：王夢偉

指導教授：趙于飛 教授

中華民國九十三年五月

多波長光彈調變式橢圓偏光術
Multi-wavelength Photoelastic Modulation
Ellipsometry

研究生：王夢偉

Student : Meng-Wei Wang

指導教授：趙于飛

Adviser : Yu-Faye Chao

國立交通大學



A Thesis

Submitted to Institute of Electro-Optical Engineering
College of Electrical Engineering and Computer Science
National Chiao Tung University
in partial Fulfillment of the Requirements
for the Degree of
Doctor of Philosophy
in
Electro-Optical Engineering

May 2004

Hsinchu , Taiwan , Republic of China

中華民國九十三年五月

國 立 交 通 大 學

博碩士論文著作權授權書

(提供授權人裝訂於紙本論文中書名頁之次頁用)

本授權書所授權之論文為本人在國立交通大學(學院)光電工程系所 _____ 組，92 學年度第 _____ 學期取得博士學位之論文。

論文名稱：多波長光彈調變式橢圓偏光術
指導教授：趙于飛

同意 不同意 (國科會科學技術資料中心重製上網)

本人具有著作財產權之上列論文全文(含摘要)資料，授予行政院國家科學委員會科學技術資料中心(或改制後之機構)，得不限地域、時間與次數以微縮、光碟或數位化等各種方式重製後散布發行或上載網路。

本論文為本人向經濟部智慧財產局申請專利(未申請者本條款請不予理會)的附件之一，申請文號為：_____，註明文號者請將全文資料延後半年再公開。

同意 不同意 (圖書館紙本影印)

本人具有著作財產權之上列論文全文(含摘要)資料，授予教育部指定送繳之圖書館及國立交通大學圖書館，基於推動讀者間「資源共享、互惠合作」之理念，與回饋社會及學術研究之目的，教育部指定送繳之圖書館及國立交通大學圖書館得以紙本收錄、重製與利用；於著作權法合理使用範圍內，不限地域與時間，讀者得進行閱覽或列印。

本論文為本人向經濟部智慧財產局申請專利(未申請者本條款請不予理會)的附件之一，申請文號為：_____，註明文號者請將全文資料延後半年再公開。

■ 同意

本人具有著作財產權之上列論文全文(含摘要)，授予國立交通大學與台灣聯合大學系統圖書館，基於推動讀者間「資源共享、互惠合作」之理念，與回饋社會及學術研究之目的，國立交通大學圖書館及台灣聯合大學系統圖書館得不限地域、時間與次數，以微縮、光碟或其他各種數位化方式將上列論文重製，並得將數位化之上列論文及論文電子檔以上載網路方式，於著作權法合理使用範圍內，讀者得進行線上檢索、閱覽、下載或列印。

論文全文上載網路公開之範圍及時間：

本校及台灣聯合大學系統區域網路	■ 立即公開
校外網際網路	■ 立即公開

上述授權內容均無須訂立讓與及授權契約書。依本授權之發行權為非專屬性發行權利。依本授權所為之收錄、重製、發行及學術研發利用均為無償。上述同意與不同意之欄位若未勾選，本人同意視同授權。

研究生：王夢偉

學號：8624802

親筆正楷：王夢偉 (務必填寫)

中華民國 93 年 7 月 9 日

國家圖書館 博碩士論文電子檔案上網授權書

(提供授權人於辦理離校手續時繳交至系所用)

本授權書所授權之論文為本人在國立交通大學(學院)光電工程系所
_____組，92學年度第_____學期取得博士學位之論文。

論文名稱：多波長光彈調變式橢圓偏光術
指導教授：趙于飛

■ 同意

本人具有著作財產權之上列論文全文(含摘要)，以非專屬、無償授權國家圖書館，不限地域、時間與次數，以微縮、光碟或其他各種數位化方式將上列論文重製，並得將數位化之上列論文及論文電子檔以上載網路方式，提供讀者基於個人非營利性質之線上檢索、閱覽、下載或列印。
上述授權內容均無須訂立讓與及授權契約書。依本授權之發行權為非專屬性發行權利。依本授權所為之收錄、重製、發行及學術研發利用均為無償。上述同意與不同意之欄位若未勾選，本人同意視同授權。

研究生：王夢偉

學號：8624802

親筆正楷：王夢偉 (務必填寫)

中華民國 93年 7 月 9 日

本授權書請以黑筆撰寫，並列印二份，其中一份影印裝訂於附錄三之一(博碩士論文授權書)之次頁；另一份於辦理離校時繳交給系所助理，由圖書館彙總寄交國家圖書館。

推薦函

中華民國 93 年 9 月 9 日

事由：推薦光電工程研究所博士班研究生 王夢偉 提出論文以參加國立交通大學博士論文口試。

說明：本校光電工程研究所博士班研究生 王夢偉 已完成光電工程研究所規定之學科及論文研究訓練。有關學科部份，王 君已修畢 18 個學分（請查閱歷年成績單），並通過學科考試。有關論文研究部份，其發表著作如附件所示。

總言之，王 君已具備國立交通大學光電工程研究所應有之訓練水準。因此推薦 王 君參加國立交通大學光電工程研究所博士班論文口試。

國立交通大學光電工程研究所
指導教授



趙子飛

國立交通大學

論文口試委員會審定書

本校光電工程研究所博士班 王夢偉 君

所提論文 多波長光彈調變式橢圓偏光術

合於博士資格標準、業經本委員會評審認可。

口試委員：

李世光

李世光 教授

周晨

周晨 教授

施宙聰

施宙聰 教授

許根玉

許根玉 教授

蘇德欽

蘇德欽 教授

指導教授：

趙于飛

趙于飛 教授

所

長：

賴暎杰

教授

賴暎杰 教授

中華民國 九十三年 五月 二十四 日

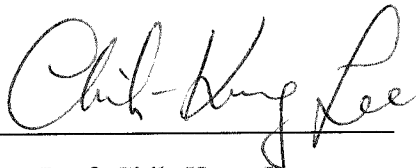
Institute of Electro-Optical Engineering
National Chiao Tung University
Hsinchu, Taiwan, R.O.C.

Date : May. 24. 2004

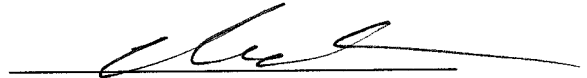
We have carefully read the dissertation entitled _____

Multi-wavelength Photoelastic Modulation Ellipsometry

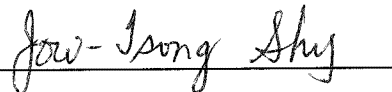
submitted by Meng-Wei Wang in partial fulfillment of the requirements of the degree of DOCTOR OF PHILOSOPHY and recommend its acceptance.



Prof. Chih-Kung Lee




Prof. Chien Chou



Prof. Jow-Tsong Shy



Prof. Ken Y. Hsu

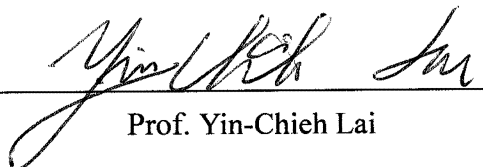


Prof. Der-Chin Su

Thesis Advisor : 

Prof. Yu-Faye Chao

Director of Institute of Electro-Optical Engineering :



Prof. Yin-Chieh Lai

多波長光彈調變式橢圓偏光術

研究生：王夢偉

指導教授：趙于飛

國立交通大學

光電工程研究所

摘要

多波長光彈調變式橢圓偏光術已可用於線上校正與即時量測。將偏光片/析光片轉動式引入光彈調變器可發展成一多波長光彈調變式橢圓偏光術。為了線上量測的封閉系統，本論文介紹一固定入射角線上校正法，將偏光片，析光片及光彈調變器一一根據待測物的反射面作零點的校正：首先，在偏光片-待測物-析光片的架構下，使用兩個事先設計的標準片或兩個適當的波長，可先根據入射面校正偏光片及析光片的方位角；隨後，再置入光彈調變器，透過方位角的轉動測得光彈調變器的方位角。

多倍頻亮度比技術可利用資料擷取系統校正光彈調變器的相位調變振幅。經由反射式及穿透式架構判斷相位調變振幅，可證明不受頻率影響，甚至經由數位化波形確認。除了相位調變振幅之外，在 632.8 奈米波長下，我們也校正靜態殘餘相位延遲。既然光彈調變器的幾何尺寸固定，我們設定相位調變振幅為針對波長 568.2 奈米的 0.383 個波長，並用於多波長相位調變振幅。線上即時的多波長光彈調變式橢圓偏光術之時間解析度已可至 40 微秒，此橢圓儀也已安裝在清華大學工科系電漿實驗室，用於監控電漿蝕刻製程。

關鍵字：線上，即時，校正，監控，光彈，調變，橢圓偏光術，多波長，光譜

Multi-wavelength Photoelastic Modulation Ellipsometry

Student : Meng-Wei Wang

Adviser : Yu-Faye Chao

Institute of Electro-Optical Engineering
National Chiao Tung University

Abstract

Multi-wavelength Photoelastic Modulation ellipsometry has been used for *in situ*/real time measurement. However, comparing to the rotating polarizer/analyzer ellipsometry, Photoelastic Modulation (PEM) ellipsometry introduces a wavelength-dependent element, the photoelastic modulator. The multi-wavelength PEM ellipsometry needs precise knowledge of the polarization of light emerging from the modulator. In this thesis, *in situ* azimuth alignment and real time phase calibration of the PEM ellipsometry has been achieved in multi-wavelength. The fixed incident angle azimuthal alignment technique is proposed to determine the azimuthal orientations of the polarizer and the analyzer to the incident plane by using two pre-designed testing samples or two probing wavelengths under a Polarizer-Sample-Analyzer (PSA) ellipsometric setup. Then, the azimuth of photoelastic modulator is directly obtained from the measurement of azimuthal rotation the PEM.

A multiple harmonic intensity ratio technique is introduced to real time calibrate the modulation amplitude (δ_o) of a photoelastic modulator by using a data acquisition system. The modulation amplitude δ_o of PEM determined by this technique is proved to be frequency independent by the reflection and transmission setups, and further confirmed by the digitized oscilloscope waveform. In addition to its modulation amplitude δ_o , we also calibrated its static phase retardation (Δ_i) at 632.8 nm. Since the physical size of PEM is constant, we calibrated the δ_o at multiple wavelengths by setting the Δ_o (i.e. $\delta_o / 2\pi$) value at 0.383λ for 568.2 nm. An *in situ*/real time multi-wavelength PEM ellipsometry has be realized with a time resolution of 40 μ s. The practical system has been installed in NTHU for monitoring the plasma etching process.

Keywords: *in situ*, real time, alignment, calibration, monitoring, photoelastic, modulation, ellipsometry, multi-wavelength, spectroscopy.

誌謝

很榮幸能將橢圓偏光術實現於線上即時監控蝕刻製程,在我學習的過程中,受到許多人的幫助.首先要感謝我的指導教授趙于飛博士這些年來的指導,支持和鼓勵.從偏極光學到量測儀器,她鼓勵我廣泛的探討研究主題.尤其要感謝她花在本論文的時間.我也要感謝清華大學工科系林滄浪教授及柳克強教授在蝕刻系統研究上可貴的共同研究及支持幫助.此外,我的口試委員李世光教授,周晟教授,施宙聰教授,許根玉教授及蘇德欽教授,提供我論文上許多深入的見解,亦表謝意.

我曾接受許多組織及個人的支持於促進國際學術合作以增強研發能力. NEW FOCUS Inc.張茂德博士夫婦提供美國光學學會的旅程獎助.德國學術交流協會提供獎學金赴德國 *SENTECH Instrument GmbH* 暑期實習及 Dr. Bernd Gruska 的指導.日本交流協會邀請及安排赴日的日本台灣交流計劃,李國鼎科技發展基金會及交通大學研發處對參加國際會議的贊助,在此一併致謝.

偏光實驗室為一個團隊合作的研究群.我要感謝早期和目前的同學們不可磨滅的貢獻:王昌國博士及劉行在早期光彈調變器的研究,林肇廉拓展到光彈調變式偏光儀及量測扭轉式液晶,林柏儒於 Mueller 矩陣的符號運算及蔡斐欣和柯凱元於光彈調變式橢圓儀的量測.我也要謝謝實驗室其他同學給我如此美好的研究生生活和像家一樣充滿友誼的實驗室.此外,我要致上我的謝意給清華大學電漿實驗室已畢業和在學的同学及寶貴的共同研究經驗:陳旭賢及張俊霖最初建立線上自動化光彈調變式偏光儀,劉育維進行線上校正及電腦程式運算,郭俊儀實現線上監控蝕刻終點.

最後,我特別要感謝我的家人給我的愛和支持.我的父親王振武和母親李乃華總是給我鼓勵及作為開明的表率,我也要感謝弟弟王夢凡博士和我患難與共的經驗分享和心靈啟發.

本研究持續由國科會及原能會資助.在此衷心感激國家給我的栽培.對這些和所有曾幫助過我求學的人,沒有你們的支持,本論文也不可能完成.我將會盡我的全力回報你們的期望.

Acknowledgments

It is the glory to achieve *in situ* ellipsometry to real time monitor plasma etching process. Many people have assisted me in my education. I would like to first thank my advisor, Professor Yu-Faye Chao, for her guidance, support and encouragement during these years. I thank her for encouraging me to wildly explore the research topics, from polarization optics to measurement instrumentation. Especially I thank her for the time she spent on this thesis. I am also grateful to Professor Tsang-Lang Lin and Professor Keh-chyang Leou in Department of Engineering and System Science of NTHU for their invaluable collaboration and helpful support on my research in plasma etching system. Furthermore, I would like to thank my Dissertation Committee members, who have been an excellent source of feedback concerning many insightful input to this work: Prof. Chih-Kung Lee, Prof. Chien Chou, Prof. Jow-Tsong Shy, Prof. Ken Y. Hsu and Prof. Der-Chin Su.

I have received support from a lot of organizations and people to promote international academic cooperation in aspiration for advancing research capability. I thank Dr. and Mrs. Milton Chang of New Focus Inc. for travel grant in Optical Society of America. I am grateful to Dr. Bernd Gruska of *SENTECH* Instrument GmbH for the summer internship sponsored by German Academic Exchange Service (DAAD). I also appreciate Japan Interchange Association for their invitation and arrangement on Japan-Taiwan Interchange Program. Special thanks go to K. T. Li Foundation and NCTU Office of Research and Development for their funds of attending international conference.

Polarized Light Laboratory (PLLab) is a teamwork research group. I like to thank the former and current members of PLLab from their numerous contribution: Dr. Charn-Kuo Wang and Shing Liu for original studies about photoelastic modulation (PEM), Andy Lin for exploration in PEM polaimetry and TN-LC measurement, Polo Lin for investigation on symbolic formulation by Mueller Matrix, and Fei-Hsin Tsai and Kai-Yuan Ko for measurement in PEM ellipsometry. I am also grateful to my other Lab members for making these years of my graduate school life at NCTU a wonderful experience, and making PLLab a warm home forever with friendship. Moreover, I like to extend my gratitude to past and present members in Plasma Lab of NTHU from their uncountable collaboration: Shu-Shien Chen and Chun-Lin Chang for primary setup of automatic *in situ* PEM ellipsometer, Yu-Wei Liu for development of *in situ* alignment and numerical programming analysis, and Chun-Yi Kuo for implementation of end point prediction by on line control etching process.

Finally, I would like to express my special thanks to my family for their love and support. My father, Chen-Wu Wang, and my mother, Nai-Hua Li, have always encouraged me and have always been my enlightened role models. I would like to thank my brother Dr. Meng-Fan Wang for sharing studying experience and inspiration.

This research has been sustainedly sponsored by National Science Council and Atomic Energy Council of R. O. C. I deeply appreciate the cultivation by my country. To these and all others who have aided me in my studies. Without your support, this thesis would not be possible. I will try my best to reward for your expectation.



Contents

Abstract (Chinese)	i
Abstract (English)	ii
Acknowledgement (Chinese).....	iii
Acknowledgement (English).....	iv
Contents	vi
List of Tables	viii
List of Figures.....	ix
Symbol Definition.....	xv
Chapter 1 Introduction.....	1
1.1 importance of multi-wavelength photoelastic modulation ellipsometry.....	1
1.2 The construction of photoelastic modulation Ellipsometry.....	4
1.3 References.....	5
Chapter 2 Fundamentals of multi-wavelength photoelastic modulation ellipsometry	7
2.1 Optical characterizations and the reflected polarized light	7
2.2 Ellipsometry.....	10
2.3 Photoelastic modulation ellipsometry.....	13
2.4 The multi-wavelength photoelastic modulation ellipsometer	15
2.5 References.....	17
Chapter 3 <i>In situ</i> azimuth alignment in photoelastic modulation ellipsometry at a fixed incident angle	23
3.1 Introduction.....	23
3.2 Theoretical Background.....	24
3.2.1 Intensity ratio alignment in PSA system.....	24
3.2.2 The azimuth alignment for the strain axis of PEM.....	25
3.3 Experiment.....	27
3.4 Results	28
3.4.1 The azimuth deviation of the polarizer and analyzer.....	29
3.4.2 The azimuth deviation of the PEM.....	29
3.5 Summary and discussion.....	29
3.6 References.....	30
Chapter 4 Real time calibrations of phase modulation amplitude of photoelastic modulator.....	37

4.1. Introduction.....	37
4.2. Theoretical background.....	39
4.3. Experimental.....	41
4.3.1 <i>real time calibration of phase modulation amplitude</i>	41
4.3.2 Correction in modulation amplitude in etching process.....	42
4.4. Result.....	43
4.4.1 <i>real time calibration of phase modulation amplitude</i>	43
4.4.2 <i>Correction in modulation amplitude in etching process</i>	43
4.5. Summary.....	44
4.6 References.....	45
Chapter 5 <i>In situ</i> / real time multi-wavelength photoelastic modulation ellipsometry.....	63
5.1. Introduction	63
5.2. Theoretical background.....	64
5.3. Experimental details.....	65
5.4. Results and discussion.....	66
5.5. Summary.....	68
5.6 References.....	68
Chapter 6 An error evaluation technique for the angle of incidence in a rotating element ellipsometer using a quartz crystal.....	87
6.1 Introduction... ..	87
6.2 The reflectance ratio of a uniaxial crystal.....	88
6.3 Experimental Procedures.....	90
6.4 Results	90
6.5 Concluding remarks	91
6.6 References.....	92
Chapter 7 Conclusion.....	101
Appendix A The samples for fixed incident angle alignment.....	105
Appendix B The analysis of etching process.....	109
Appendix C Fresnel reflection coefficients of uniaxial crystals.....	112
Vita (Chinese).....	115
Curriculum Vitae.....	116
Publication List.....	117

List of Tables

Chapter 3

Table 3.1 Measured Ψ at intersections.....32

Table 3.2 The ellipsometric parameter Ψ measured by PEM and Rodolph ellipsometers.....32

Chapter 4

Table 4.1 The measured modulation amplitudes almost shifted from the displayed value by 0.02λ in reflection setup.....47

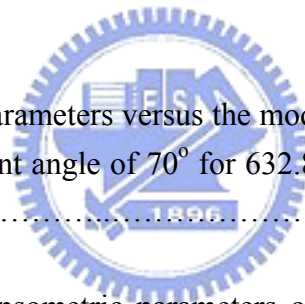
Table 4.2 The measured modulation amplitudes almost shifted from the displayed value by 0.02λ in transmission setup.....48

Chapter 5

Table 5.1 The ellipsometric parameters versus the modulation amplitudes: A SiO_2 thin film is measured at the incident angle of 70° for 632.8 nm after considering the static retardation.....70

Table 5.2. The measured ellipsometric parameters of a standard SiO_2 thin film for various wavelengths after considering the static retardation.....71

Table 5.3 The modulation amplitude calculated for other wavelengths and the measured values by taking the modulation amplitude at 0.383λ for 568.2 nm71



List of Figures

Chapter 2

- Fig. 2.1 Light interacting with a plane parallel interface between air and a material with complex index of refraction n_2 . The plane of incidence is defined as the plane which contains both the incoming beam and the normal to the surface. The amplitude of the electric field wave in the plane of incidence and perpendicular to the plane of incidence are called E_p and E_s , respectively.....17
- Fig. 2.2 Reflections and transmissions for two interfaces. The resultant reflected beam is made up of the initially reflected beam and infinite series of beams which are transmitted from medium 2 back into medium 1.18
- Fig. 2.3 Schematic setup of photoelastic modulation ellipsometer.....19
- Fig 2.4 Schematic diagram of photoelastic modulator.....20
- Fig. 2.5 Schematic configuration of data acquisition and processing system.....21
- Fig 2.6 The flowchart of *in situ* / real time multi-wavelength PEM ellipsometer...22

Chapter 3

- Fig. 3.1 Schematic setup of photoelastic modulation multi-wavelength ellipsometer.33
- Fig. 3.2 Angular positions of polarizer (α) and analyzer (β) where intensity ratio $A=B$, for the SiO_2/Si thin film sample (105 nm) and bare silicon wafer (2 nm). These two curves intersect each other at the incident plane $0.03^\circ \pm 0.02^\circ$ for polarizer and $-0.11^\circ \pm 0.02^\circ$ for analyzer. The signs (asterisk and circle) show the experimental data for 105 nm and 2 nm sample, respectively, and the lines show their linear polynomial fit approximation.....34
- Fig. 3.3 Angular positions of polarizer (α) and analyzer (β) where intensity ratio $A=B$, for the SiO_2/Si thin film sample (105 nm) with two probing wavelength, 488 nm and 647nm. These two curves intersect each other at the incident plane $-0.01^\circ \pm 0.05^\circ$ for polarizer and $-0.07^\circ \pm 0.05^\circ$ for analyzer. The signs (asterisk and circle) show the experimental data for 488 nm and 647 nm sample, respectively, and the lines show their linear polynomial fit approximation.35

Fig. 3.4 DC intensity distribution of the PEM ellipsometer. The azimuth angle of analyzer is at 0° versus the azimuth angle of the PEM. The sign (circle) shows the experiment data and the solid line shows the azimuth deviation of PEM is $0.2764^\circ \pm 0.0003^\circ$36

Chapter 4

Fig. 4.1 Schematic setup of photoelastic modulation ellipsometer.....49

Fig. 4.2 Schematic setup of photoelastic modulation polarimeter.....50

Fig. 4.3 Schematic setup of the IPC etcher with PEM ellipsometer.....51

Fig. 4.4 The configuration of the PEM ellipsometer for IPC etcher.....52

Fig. 4.5 The modulation amplitude are determined by the harmonic intensities ratios under varies displayed Δ_0 in a reflection setup. Circles and asterisks are the measured data for (I_{1f}/I_{3f}) and (I_{2f}/I_{4f}) , respectively. The lines are their polynomial fit: the slope of I_{1f}/I_{3f} is 99.75%, and I_{2f}/I_{4f} is 96.64%. An ideal line is plotted, i.e. the measured data equals to the displayed value.....53

Fig. 4.6 The modulation amplitude are determined by the harmonic intensities ratios under varies displayed Δ_0 in a transmission setup. Circles and asterisks are the measured data for (I_{1f}/I_{3f}) and (I_{2f}/I_{4f}) , respectively. The lines are their polynomial fit: the slope of I_{1f}/I_{3f} is 92.73% and I_{2f}/I_{4f} is 99.84%. An ideal line is plotted, i.e. the measured data equals to the displayed value.....54

Fig. 4.7 The modulation amplitude are determined by the harmonic intensities ratios under varies displayed Δ_0 : reflection (circles, I_{1f}/I_{3f}) and transmission (asterisks, I_{2f}/I_{4f}). Line is the polynomial fit, whose slope is 99.80%. An ideal line is plotted, i.e. the measured data equals to the displayed value.....55

Fig. 4.8 The measured ellipsometric parameters Ψ and Δ of SiO_2/Si : before (circles) and after (asterisks) calibration under varies modulation amplitude. The line is the polynomial fit of the measured data after calibration.....56

Fig. 4.9 The digitized oscilloscope waveform of a half-wave retardation:.....57

Fig. 4.10 The zooming in of Fig. 4.9.....	58
Fig. 4.11 Model of a double-layer wafer for etching.....	59
Fig. 4.12 The distribution Ψ under etching: Upper one is the film etched from around 5000 Å of polysilicon and lower one is the one etched with 10000 Å. (dotted line) is the theoretical calculated value; (solid line) measured value.....	60
Fig. 4.13 The distribution of Ψ and Δ for film (a) etched from 5000 Å; (b) etched from 10000 Å. (dotted line) measured value x correction factor; (solid line) theoretical value.....	61
Fig. 4.14 The real time calibration of modulation magnitude of PEM: fluctuated intensities of 1st and 3rd harmonics (upper), the monitoring of smooth varied modulation magnitude (lower).....	62
Chapter 5	
Fig. 5.1 The schematic setup of PEM ellipsometry.....	72
Fig. 5.2 The calibration of modulation amplitude in the reflection setup: both odd (o) and even (*) intensity ratios are measured, the ideal line is when measured values = displayed values.....	73
Fig. 5.3 The calibration of modulation amplitude under different wavelengths: 514.5 nm (o), 647.1 nm (*) and panel displayed values (line).....	74
Fig. 5.4 The modulation amplitude distribution versus azimuth position of analyzer: The intensity ratios of 1f/3f are measured in the reflection setup. A SiO ₂ thin film of 365 Å is measured at the incident angle of 70°	75
Fig. 5.5 The digitized oscilloscope waveform of half-wave retardation in the transmission setup: P = -45° and A = 45°; the solid line are the calculated waveform of 0.50λ (right) and 0.52λ (left).....	76
Fig. 5.6 The digitized oscilloscope retardation waveform of half-wave retardation at P = 45° and A = -45°	77
Fig. 5.7 The ellipsometric parameters versus the modulation amplitudes: A SiO ₂ thin	

film of 365 Å is measured at the incident angle of 70° and $\lambda=632.8$ nm.
 (A) Ψ : before calibration (o) ; after calibration (*)
 (B) Δ : before calibration (o) ; after calibration (x) ; after introduce the static phase retardation (*).....78

Fig. 5.8 Ψ and Δ graph of SiO₂ thin film at the incident angle of 70° with the discrete wavelengths of a KrAr tunable laser.....79

Fig. 5.9 The modulation amplitude σ of PEM versus wavelengths, by setting $\Delta_0=0.383$ at $\lambda=568.2$ nm.....80

Fig. 5.10 Two wavelength real time PEM ellipsometry was employed with a rotating chopper to switch two laser light sources.....81

Fig. 5.11 The measured intensity was chopped in about 0.4 sec to demonstrate the 0.1 sec time consumption to sketch sample condition for real time monitoring.....82

Fig. 5.12 Real time monitoring of polysilicon etching process: the traces of Ψ and Δ (upper), the calculated polysilicon thickness (lower).....83

Fig. 5.13 The modulation amplitude σ alternated in 1 ms between two wavelengths, 632.8nm and 488.0nm, calibrated simultaneously in 40 μ s.....84

Fig. 5.14 Two real time obtained ellipsometric parameters Ψ and Δ of a standard SiO₂ thin film of 364 Å thickness at the incident angle of 70° under two wavelengths, 632.8 nm and 488.0 nm.85

Fig. 5.15 The short intervals where two wavelengths are blocked (upper) or mixed (lower) in the acquired signal waveform.....86

Chapter 6

Fig. 6.1. The reflection geometry: θ_i is the incident angle, xy plane is the reflecting face of the crystal, zx plane is the incident plane, the z axis is the normal line. OA is the optical axis of the crystal.....93

Fig. 6.2. The numerically simulated Ψ as a function of azimuthal angle of θ_a while $\theta_c=90^\circ$: (a) quartz crystal: $n_o=1.544$, $n_e=1.553$ at the incident angle of 45° (line), and 44.94° (dot); (b) yttrium orthovanadate crystal: $n_o=1.9929$, $n_e=2.2154$ at the incident angle of 45° (line), and 44.5° (dot).....94

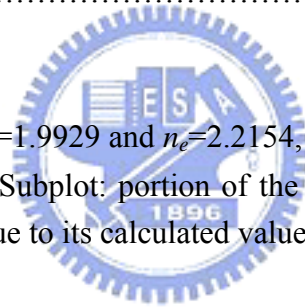
Fig. 6.3. The numerically simulated ψ as a function of azimuthal angle of θ_a while $\theta_c = 90^\circ$, quartz crystal of $n_o = 1.544$, $n_e = 1.553$ at the incident angle of 57° (line), and 56.94° (dot), respectively.....95

Fig. 6.4. A schematic set-up of the PSA ellipsometer: L, light source (He-Ne laser); P, polarizer; A, analyzer; D, detector.....96

Fig. 6.5. Ψ verses θ_a : Quartz
 $\theta_c=90^\circ$, $n_o=1.544$, $n_e=1.553$: (a) $\theta_i = 45^\circ$ (line: calculated •: measured) and $\theta_a = 0^\circ$;
 (b) $\theta_i = 44.94^\circ$ (line: calculated •: measured) and $\theta_a = -1.78^\circ$. Subplot: portion of the main plot, “ I “ is the standard deviation of the measured value to its calculated value.....97

Fig. 6.6. Ψ verses θ_a : BK7
 The standard deviation is 0.02° . The line indicates the mean value which is 17.29°98

Fig. 6.7. Ψ verses θ_a : YVO4
 $\theta_c=136.01^\circ$ for YVO4 with $n_o=1.9929$ and $n_e=2.2154$, $\theta_i = 44.94^\circ$ (line: calculated •: measured) and $\theta_a = 7.24^\circ$. Subplot: portion of the main plot, “ I ” is the standard deviation of the measured value to its calculated value.....99



Appendix A

Fig A.1 Ψ versus Δ for an air-film-silicon at the incident angle of 70° and wavelength of 633 nm. The film refractive index is taken as 1.46; the curve is plotted from 0 to 270 nm with 10 nm thickness increment. The 105 nm thin film (asterisk): $\Psi=42.82^\circ$, $\Delta=80.30^\circ$; the 2 nm native oxide (circle): $\Psi= 10.65^\circ$, $\Delta=164.45^\circ$106

Fig A.2 Ψ versus Δ for an air-film-silicon at the incident angle of 70° . The curve is plotted for a thin film of thickness 105 nm under different wavelength, which is from 488 nm to 647 nm with 20 nm increment. At wavelength of 488nm (asterisk) $\Psi=83.54^\circ$, $\Delta=146.11^\circ$; at wavelength of 647 nm (circle): $\Psi =42.42^\circ$, $\Delta=79.36^\circ$ 107

Fig. A.3 Intensity ratio of A and B plotted against angular position of polarizer (α) at a fixed angular position of analyzer (β) for the SiO₂/Si 105 nm thin film sample and native oxide 2 nm silicon sample. The intensity ratios are scaled according to

different sample and denoted as (105 nm) and (2 nm), respectively.....108

Appendix B

Fig. B.1 The distribution of Ψ and Δ for film under etching with 70 Å gate oxide...110

Fig. B.2 The distribution of Ψ and Δ for film under etching with 800 Å field oxide.111

Appendix C

Fig. C.1. The reflection geometry: θ_i is the incident angle, xy plane is the reflecting face of the crystal, zx plane is the incident plane, the z axis is the normal line. OA is the optical axis of the crystal.....114



Symbol Definition

r_p : the Fresnel reflection coefficient for the parallel polarizations

r_s : the Fresnel reflection coefficient for the perpendicular polarizations

ρ : the complex reflection coefficient ratio defined as $\rho = r_p / r_s = \tan\Psi e^{i\Delta}$

Ψ : ellipsometric parameter defined as the absolute value of complex reflection coefficient ratio

Δ : ellipsometric parameter defined as the phase angle of complex reflection coefficient ratio

P: azimuth of polarizer from the incident plane

A: azimuth of analyzer from the incident plane

α : small angle deviation of azimuths of polarizer

β : small angle deviation of azimuths of analyzer

γ : the strain axis of photoelastic modulator deviated from the incident plane

θ_o : the azimuth deviation of the photoelastic modulator

Δ_p : phase retardation of photoelastic modulator defined as $\Delta_p = \Delta_i + \delta_o \sin\omega t$

δ_o : the modulation amplitude of photoelastic modulator

Δ_o : measured modulation amplitude defined as $\delta_o / 2\pi$

Δ_i : the static phase retardation of photoelastic modulator

χ_i : incident polarization states

χ_r reflected polarization states

n : refractive index

k : extinction coefficient

n_o : ordinary refractive index

n_e : extraordinary refractive index

θ_i : incident angle

θ_a : the azimuth angle of the optical axis of a uniaxial crystal

θ_c : the angle between the normal to the cleavage plane and the optic axis

Chapter 1

Introduction

1.1 Importance of multi-wavelength photoelastic modulation ellipsometry

The increasing importance of techniques like plasma etching in semiconductor processing has provided a strong incentive to develop non-invasive diagnostics that can monitor *in situ* material evolution. Such characterizations can be used either to probe the growth mechanisms and the material structure from a fundamental point of view or to provide real time process control. *In situ* electronic probe are generally incompatible with the reactive environment of plasma etching chamber. On the contrary, optical diagnostics can be used in any transparent ambient. Moreover, detailed knowledge of surface and film composition, thickness and microstructure can be obtained by non-destructive techniques based on optical measurement. Optical measurements can be used to monitor and control surface growth, coating, cleaning, annealing, etching and other processes associated with fabrication of material surfaces. Among the various optical techniques, ellipsometry [1] takes advantage of the simultaneous measurement of two quantities (amplitude and phase) and employs polarization optics to measure the optical constants and thicknesses of thin films. It can provide real-time feedback on surface and film quality and thickness for monitoring and process control [2]. Film growth and etching, certainly, are two key processes used in materials growth and devices fabrication, especially in Nano-Structure, Bio-Technology and Micro ElectroMechanical Systems(MEMS).

Spectroscopic ellipsometry (SE) [3] allows measurements of the complex dielectric functions of multiplayer thin film structure. Different wavelengths have different penetration depths, especially for semiconductor sample. A shorter (above-gap) wavelength would be more sensitive to surface changes, while a longer (below-gap) wavelength would penetrate to underlying interfaces and be sensitive to overall layer thickness. On the other hand, a fully spectroscopic system would provide a great deal more information, but at the cost of much operation time, more complex and expensive system, and the need for more elaborate data analysis. A broadband lamp source would be needed, which would have significantly lower signal to noise than laser sources. Either a scanning monochromator (which would be slow) or a polychromator with detector array (with higher electronic complexity) could be used to select wavelengths. Development of such a system would be a major undertaking. While spectroscopic capability would be very valuable in a research instrument, it is probably not necessary for most real time monitoring applications.

As a consequence of recent advances in optical instrumentation and signal processing, *in situ* / real time ellipsometry became compatible with most of the kinetics involved in semiconductor processing techniques [4]. Such fast measurements are required to monitor the sample status like multi-layer stack plasma etching. The optical system originally uses a single wavelength laser source [5] multiple (two or more) wavelength data would provide useful additional information content, at relatively little increase in complexity and expense. Furthermore, multi-wavelength laser or several laser sources integrated through fiber optics can be used directly.

Two different experimental techniques, based on polarization modulation, are commonly used to perform automatic measurement. Rotating Element Ellipsometry

(REE) has the advantage of a conceptual simplicity and a wavelength insensitivity. Then they allow high precision measurements, in particular using Rotating Analyzer Ellipsometry (RAE) [6]. However, as a consequence of the low frequency modulation provided by the mechanical rotation, this first technique has been limited firstly to static measurements or to *in situ* applications involving slow kinetics. However, fast real time measurements with reasonable repetition rates are now available. In contrast, photoelastic modulation (PEM) ellipsometry use photoelastic modulator to perform the polarization modulation [7]. The main advantage of this technique is the use of a modulation system, about three orders of magnitude faster (typically 50kHz) than mechanical rotation of a polarizer [8,9]. PEM ellipsometer have already been successfully installed on a plasma etching system for monitoring the etching process [10]. Furthermore, the rotating element ellipsometry can cause the light beam to deviate around its incident direction hence embeds errors in the measurements. This parasitic error can be eliminated because of no moving part in the PEM ellipsometry. The time resolution of this system under a single wavelength is 0.1 sec; besides it can only measure the thickness and refractive indices of a flat surface.

Recently, multi-wavelength ellipsometry has been used in real time measurement [11]. It is our interest to improve the current apparatus into a multi-wavelengths type system [12]. However, as compared to REE, PEM introduces a wavelength-dependent element, the photoelastic modulator. Multi-wavelength PEM ellipsometry needs a precise knowledge of the polarization of light emerging from the modulator. The point has been addressed in detail. In particular, a clear improvement of the precision of PEM has been achieved by using an *in situ* / real time alignment technique to calibrate the polarization optical instrument [13-15]

1.2 The construction of photoelastic modulation Ellipsometry

The optical diagnostics based on phase modulation are described in Chapter 2. The multi-wavelength PEM ellipsometer is presented. The signal processing was based on the Fourier analysis of a data acquisition system.

The *in situ*/ real time calibration of PEM ellipsometric system will be presented from Chapter 3 to Chapter 5. Chapter 3 is devoted to the azimuth alignment technique with a fixed incident angle, which is prepared for the closed chamber system. The azimuth alignment will be carried out by two testing samples or two probing wavelengths without changing its physical setup, namely *in situ*. The calibration of phase modulator for real time application is presented in chapter 4. A multiple harmonic intensity ratio technique for calibrating the modulation magnitude of a photoelastic modulator will be introduced. A data acquisition system is utilized to investigate the frequency response of the system in the reflection and transmission setups and the calibration is confirmed by its digitized oscilloscope waveform. Furthermore, a correction factor is introduced to correct the effect caused by the shift modulation amplitude in the processing of etching. An *in situ* multi-wavelength PEM ellipsometry for real time measurement are presented then in Chapter 5. Under a fixed incident angle, the modulation magnitude at multiple wavelengths will be calibrated by setting a constant retardation value for its central wavelength. In addition to the modulation magnitude, the static phase retardation of modulator can also be obtained. These calibrations provided enough information for measuring multi-wavelength ellipsometric parameters of a sample by the multiple harmonic intensity ratio technique in real time. In chapter 6, we also evaluate the error of the angle of incidence for a rotating element ellipsometer by a uniaxial quartz crystal.

We have also applied this technique to determine the orientation of optical axis of yttrium orthovanadate (YVO_4) crystal to explore the feasibility of ellipsometry.

Finally, Chapter 7 concludes with the calibration and our recommendations for the future prospects of the multi-wavelength PEM ellipsometry.

1.3 References

- [1] R. M. A. Azzam and N. M. Bashara, *Ellipsometry and Polarized Light* (North Holland, Amsterdam, 1977).
- [2] S. A. Henck, *J. Vac. Sci. Technol. A* **10**, 934 (1992).
- [3] D. E. Aspnes, *Thin Solid Films* **89**, 249 (1982).
- [4] I. San, Y. M. Li, H. V. Nguyen, and R. W. Collins, *Rev. Sci. Instrum.* **63**, 3842 (1992).
- [5] Y. F. Chao, W. C. Lee, C. S. Hung, and J. J. Lin, *J. Phys. D.: Appl. Phys.* **31**, 1968 (1998).
- [6] D. E. Aspnes and A. A. Studna, *Appl. Opt.* **14**, 220 (1975).
- [7] S. N. Japerson and S. E. Schnatterly, *Rev. Sci. Instrum.* **40**, 761 (1969).
- [8] O. Acher, E. Bigan and B. Drevillion, *Rev. Sci. Instrum.* **60**, 65 (1989).
- [9] S. Ducharme, H. Machlab, P. G. Snyder, J. A. Woollam, and R. A. Synowicki, *SPIE Proceedings* **2839**, 373 (SPIE, Denver, 1996).
- [10] H. L. Maynard, N. Layadi, J. T. C. Lee, *J. Vac. Sci. Technol. B.* **15**, 109 (1997).
- [11] H. L. Maynard and N. Layadi, *Thin Solid Films* **313-314**, 398 (1998).
- [12] M. W. Wang, F. H. Tsai, and Y. F. Chao, *Thin Solid Films* **355-356**, 78 (2004).
- [13] Y.F. Chao, M.W. Wang, and Z. C. Ko, *J. Phys. D: Appl. Phys.* **32**, 2246 (1999).
- [14] M. W. Wang and Y. F. Chao, *Jpn. J. Appl. Phys.* **41**, 3981 (2002).
- [15] M. W. Wang, Y. F. Chao, K. C. Leou, F. H. Tsai, T. L. Lin, S. S. Chen, and Y. W. Liu, *Jpn. J. Appl. Phys.* **43**, 827 (2004).



Chapter 2

Fundamentals of multi-wavelength photoelastic modulation ellipsometry

Optical characterization techniques such as ellipsometry is widely used to measure film thicknesses or optical constants. In this chapter, optical properties of polarized light are briefly reviewed first. Formulated from Snell's law, Fresnel equation, and thin film interference expression, ellipsometry is employed to calculate film thicknesses and optical constants through modeling. After introducing the azimuth alignment and phase modulation calibration, the advantage of photoelastic modulation ellipsometry can be presented. The multi-wavelength photoelastic modulation ellipsometer is configured by data acquisition system at the end.

2.1 Optical characterizations and the reflected polarized light

The optical characteristic of a sample is embedded in its refractive index. Such as the anisotropic medium, the refractive index does depend on the polarization of light [1]. The real part of the refractive index is generally referred as *birefringence*, while the imaginary part is usually called as *dichroism*. Another important mechanism of polarization modification occurs at an interface, even between two isotropic media. Under non-normal incidence, the polarization of the reflected and the transmitted differ from the incident polarization. The instrument for measuring this phenomenon is called *ellipsometer*. However, the ellipsometric technique is generally involved to study non-transparent materials. As a consequence, ellipsometry in reflection configuration is much more widespread than in transmission. Dichrographs are more generally used in chemistry or biology. They

are called *linear* or *circular dichroism*, according to the eigen-polarization of the medium.

Ellipsometry measures the light making a reflection from the surface of interest [2]. In order to write the equations which describe the effect of the reflection on the incident light, it is necessary to define a reference plane, which is considered as our reference zero. Figure 2.1 schematically shows a light beam reflecting from the surface. The incident beam and the direction normal to the surface define a plane which is perpendicular to the surface and this is called the *plane of incidence*. Note that the outgoing beam is also in the plane of incidence. As indicated in Fig 2.1, the angle of incidence is the angle between the light beam and the normal to the surface. The effect of the reflection depends on the polarization state of the incoming light, the angle of incidence and physical structure of the medium. In Fig. 2.1, we show the amplitude of the electric wave in the plane of incidence as E_p and the amplitude of the electric wave perpendicular to the plane of incidence as E_s .

We are interested in the ratio of the amplitude and phase of the outgoing wave compared to that of the incoming wave. We first focus on a single interface and will develop the more general case later. When only one interface is considered, this ratio is called the *Fresnel reflection coefficients*, and it will be different for s-waves and p-waves. Let us suppose that the interface separates medium 1 and medium 2, with respective indices of refraction n_1 and n_2 and angles of incidence and refraction θ_1 and θ_2 (related by Snell's law). When the beam is incident from medium 1 onto medium 2, the Fresnel reflection coefficients are given by

$$\begin{aligned}
r_p^{12} &= \frac{n_2 \cos \theta_1 - n_1 \cos \theta_2}{n_2 \cos \theta_1 + n_1 \cos \theta_2} \\
r_s^{12} &= \frac{n_1 \cos \theta_1 - n_2 \cos \theta_2}{n_1 \cos \theta_1 + n_2 \cos \theta_2}
\end{aligned}
\tag{2.1}$$

where the superscripts refer to either p-waves or s-waves and the subscripts refer to the media which the interface separates.

When more than one interface is present, such as suggested by Fig 2.2. The resultant reflected wave returning to medium 1 will consist of light which is initially reflected from the first interface as well as light which is transmitted by the first interface, reflected from the second interface, and then transmitted by the first interface going in the reverse direction, and so on. Each successive transmission back into medium 1 is smaller than the last, and the infinite series of partial waves makes up the resultant reflected wave. We are interested in the phase and amplitude relationships between the p-wave and the s-wave. The ratio of the amplitude of the outgoing resultant wave to the amplitude of the incoming wave is defined as the *reflection coefficient*, and is analogous to the *Fresnel reflection coefficients* for a single interface. For a single film with thickness d (two interfaces) this is

$$\begin{aligned}
r_p &= \frac{r_p^{12} + r_p^{23} e^{-j2\delta}}{1 + r_p^{12} r_p^{23} e^{-j2\delta}} \\
r_s &= \frac{r_s^{12} + r_s^{23} e^{-j2\delta}}{1 + r_s^{12} r_s^{23} e^{-j2\delta}}
\end{aligned}
\tag{2.2}$$

where $\delta = 2\pi(d/\lambda)n_2 \cos \theta_2$. When $k \neq 0$, the absorption of the medium, the Fresnel coefficient, n_2 and $\cos \theta_2$ (and hence δ) are complex numbers. When $k=0$, non-absorbents, all these numbers are real. In general, except for very special circumstances, r_p and r_s are complex numbers. δ is the phase change in the wave, as

it moves from the top of the film to the bottom of the film. Hence, 2 is the phase difference between the part of the wave reflecting from the top surface and the part of the wave which has traversed the film twice (in and out).

Although the tabulated optical constants are simple values for each wavelength, the values are not independent of each other. The value of n and k should vary smoothly as one varies the wavelength in a continuous manner. Dispersion relationships are simply equations which give the values of n and k as a function of wavelength. Although some of the possible relationships are strictly empirical, most are based on physical principles. The best-known dispersion relationship was developed by L. Cauchy. The index n (or k) decreased with increasing wavelength (in the visible range) and could be expressed approximately as

$$n(\lambda) = n_a + \frac{n_b}{\lambda^2} + \frac{n_c}{\lambda^4} \quad (2.3)$$

where n_a , n_b , and n_c are known as the *Cauchy coefficients*. n_a gives the constant value at long wavelengths, and n_b controls the curvature in the middle of the visible spectrum and n_c influences the spectrum to a greater proportions for shorter wavelengths. Although one can rationalize this expression from physical principle, it is usually used in an empirical manner.

2.2 Ellipsometry

Ellipsometry measures the ratio of the reflective coefficient between P -wave and S -wave, namely as

$$\rho = \tan \Psi e^{i\Delta} = \frac{r_p}{r_s} \quad (2.4)$$

where the subscripts p and s refer to the plane wave electric field components, respectively, parallel and perpendicular to the plane of incidence. The magnitude and the phase of ρ are contained in the $\tan\Psi$ and its the exponential function, respectively. The quantities Ψ and Δ (sometimes only $\cos\Delta$) are measured by ellipsometer and are named as ellipsometric parameters. The information of sample is contained in the reflection coefficients, and hence in ρ ; quantities such as thicknesses and the optical constants of the medium can be deduced through modeling.

It is often not possible to extract the thicknesses or optical constants of interest directly from measured optical data, particularly if more than one or two parameters are to be obtained from the analysis. As an alternative to direct calculation methods, regression methods may be used to extract the sample parameters of interest from the measured optical data. The problem of optical data analysis can be stated as follows. We have an experimentally measured set of optical data, consisting of ellipsometric parameters, from a given sample. We also have a model for the sample which allows us to calculate the ellipsometric parameters for the model given the thicknesses and optical constants of all layers. We wish to adjust the values of some of the parameters in the model (thicknesses and optical constants) so that the data calculated from the model matches the measured data as closely as possible. To do this, we require some kinds of merit function which indicate how well the experimentally measured data match the calculated model data.

Mean square error (MSE) is commonly used merit function to judge the quality of the match between the measured and calculated data:

$$\text{MSE} = \sum_1^N [(\Psi_m - \Psi_c)^2 + (\Delta_m - \Delta_c)^2]. \quad (2.5)$$

In this equation, Ψ_m and Δ_m denote the experimentally measured data values, Ψ_c and Δ_c are the calculated model data points. There are N total ellipsometric parameters Ψ and Δ . The calculated data predicted from Snell's law, Fresnel equation, and thin film interference expression contains the model parameters which are to be varied in order to fit the experimental data. This function will exhibit a minimum value when the model matches the experimental data as closely as possible.

There are three ellipsometric methods that have been widely used: (I) Null Ellipsometry, the known polarized light is directed to the sample then through appropriate polarizing elements (compensator, polarizer) arrangement in such a way that the net outcome of light is zero, or 'null'. The null result can be obtained by several distinct arrangements of the polarizing elements, their azimuths of polarizer and analyzer can reveal the values of Ψ and Δ . (II) Rotating Element Ellipsometry, light of a specific polarization state is directed to the sample then the reflected light passes through an exit polarizer. The outcome intensity is measured by rotating one of the polarizing elements including polarizer, analyzer and compensator. The values of Ψ and Δ are determined by analyzing the measured data. (III) Modulation Ellipsometry, an oscillating compensator (the photoelastic modulator) is placed in the optical path (either before or after sample) along with other static polarizing elements. The intensity of the beam transmitted through the entire system is measured as the modulator retardation is varied over a specified range. Since the modulator retardation is sensitive to the changes of wavelength, precise calibration is required. This work is trying to develop a multi-wavelength spectroscopic ellipsometry by

using photoelastic modulator, so we shall put more effort in the photoelastic modulation ellipsometry.

2.3 Photoelastic modulation ellipsometry

A typical PEM ellipsometer consists of the Source–Polarizer–Photoelastic Modulator–Sample–Analyzer–Detector configuration, which is displayed in Fig. 2.3. The respective orientations of the polarizer, photoelastic modulator and analyzer, referred to the plane of incidence, are denoted as P, PEM and A. A photoelastic modulator consists of a fused silica bar submitted to a periodical stress, which is induced by a piezoelectric transducer, shown in Fig. 2.4, forming the optical anisotropy in the silica bar. As a consequence, the refractive index for a light beam with its polarization parallel to the strain differs from the index of a beam with its polarization perpendicular to the stress. Thus a photoelastic modulator induces a modulated phase shift Δ_p between these two eigen-modes.

The phase of an ideal photoelastic modulator is modulated as:

$$\Delta_p = \delta_o \sin \omega t \quad (2.6)$$

where δ_o is the modulation amplitude and is proportion to the excitation voltage. From Fourier expansion of the modulation, one can express the modulation in the followings

$$\begin{aligned} \sin \Delta_p &= 2J_1(\delta_o) \sin \omega t + 2J_3(\delta_o) \sin 3\omega t + \dots, \\ \cos \Delta_p &= J_0(\delta_o) + 2J_2(\delta_o) \cos 2\omega t + 2J_4(\delta_o) \cos 4\omega t + \dots, \end{aligned} \quad (2.7)$$

where $J_n(\delta_o)$ is the n^{th} Bessel function of δ_o .

Generally a high modulation frequency (30-80kHz) PEM ellipsometry is adapted for *in situ* measurements. Besides for reducing the noise level, one have to consider the time consumption of signal analysis in the DAQ system, the real time measurements are integrated in millisecond scale. In theory, the time resolution of PEM can be reduced to 20 μ s, which is considerable faster than the one can be obtained using rotating analyzer ellipsometry (RAE). Since here is not enough description of the spectroscopic behavior of the photoelastic modulator, the RAE ellipsometry was developed before PEM ellipsometry in spectroscopic region. This can be conquered in multi-wavelength structure. In a similar way, improvement of PEM ellipsometry were obtained by combining various conjugate measurements, using the so-called “zone averaging” procedure [3]. The precision is known to strongly vary as function of Ψ and Δ , in particular without a compensating optical element in the RAE measurement of $\cos^2 \Delta$. Therefore RAE are very insensitive to Δ when Δ is near 0° and 180° , in particular RAE measurements are generally inaccurate when dealing with low absorption range and ultra thin film structure. This experimental problem can be overcome in the case of PEM ellipsometry.

In order to acquire the accurate data with a PEM ellipsometry, it is necessary to determine a number of parameters of the optical system, such as azimuths of the optical elements, and the phase modulation amplitude of the PEM ellipsometry. A three intensity technique is developed to align the azimuth angle of the polarizer and analyzer to the incident plane, and then the azimuth of optic axis of photoelastic modulator is aligned to incident plane by a intensity ratio technique. An *in situ* ellipsometer is mainly used to monitor the closed processing system, like plasma etching chamber, one have to determine all azimuth angles in a fixed incident angle, so two sample or two wavelengths are used. Furthermore, the phase angle

modulated by photoelastic modulator can be calibrated by multiple harmonic intensity ratio technique. Chosen intensities from higher signal to noise ratio, the odd and even harmonics are used to determine the modulation magnitude. Under a wide range variation of modulation amplitude, we also investigate the frequency response of the system.

This calibration is very important, as the azimuthal locations of ellipsometer must be known in order to calculate Ψ and Δ . We also have to determine the system error by a zone average technique to obtain the accurate value of Ψ and Δ , i.e. taking the value at $P = \pm 45^\circ$. Since the error of incident angle is embedded in Ψ and Δ under the rotating element ellipsometry, we can evaluate the error by using a uniaxial quartz crystal in chapter 6.

2.4 The multi-wavelength photoelastic modulation ellipsometer

The configuration of multi-wavelength PEM ellipsometer has been shown in Fig 2.3. A linear polarized light passes through the photoelastic modulator forming a modulated polarized light. The modulator consists of a rectangular bar of a transparent material (fused silica) attached to a piezoelectric transducer oscillating at the frequency ω (50 kHz), which generates a periodical phase shift Δ_p between two orthogonal directions of the transmitted light.

In our system, a tunable multi-wavelength KrAr laser light passes through the polarizer which produces a well-defined linear polarization state. The high quality sheet polarizers are used as polarizer and analyzer, whose extinction ratios exceed $1:10^4$. The polarizer and photoelastic modulator are located in the first arm. Stepping motors are used for automatic rotation; the polarizer is oriented with its polarization axis at $\pm 45^\circ$ and the modulator is oriented with its optical axis at 0° with

respect to the plane of incidence. The spot size on the sample is about 1 mm in diameter. A second arm contains the analyzer which can also be automatically rotated by a stepping motor; the polarization axis of the analyzer is oriented at $\pm 45^\circ$ with respect to the plane of incidence. A silicon PIN photodiode is used as detector and the available wavelength range is in visible spectrum. The detector has linear response in the optical power independent of frequency up to the modulation frequency. The adaptation of the two optical arms allows spectroscopic measurements at various angles of incidence. On the other hand, the ellipsometer can be used for *in situ* application. In particular, the two arms can be adapted through optical windows to most of the semiconductor process reactors.

The configuration of data acquisition and digital signal process system is displayed in Fig. 2.5. This system can be divided into two distinct parts. The first part is the analog read-out system. After a broadband amplified photodiode to condition signal, the signal are amplified to adjust the amplitude from detector to match the range of analog to digital converter (ADC, 12-bits, 5 MHz). The high precision fast analog to digital converter is used to convert the modulated signal into digital form for further analysis by the computer. On the other hand, the Fourier analysis of the signal is then carried out in LabVIEW computer program. The instrumentation program is dedicated to Fast Fourier Transform (FFT) computation. Then, the DC component together with the harmonics of the signal are computed by 100ms. Moreover, after utilizing signal waveform computation by MatLab computer program, the ellipsometric parameters Ψ and Δ can be obtained simultaneously in 40 μ s. Eventually, our calibration technique allows the on-line control of the modulation amplitude. The PC computer is devoted to overall operation of the ellipsometer. Therefore, this multi-wavelength PEM ellipsometer

can be a powerful tool for real time control processing. Fig 2.6 represents the operation procedure of *in situ* / real time multi-wavelength PEM ellipsometer.

2.5 References

- [1] E. Collett, *Polarized Light : Fundamentals and Applications* (Marcel Dekker, New York, 1993).
- [2] H. G. Tompkins, and W. A. McGahan, *Spectroscopic Ellipsometry and Reflectometry: A User's Guide* (Wiley, New York, 1999).
- [3] F. A. Modine, G. E. Jellison, and G. R. Gruzalski, *J Opt. Soc. Am.* **73**, 893 (1982).

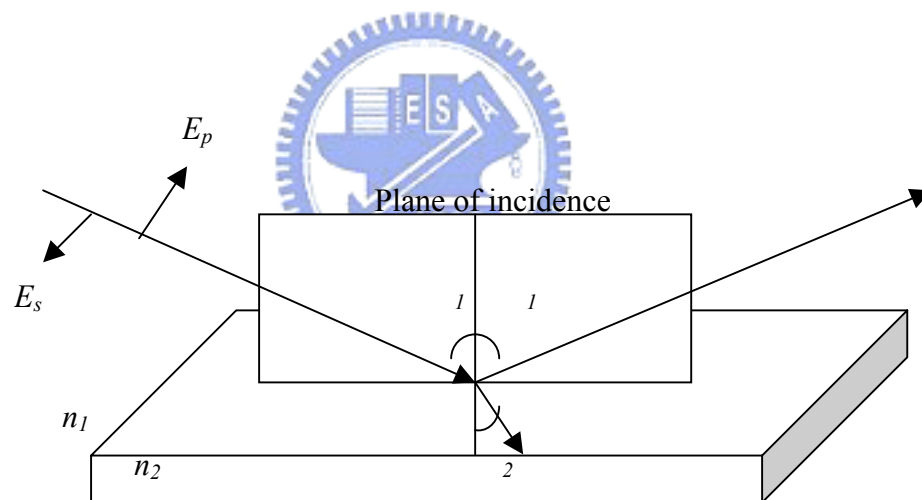


Fig. 2.1 Light interacting with a plane parallel interface between air and a material with complex index of refraction n_2 . The plane of incidence is defined as the plane which contains both the incoming beam and the normal to the surface. The amplitude of the electric field wave in the plane of incidence and perpendicular to the plane of incidence are called E_p and E_s , respectively.

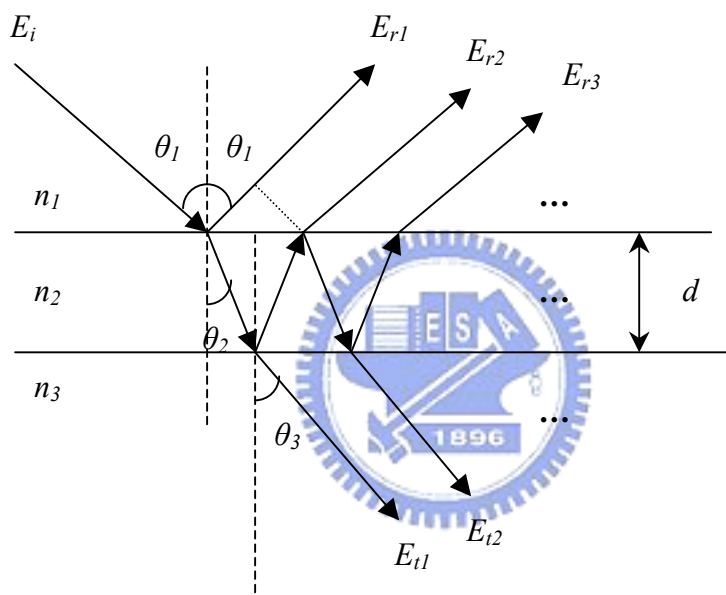


Fig. 2.2 Reflections and transmissions for two interfaces. The resultant reflected beam is made up of the initially reflected beam and infinite series of beams which are transmitted from medium 2 back into medium 1.

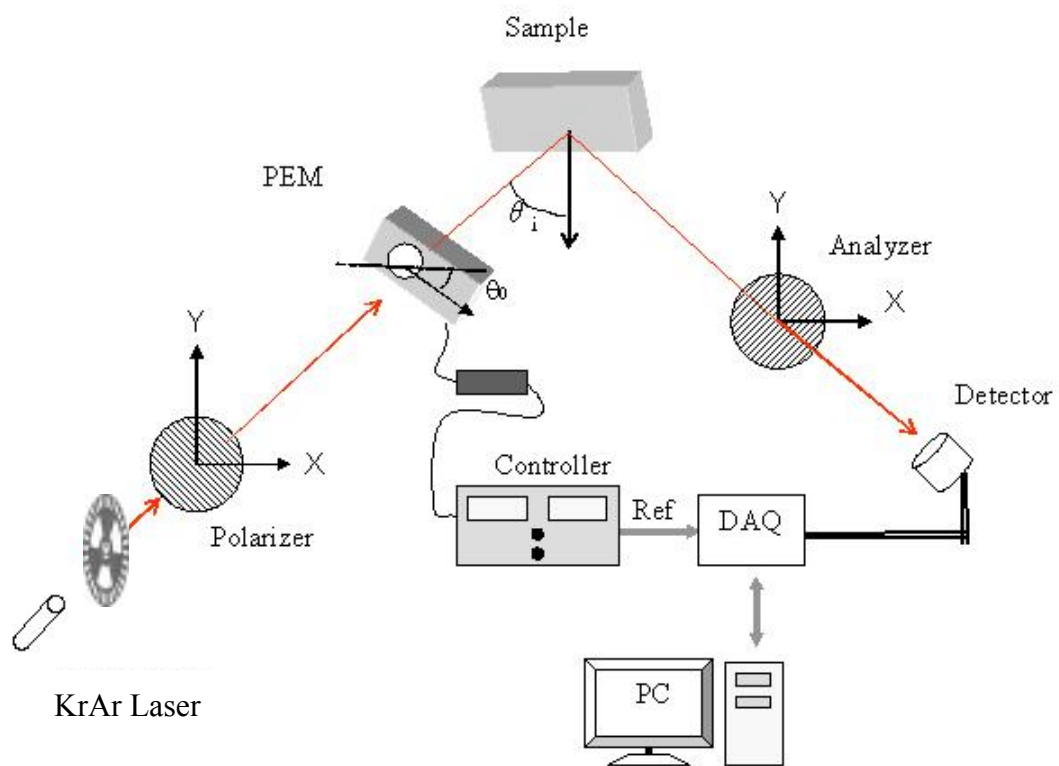


Fig. 2.3 Schematic setup of photoelastic modulation ellipsometer

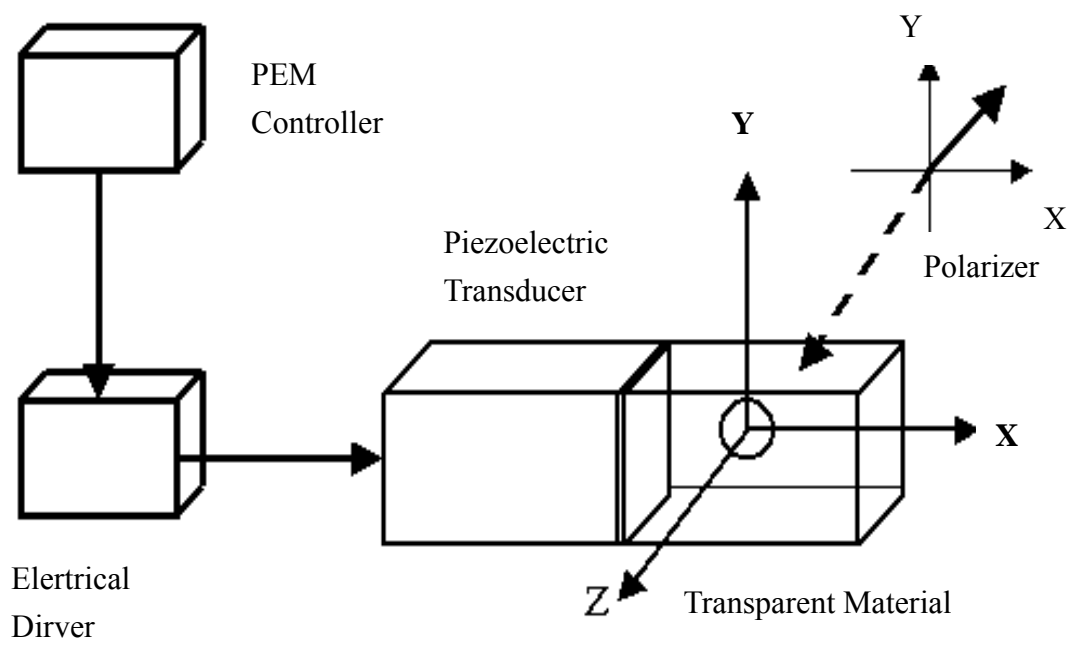


Fig 2.4 Schematic diagram of photoelastic modulator

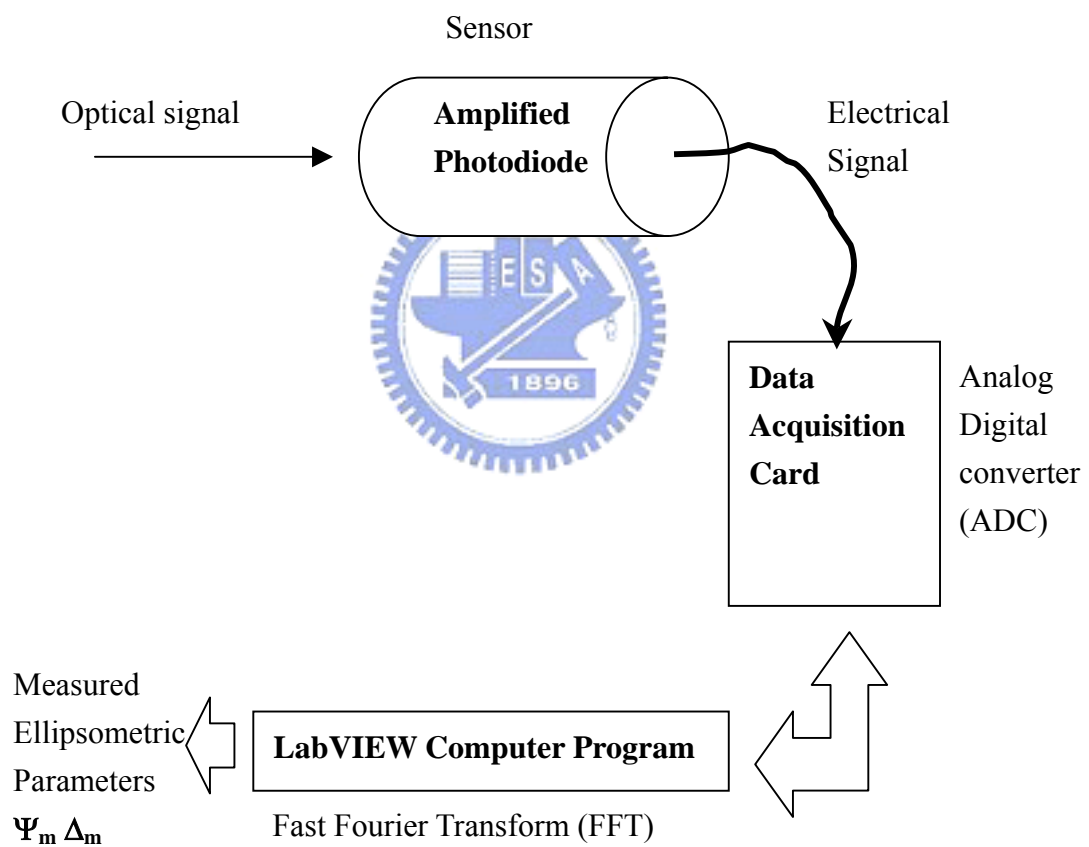


Fig. 2.5 Schematic configuration of data acquisition and digital signal process system

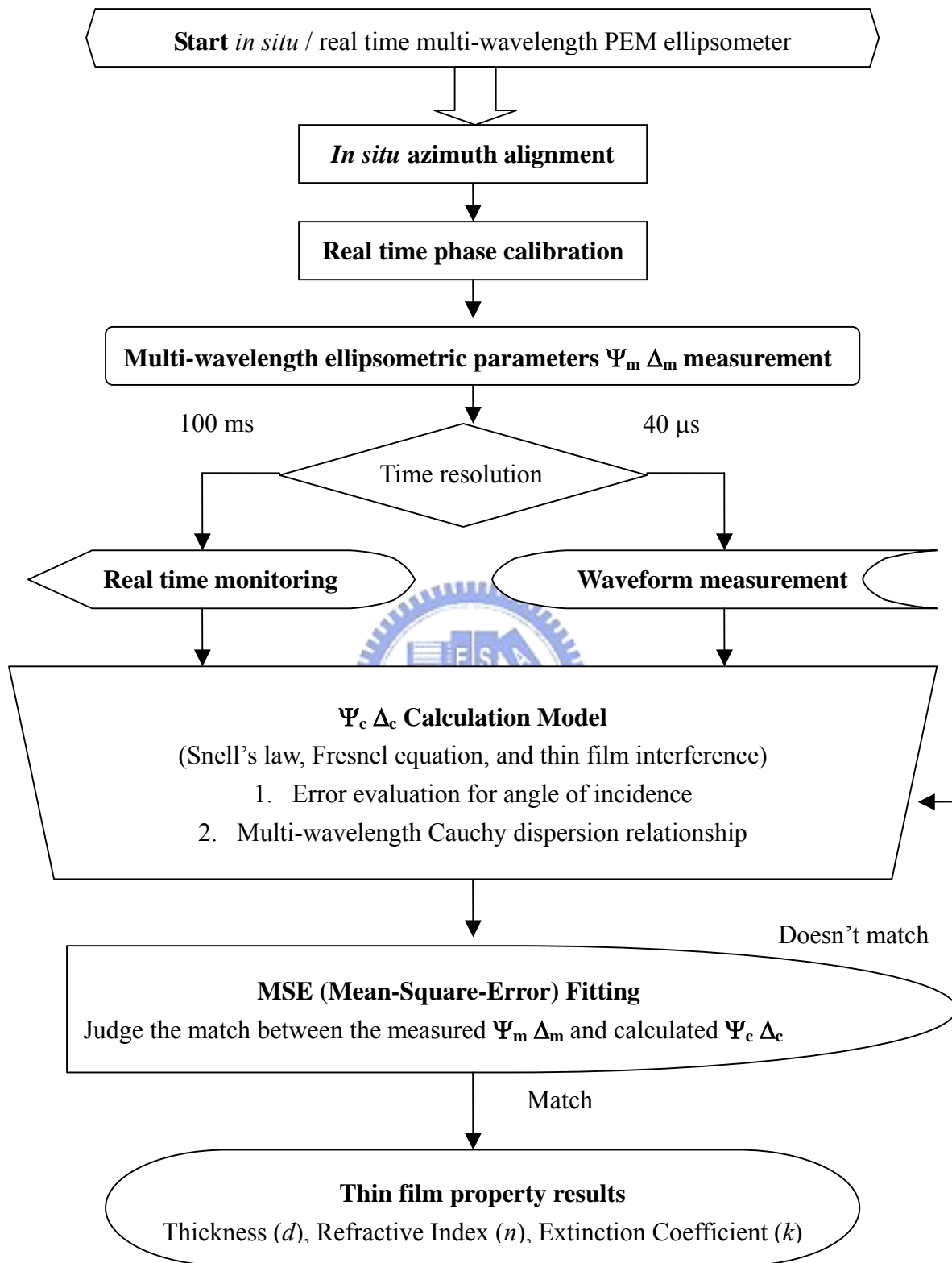


Fig. 2.6 The flowchart of *in situ* / real time multi-wavelength PEM ellipsometer

Chapter 3

***In situ* azimuth alignment in photoelastic modulation ellipsometry at a fixed incident angle**

Ellipsometry has recently emerged as a powerful optical technique to study thin films, because of its ability to perform *in situ* and spectroscopic studies. This technique is a nondestructive testing technique; its precision is comparable to interferometry but insensitive to the surface conditions of sample. In a photoelastic modulation ellipsometry, a fixed incident angle azimuthal alignment technique is proposed by high intensity ratio measurement. This technique is used to determine the azimuthal orientations of the polarizer, the photoelastic modulator and the analyzer to the incident plane.

3.1 Introduction

Photoelastic Modulation ellipsometry can not only control the phase retardation of PEM for wide range of wavelengths, but also use its harmonic modulation for synchronous detection without moving any part of the ellipsometric system [1, 2]. It is essential to align the azimuths of the optical components in ellipsometer for accurate measurements because any improper azimuth setting in the system can cause significant errors [3, 4]. Instead of null method [5], we improved Steel's intensity ratio technique [6] and separately aligned the azimuths of the polarizer (P) and analyzer (A) to the specimen surface in a polarizer-sample-analyzer (PSA) system through two incident angles [7]. We also need two incident angles to determine [8] the relative azimuth position of the strain axis of the Photoelastic Modulator (PEM) to the transmission axes of the polarizer and analyzer. We first align them in a straight-through setup, and then align the P-PEM-A system to the incident plane [9]. This at least two incident angles alignment technique is not suitable for a closed


chamber system. For the closed chamber, we extend the similar technique to align all of the optical components (namely P, PEM and A) to the reflective surface of a specimen at fixed incident angle. This development allows us to install the ellipsometer in a pre-designed closed system [10] for monitoring the film deposition or etching.

3.2 Theoretical Background

The basic setup of the ellipsometric system is shown in Fig. 3.1. The alignment for all the azimuths in the system is divided into the following two successive procedures.

3.2.1 Intensity ratio alignment in PSA system

Before inserting the PEM, we align the polarizer and analyzer to the incident plane by an intensity ratio technique. The ellipsometric parameters Ψ and Δ are defined as



$$\tan \Psi e^{i\Delta} = \frac{r_p}{r_s}, \quad (3.1)$$

where r_p and r_s are the reflection coefficients in the plane parallel (p) and perpendicular (s) to the incident plane, respectively. By considering the polarizer and analyzer separately, Chao [9] improved Steel's [6] intensity ratio technique to align the polarizer and analyzer to the incident plane. In the intensity ratio technique, the following two intensity ratios are defined

$$A(\alpha, \beta) = \frac{I(45^\circ + \alpha, \beta)}{I(45^\circ + \alpha, 90^\circ + \beta)}, \quad (3.2)$$

$$B(\alpha, \beta) = \frac{I(-45^\circ + \alpha, \beta)}{I(-45^\circ + \alpha, 90^\circ + \beta)},$$

where $I(P, A)$ is the intensity distribution at P and A of azimuths of polarizer and analyzer, with small angle deviation α and β from the incident plane, respectively. These intensity ratios are expanded to the first order approximation around their

respective scales, that is around α and β near to zero, one can have the following expressions;

$$\begin{aligned} A(\alpha, \beta) &\cong \tan^2 \Psi - 2[2 \tan^2 \Psi \alpha - \sec^2 \Psi \tan \Psi \cos \Delta \beta], \\ B(\alpha, \beta) &\cong \tan^2 \Psi + 2[2 \tan^2 \Psi \alpha - \sec^2 \Psi \tan \Psi \cos \Delta \beta]. \end{aligned} \quad (3.3)$$

The above two linear equations have opposite gradients and intersect with one other when

$$2 \tan^2 \Psi \alpha - \sec^2 \Psi \tan \Psi \cos \Delta \beta = 0 \quad (3.4)$$

at $\tan^2 \Psi$. This property can be used to align the polarizer and analyzer to the incident plane by solving two linear equations of different Ψ and Δ . It is easier to identify the intersection of those two equations by opposite sign of $\cos \Delta$. The two-incident angles [7], two-samples and two-wavelengths alignment technique are all based on this concept. We will explain the later two methods in the appendix A.

3.2.2 The azimuth alignment for the strain axis of PEM

Having precisely located the incident plane in the PSA system, we then directly determine the strain axis of PEM to the incident plane. If the strain axis of PEM deviates from the incident plane by θ , the final polarization state through the system can be expressed as

$$S_f = M_A(A) \cdot R_{SAM}(\Psi, \Delta) \cdot M_{PEM}(\theta, \Delta_p) \cdot S_p, \quad (3.5)$$

where the linearly polarized light, S_p , successively emerges through a PEM, $M_{PEM}(\theta, \Delta_p)$, then is reflected from the sample surface, $R_{SAM}(\Psi, \Delta)$, and finally measured by the detector through the projection of an analyzer, $M_A(A)$. When the initial light source is linearly polarized at 45° to the reference zero of the system, the previous expression can be formulated as

$$I(A) = I_o [L \sin^2 A + M \cos^2 A \tan^2 \Psi + N \sin A \cos A], \quad (3.6)$$

where

$$\begin{aligned}
L &= 0.5\{1 + \cos \Delta_p + (1 - \cos \Delta_p)(1 - \sin 4\theta)\}, \\
M &= 0.5\{1 + \cos \Delta_p + (1 - \cos \Delta_p)(1 + \sin 4\theta)\}, \\
N &= 0.5[1 + \cos \Delta_p - (1 - \cos \Delta_p) \cos 4\theta] \tan \Psi \cos \Delta - \sin \Delta_p \cos 2\theta \tan \Psi \sin \Delta.
\end{aligned}$$

When the azimuth angle of the analyzer is set at 0° and 90° , respectively, the expression of intensity can be reduced as

$$I(0^\circ) = 0.5I_o \tan^2 \Psi \{2 + (1 - \cos \Delta_p) \sin 4\theta\}, \quad (3.7)$$

$$I(90^\circ) = 0.5I_o \{2 - (1 - \cos \Delta_p) \sin 4\theta\}. \quad (3.8)$$

If the retardance Δ_p of the modulator is modulated as

$$\Delta_p = \delta_o \cos \omega t,$$

then the intensity can be Fourier expanded by its harmonic function

$$\cos \Delta_p = J_o(\delta_o) - 2J_2(\delta_o) \cos 2\omega t \dots$$

By taking the zero-order Bessel function $J_o(\delta_o)$ at its zero point, i.e., $\delta_o = 0.383\lambda$, we can simplify the DC component of its intensity as

$$I_{dc}(0^\circ) = 0.5I_o \tan^2 \Psi \{2 + \sin 4\theta\}, \quad (3.9)$$

$$I_{dc}(90^\circ) = 0.5I_o \{2 - \sin 4\theta\}. \quad (3.10)$$

From the eq. (3.9), the azimuth deviation of the PEM θ_o can be obtained by the DC component of the intensity, which are taken at two azimuths of the PEM separated by 45° through the following relation

$$\sin 4\theta_o = 2 \frac{I_{dc}(0^\circ)_{\theta=\theta_o} - I_{dc}(0^\circ)_{\theta=\theta_o+45^\circ}}{I_{dc}(0^\circ)_{\theta=\theta_o} + I_{dc}(0^\circ)_{\theta=\theta_o+45^\circ}}. \quad (3.11)$$

In addition to the azimuth, the ellipsometric parameter Ψ can also be obtain by the same measurements and related as

$$\tan^2 \Psi = \frac{I_{dc}(0^\circ)_{\theta=\theta_o+45^\circ}}{I_{dc}(90^\circ)_{\theta=\theta_o}}. \quad (3.12)$$

It is sufficiently to analyze the error of the azimuth deviation due to the fluctuation of light intensity. According to the intensity ratio of eq. (3.11), one can easy to prove the deviation of azimuth $\delta\theta_o$ resulting from those fluctuations is

$$\delta\theta_o = \frac{\tan 4\theta_o}{4 \tan^2 \psi} \frac{\delta I}{I}. \quad (3.13)$$

3.3 Experiment

In the beginning, we employed a standard technique to locate the incident plane. A marked polarizer (Melles Groit sheet polarizer of extinction ratio 10^{-4}) was used to locate the minimum reflection at the Brewster angle of a nonabsorbent, which was considered as the reference zero. The azimuth angles of polarizer and analyzer were aligned to locate the minimum transmission by a power meter (Newport 818-SL). After the rough alignment, the polarizer and analyzer were then positioned at the required incident angle, 70° in this experiment, in a PSA system to determine incident plane by the intensity ratio technique. The intensities of $I(\pm 45^\circ + \alpha, \beta)$ and $I(\pm 45^\circ + \alpha, 90^\circ + \beta)$ were measured as α varies from -5° to 5° with an increment of 1° , and β varies from -1° to 1° with increment of 0.5° . Two pre-designed SiO₂/Si thin films were chosen according to their thickness: 105 nm and 2 nm, respectively. For comparison, two wavelengths (Melles Griot Krypton Argon mix-gas ion tunable laser 643AP) were also used to probe a single sample, the SiO₂/Si thin film of thickness 105 nm used previously.

After the azimuth angles of the polarizer and analyzer were aligned precisely, the PEM (Hinds PEM 90) was arranged between the polarizer and sample in a P-PEM-S-A type ellipsometer. During measurement process, we adjusted the polarizer at $\pm 45^\circ$, the analyzer at 0° and 90° , respectively. For comparison, we set the amplitude of phase modulation at 0.383 of the HeNe laser (5mw Melles Griot),

and measured the DC intensity under varies azimuth angle of PEM from -90° to 90° with an increment of 5° . The azimuth deviation of the PEM can be determined from the DC intensity at two azimuths of the PEM, which is separated by 45° to each other; the $\tan\Psi$ can also be obtained by the DC intensity when the azimuth of analyzer at 0° and 90° , respectively.

3.4 Results

Because the polarizer and analyzer are aligned to the incident plane before inserting the PEM, we will present the result separately.

3.4.1 The azimuth deviation of the polarizer and analyzer

According to our analysis, we convert all the measured intensities into intensity ratios A and B. Two parameters can be obtained from the distribution of these ratios: the position of intersections (,) and the value at the intersection ($\tan^2\Psi$). A typical result is shown in the appendix A (Fig. A.3). From the graphical distribution of intersections, we can obtain the incident plane by least squares fitting. In this report, we are able to locate the incident plane within 0.04° difference between two samples and two probing wavelengths, such as shown Fig. 3.2 and Fig. 3.3. The azimuth of polarizer is located at $0.03 \pm 0.02^\circ$ verses $-0.01 \pm 0.05^\circ$; while the azimuth of analyzer is positioned at $-0.11 \pm 0.02^\circ$ verses $-0.07 \pm 0.05^\circ$ by two samples and two wavelengths, respectively. The value at the intersections ($\tan^2\Psi$) is the reflectance of the sample, which can be used to measure the incident angle of the system. We list the reflectance of two samples and two wavelengths in Table 3.1. The thickness deduced from the measured values is about 3 nm thicker than what we originally measured for both bare silicon and 105 nm film. We will discuss this in next section. The incident angle deduced from the measurement of the bare silicon is $69.93 \pm 0.02^\circ$, which is similar to what we measured in an anisotropic medium in chapter 6 [11].

3.4.2 The azimuth deviation of the PEM

After carefully locating the incident plane in the PSA system, we then insert the PEM in the system, and directly determine the azimuth deviation of the strain axis of PEM from eq. (3.11). The azimuth deviation evaluated by this technique is $0.2764 \pm 0.0003^\circ$; the intensity distribution predicted from this determination is compared with the measured intensity in Fig. 3.4. From the same intensity measurements the ellipsometric parameter Ψ of a thick platinum film is obtained at the incident angle of 70° . Table 3.2 lists the results from Rodolph AutoEL III and this technique for comparison.

3.5 Summary and discussion

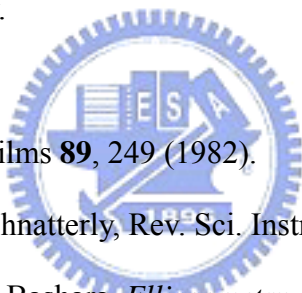
In addition to the azimuths of polarizer and analyzer, the strain axis of PEM can also be determined at the same incident angle by intensity ratio technique. This intensity ratio technique not only can reduce the error caused by the intensity fluctuation, it also simultaneously determine the ellipsometric parameter Ψ , which can be used to determine the incident angle *in situ*. Just like two incident-angle-alignment technique, it requires at least two testing samples or two-wavelengths to align the system prior to any measurement at a working incident angle. This technique is particularly suitable to a pre-designed closed system for the real time monitoring, in which a multi-incident-angle technique is not possible.

As the accuracy of the measurement fully depends on the stability of intensity, a stable light source can improve the determination of the azimuths of polarizer, analyzer and the strain axis of PEM. Since the intensity of KrAr tunable laser is not as stable as HeNe laser, the error for determining the azimuth in two probing wavelengths is 0.05° , while the error of two samples in HeNe laser is 0.02° . The instability of light source also decreases the accuracy of ellipsometric parameter determination. For fixed incident angle alignment, a stable source is suggested for

two wavelength technique. For determining the azimuth of PEM, we choose the azimuth position as close to zero as possible, because the effect of $\cos\Delta_p$ can be ignored at 0° and 45° when the azimuth of analyzer at 0° or 90° . According to our error analysis, the error increases with the azimuth position of PEM, especially when the azimuth setting of PEM closes to 22.5° .

The PEM ellipsometer can be aligned systematically on-line by a fixed incident-angle-azimuths-alignment technique. The advantage of this PEM ellipsometry is to use its harmonic modulation to monitor the process *in situ* / real time. However, the major problem in this system is the setting of the phase retardation of PEM for different wavelength; we are pursuing the calibration of phase retardation of PEM for multi-wavelength ellipsometry.

3.6 References

- 
- [1] D. E. Aspnes, Thin Solid Films **89**, 249 (1982).
- [2] S. N. Japerson and S. E. Schnatterly, Rev. Sci. Instrum. **40**, 761 (1969).
- [3] R. M. A. Azzam and N. M. Bashara, *Ellipsometry and Polarized Light* (North-Holland, Amsterdam, 1980), p. 387.
- [4] D.E. Aspnes and A.A. Studna, Appl. Opt. **10**, 1024 (1971).
- [5] F. L. MaCrackin, E. Passaglia, R. R. Stromberg, and H. L. Steinberg, J. Res. Natl. Bur. Stand. A **67**, 363 (1963).
- [6] M. R. Steel, Appl. Opt. **10**, 2370 (1971).
- [7] Y. F. Chao, C. S. Wei, W. C. Lee, S. C. Lin, and T. S. Chao, Jpn. J. Appl. Phys. **34**, 5016 (1995).
- [8] Y. F. Chao and C. K. Wang, Jpn. J. Appl. Phys. **37**, 3558 (1998).
- [9] Y. F. Chao, C. K. Wang, and S. Liu, Jpn. J. Appl. Phys. **38**, 6919 (1999).
- [10] H. L. Maynard and N. Layadi, Thin Solid Films **313-314**, 398 (1998).

[11] Y. F. Chao, M. W. Wang, and Z. C. Ko, J. Phys D: Appl. Phys. **32**, 2246 (1999).



Table 3.1 Measured Ψ at intersections

Wavelengths (nm)	632.8		647.1	488.0
	bare	thin film		
Ψ (deg)	10.65	44.46	43.96	83.61

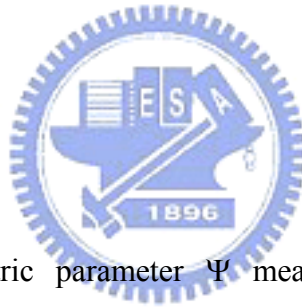


Table 3.2 The ellipsometric parameter Ψ measured by PEM and Rudolph ellipsometers

Ψ (deg)	P= 45	P= - 45	Average
PEM	34.41	34.19	34.30
Rudolph			34.15

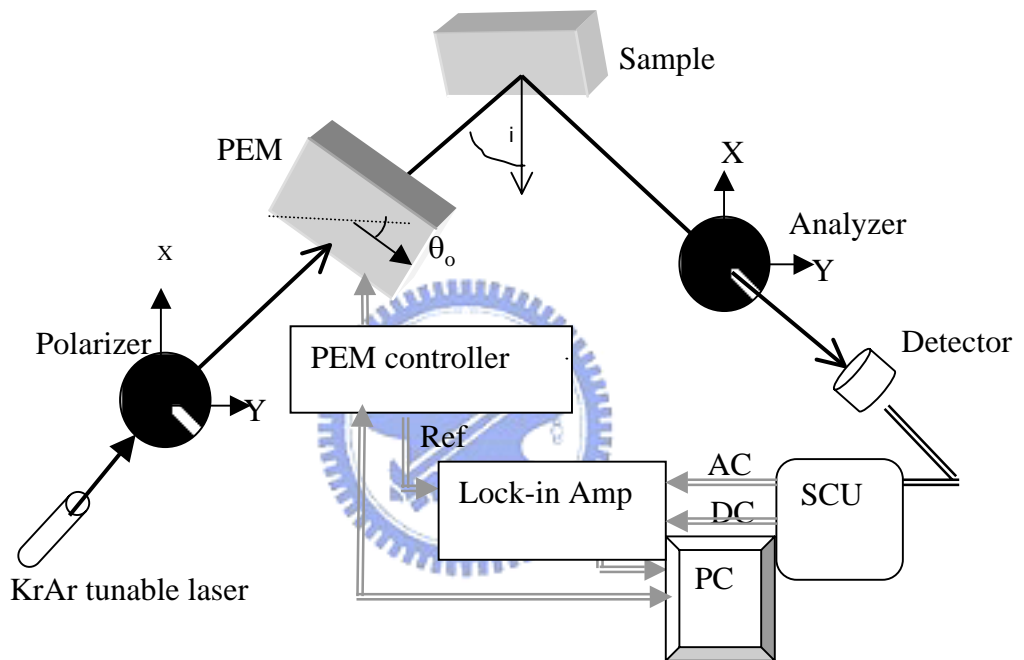


Fig. 3.1 Schematic setup of photoelastic modulation multi-wavelength ellipsometer.

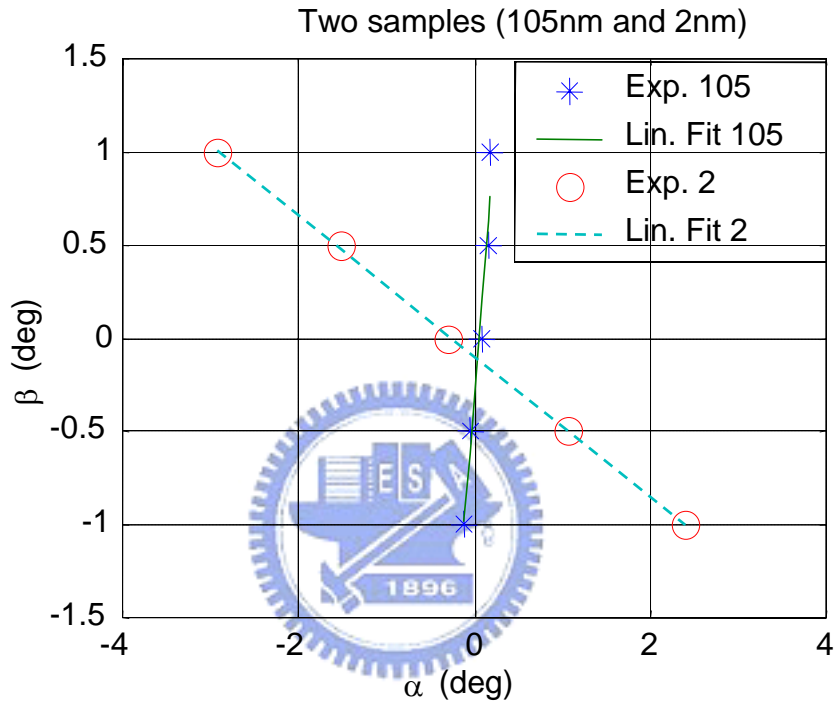


Fig. 3.2 Angular positions of polarizer (α) and analyzer (β) where intensity ratio $A=B$, for the SiO_2/Si thin film sample (105 nm) and bare silicon wafer (2 nm). These two curves intersect each other at the incident plane $0.03^\circ \pm 0.02^\circ$ for polarizer and $-0.11^\circ \pm 0.02^\circ$ for analyzer. The signs (asterisk and circle) show the experimental data for 105 nm and 2 nm sample, respectively, and the lines show their linear polynomial fit approximation.

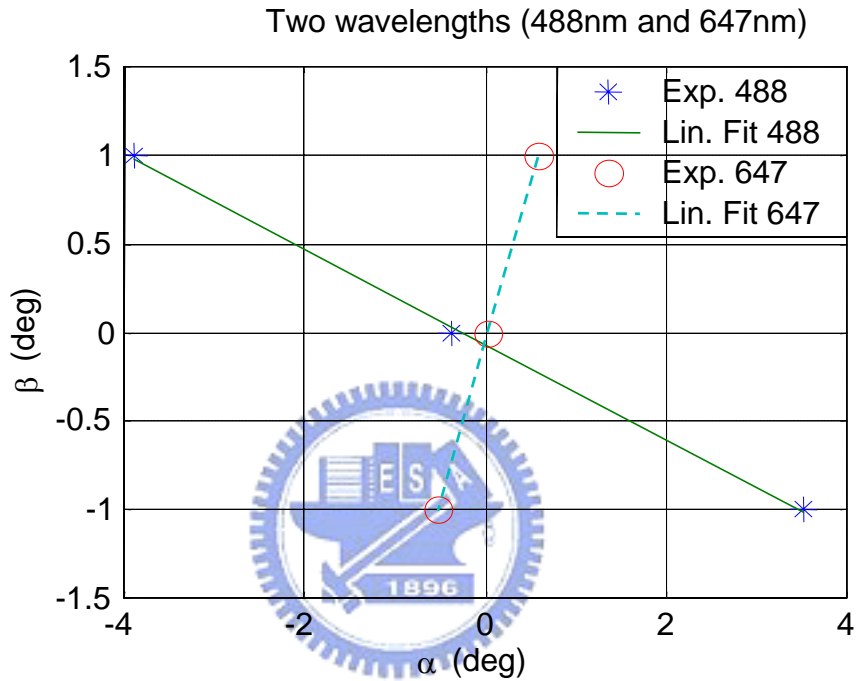


Fig. 3.3 Angular positions of polarizer (α) and analyzer (β) where intensity ratio $A=B$, for the SiO_2/Si thin film sample (105 nm) with two probing wavelength, 488 nm and 647 nm. These two curves intersect each other at the incident plane - 0.01° 0.05° for polarizer and -0.07° 0.05° for analyzer. The signs (asterisk and circle) show the experimental data for 488 nm and 647 nm sample, respectively, and the lines show their linear polynomial fit approximation.

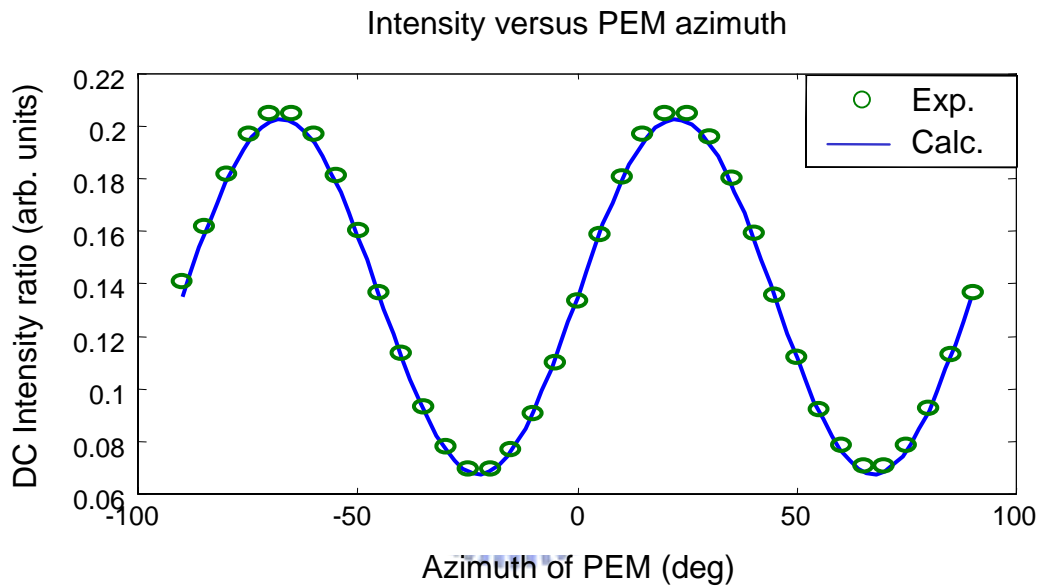


Fig. 3.4 DC intensity distribution of the PEM ellipsometer. The azimuth angle of analyzer is at versus the azimuth angle of the PEM. The sign (circle) shows the experimenter data and the solid line shows the azimuth deviation of PEM is $0.2764^\circ \pm 0.0003^\circ$.

Chapter 4

Real time calibrations of phase modulation amplitude of photoelastic modulator

A real time monitoring system is needed to measure the film thickness for controlling the decreasing dimension required in semiconductor processes. The ellipsometric technique has been used to measure the film thickness and refractive index since 70th. In the beginning of 90th, the *in situ* / real time ellipsometric system started to develop. A multiple harmonic intensity ratio technique is proposed to calibrate the modulation amplitude (δ_o) of a photoelastic modulator (PEM). A data acquisition system is utilized to investigate the frequency response of this technique. We also introduce a correction factor to correct the effect caused by the shifted modulation amplitude in the process of etching.

4.1. Introduction

PEM ellipsometry [1] is able to measure optical properties in real time [2] with minimum background noise. However, in contrast to the rotating element setups, the modulation amplitude of PEM has to be adjusted precisely to the zero point of the zero order Bessel function in order to obtain accurate measurements in the PEM ellipsometry [3]. Although we [4] did establish a technique for locating the zero point of zero order Bessel function for PEM, the position does vary under different environment, such as temperature; it is our interest to develop a method for correcting this zero point problem under various process. In addition to provide a correction technique for the modulation amplitude of PEM ellipsometry in the process of etching, we also like to introduce a standard real time calibration technique for the modulation amplitude of PEM, which can be employed for PEM polarimetry or ellipsometry under any incident angle.

Even one can align all the azimuths of the optical components in a PEM ellipsometer at a fixed incident angle [5], the phase modulation amplitude of its PEM still needs to be calibrated. It is known that PEM can be used in polarimetry and ellipsometry [6]. Here, we develop a real time calibration technique for modulation amplitude of both systems by a multiple harmonic intensity ratio (MHIR) technique without rearranging the experimental setup. Due to the progress of data acquisition (DAQ) system, we analyze the multiple harmonic components, which are obtained by Fourier expanding the measured value of the PEM ellipsometry/polarimetry system. Since the signal to noise ratio can be influenced by a weak signal, two experimental setups (a reflection style and a transmission style) are not only used to determine the phase modulation but also to investigate the frequency response of this technique. Before any coarse adjustment, we calibrate the modulation amplitude of a modulator (Hinds PEM90) and observe a 4% shifting in comparison with its displayed scale (provided by the vender). The analogue oscilloscope waveform of a half wave modulation is suggested for the calibration of PEM in its operation menu [6]. A multiple-paths [7] method is used to amplify the modulation amplitude for higher resolution; both techniques are operated in a straightforward setup and calibrate the modulation amplitude by their analogue oscilloscope waveform. Since one can obtain the digitized oscilloscope waveform by the DAQ system, we also compare the theoretical waveform with the digitized oscilloscope waveform under a straightforward setup; the results consist with what is obtained in the MHIR

For real time monitoring a etching process, a PEM ellipsometry is installed in a pre-designed plasma etching chamber [8]. To study the extinction coefficient k of polysilicon [9], which may be affected by the chemistry of etches, we deliberately use a very thick polysilicon film in order to analyze the etching process. We use one sample to correct the mislabeled modulation amplitude and find the refractive index

(including the extinction coefficient) of the sample; then we use another one to fit the measured data with the simulated value. After we simulated the distribution of Ψ and Δ for gate oxide in order to illustrate the film's thickness behavior in the etching process (appendix B), we suggest to provide the distribution of Ψ and Δ with respect to the film thickness instead of looking for the appropriate probing wavelength [3], which consists of high extinction coefficient for the sample. Because of this choice, we are able to identify the mislabeled modulation amplitude of PEM, which consists with our observation in MHIR technique with different modulator. Since two lock-in amplifiers both of which operate with limited harmonics, we introduce a correction factor instead of using a MHIR to re-calibrate the PEM for solving this problem.

4.2. Theoretical background

The basic setup of the PEM ellipsometer is shown in Fig. 4.1. If the azimuth angle of the initial linear polarized light is set at -45° , the measured intensity can be simplified as

$$I(A) = 0.5I_o[\sin^2 A + \tan^2 \Psi \cos^2 A - \tan \Psi \sin 2A (\cos \Delta \cos \Delta_p + \sin \Delta \sin \Delta_p)] \quad (4.1)$$

Since the phase retardation of PEM is modulated as $\Delta_p = \delta_o \sin \omega t$, one can substitute the Fourier expansions of the harmonic functions

$$\begin{aligned} \sin \Delta_p &= 2J_1(\delta_o) \sin \omega t + 2J_3(\delta_o) \sin 3\omega t + \dots, \\ \cos \Delta_p &= J_0(\delta_o) + 2J_2(\delta_o) \cos 2\omega t + 2J_4(\delta_o) \cos 4\omega t + \dots, \end{aligned}$$

into equation (4.1), and obtain the following relations between the measured intensity and its corresponding harmonic component,

$$\begin{aligned}
I_{dc}(A) &= 0.5I_0[\sin^2 A + \tan^2 \Psi \cos^2 A - \tan \Psi \cos \Delta J_0(\delta_o) \sin 2A], \\
I_{1f}(A) &= -I_0[\tan \Psi \sin \Delta J_1(\delta_o) \sin 2A] \sin \omega t, \\
I_{2f}(A) &= -I_0[\tan \Psi \cos \Delta J_2(\delta_o) \sin 2A] \cos 2\omega t, \\
I_{3f}(A) &= -I_0[\tan \Psi \sin \Delta J_3(\delta_o) \sin 2A] \sin 3\omega t, \\
I_{4f}(A) &= -I_0[\tan \Psi \cos \Delta J_4(\delta_o) \sin 2A] \cos 4\omega t.
\end{aligned} \tag{4.2}$$

It is very interesting to notice that the even/odd harmonics are related by the similar physical parameters except the orders of its Bessel function. By taking the intensity ratio technique, we can determine modulated amplitude of PEM but avoid the effect of its physical setup, i.e.

$$\frac{I_{1f}}{I_{3f}} = \frac{J_1(\delta_o)}{J_3(\delta_o)}; \quad \frac{I_{2f}}{I_{4f}} = \frac{J_2(\delta_o)}{J_4(\delta_o)}. \tag{4.3}$$

It is obvious that these ratios are independent of the azimuth position of the analyzer and the physical parameters of the examined sample. Furthermore, this multiple harmonic intensity ratio technique can also be used to determine the ellipsometric parameters Ψ and Δ . That is to set $A = \pm 45^\circ$, through the following expressions

$$\begin{aligned}
\sin 2\Psi &= \frac{\sqrt{\left(\frac{I_{1f}(45^\circ)}{J_1(\delta_o)}\right)^2 + \left(\frac{I_{2f}(45^\circ)}{J_2(\delta_o)}\right)^2}}{I_{dc}(45^\circ) + I_{dc}(-45^\circ)}, \\
\tan \Delta &= \frac{I_{1f}(45^\circ)J_2(\delta_o)}{I_{2f}(45^\circ)J_1(\delta_o)},
\end{aligned} \tag{4.4}$$

one can obtain Ψ and Δ independently.

Since a DAQ system can digitize the analog oscilloscope waveform, a transmitted system setup is utilized for analyzing the time variation of intensity. By setting $P = -45^\circ$ and $A = 45^\circ$ to the optic axis of PEM, and substituting the ellipsometric parameters of air (i.e. $\Psi = 45^\circ$; $\Delta = 0^\circ$) into equation (4.1), we can formulate the temporal behavior of the intensity in the following form,

$$I(t) = I_o[1 - \cos(\delta_o \sin \omega t)], \quad (4.5)$$

this waveform can be digitized by DAQ system. The analog oscilloscope waveform is a typical method for calibrating the modulation amplitude δ_o of a PEM. Normally, a half wave modulation is considered because it consists a flat top in the waveform; if the δ_o is higher than half wave, a dip will appear in the waveform. This property has been employed for calibrating the δ_o in the operation menu, which only qualitatively resolve the δ_o . Instead of using the multiple-path, one can zoom in the digitized waveform and compare with the theoretical waveform directly.

In addition to the MHIR technique, one also can correct the effect of δ_o in the process of etching; without setting the zero point of zero order Bessel function, one can formulate the ellipsometric parameter Ψ by introducing the correction factor f_c , i.e.

$$\sin 2\Psi = \sqrt{\left(\frac{I_{1f}}{2I_{dc}J_1(\delta_o)}\right)^2 + \left(\frac{I_{2f}}{2I_{dc}J_2(\delta_o)}\right)^2} \times f_c \quad (4.6)$$

$$f_c = 1 + J_0(\delta_o)\sin 2\Psi \cos \Delta$$

Normally, one can set $\delta_o=2.405$, i.e. 0.383λ , where $J_0(\delta_o)=0$, i.e. $f_c=1$. It is known [10] that the optical properties of material under etching can be different from the published reference values. In this work, we measure the Ψ and Δ under etching, and then deduce the optical properties by fitting. Since one have to calibrate certain parameter in the process of etching, we suggest two long etching processes to carried out the calibration of refractive index, the oxide layer and the correction factor of the PEM, which is caused by the mislabeled retardation amplitude δ_o .

4.3. Experimental

4.3.1 Real time calibration of phase modulation amplitude

A data acquisition system (NI PCI-6111) is used in the PEM (Hinds PEM90/CF50) ellipsometry; both the reflection (Fig. 4.1) and transmission (Fig. 4.2) styles

are studied in this report. Since we like to illustrate which ratio to use in the calibration process, we deliberately choose a SiO₂/Si thin film of 364 Å at the incident angle of 75°, whose Δ is closer to 90° in the reflection; but choose the air, whose Δ is closer to 0° in the transmission. In the reflection and transmission setups, we systematically aligned all the azimuth positions by a fixed incident angle alignment technique [5] and a direct determination technique [11], respectively. In both cases, the strain axis of PEM is positioned at 0°, and the azimuth of polarizer and analyzer are kept at -45° and 45°, respectively. The amplitude of the modulation is varied from 0.368 λ to 0.550 λ with closer steps around 0.383 λ . In addition to the dc component, four more harmonic intensities are obtained. After deducing the modulation amplitudes by using the intensity ratios of I_{1f}/I_{3f} (odd-ratio) and I_{2f}/I_{4f} (even-ratio) from eqs. (4.2) and (4.3), we then compared it with the provided display. The ellipsometric parameters of the SiO₂/Si thin film are also obtained by using equation (4.4). The digitized oscilloscope waveforms of a half-wave retardation are recorded to compare with the theoretical waveforms from eq. (4.5) before and after the calibration.

4.3.2 Correction in modulation amplitude in etching process

Two wafers are etched and measured in the plasma-etching chamber (ICP power 1000W, Bias 200W, pressure 10mTorr, flow (Cl₂/Ar) 95sccm / 5sccm), such as shown in Fig. 4.3. The basic structures of the wafers are polysilicon around 500 nm (wafer A) and 1000 nm (wafer B) deposited on thermally grown silicon dioxide with thickness of 100 nm on p-type silicon substrate.

The photoelastic modulation ellipsometer, such as shown in Fig. 4.4 consists of three parts: (A) modulated light source, the diode laser (635nm) followed by a polarizer and a PEM (Hinds 90/FS50), the transmission axis of polarizer and analyzer are set at 45° and the optical axis of PEM is set at 0°; (B) the detection system, the

intensity is measured by a photo detector and separated by a signal control unit (SCU-90) through two Lock-in amplifiers (EG&G 7265 and 7220) the DC, 1f and 2f signals are measured; (C) signal process system, the measured values are sent into PC by GPIB then converted to the ellipsometric parameters, Δ can be directly obtained by eq. (4.4) and Ψ also can be determined by eq. (4.6) with correction factor of modulation amplitude δ_o .

4.4. Result

4.4.1 Real time calibration of phase modulation amplitude

The modulation amplitudes δ_o of PEM are determined by MHIR, such as expressed in eq. (4.3). The measured modulation amplitudes Δ_o (i.e. $\delta_o / 2\pi$) against to its displayed values are plotted in Figs. 4.5 and 4.6 and listed in Tables 4.1 and 4.2 with the standard deviation. From both graphs, one can clearly see that they are almost parallel shifted from the displayed value by 0.02λ . Due to the value of Δ , the slopes of even-ratio in reflection ($\cos \Delta \ll \sin \Delta$) and odd-ratio in transmission ($\sin \Delta \ll \cos \Delta$) are off more than 4%, but less than 1% of the other ratio for both cases. Finally, we collected the measured modulated amplitudes of even-ratio in transmission and odd-ratio in reflection in the same plot, such as shown in Fig. 4.7. Since the ellipsometric parameters can be independently determined in the multiple harmonic measurements, the obtained Δ and Ψ of a SiO₂/Si thin film under varied Δ_o before and after the calibration are plotted in Fig. 4.8. The measurements of ellipsometric parameters are clearly improved after the calibration, especially when the modulation amplitude around 0.383λ . In the transmission setup, the temporal waveforms of a half-wave retardation are plotted in Fig. 4.9. The dip is clearly observable in the zooming in the half waveform, such as shown in Fig. 4.10.

4.4.2 Correction in modulation amplitude in etching process

The thicker wafer is used to extract the extinction coefficient under etching.

By comparing with the theoretical calculation of a double-layer film (Fig. 4.11), we obtain refractive index $n=3.631$ and extinction coefficient $k=0.0055$ for poly silicon; the thickness of oxide layer is 720 \AA instead of pre-designed 1000 \AA . It is known that the distribution of Ψ does depend on the zero point of $J_0(\delta_0)$, this phenomena can be observed by the traces of Ψ for both wafers, such as shown in Fig. 4.12. After introducing the correction factor, we can identify the expected significant change in the wafer A, which is about 900 \AA prior to the endpoint of etching, such as in Fig. 4.13.

4.5. Summary

For a closed chamber system, we not only align all the optical components of a PEM ellipsometry by a fixed incident angle [5]; we also introduce a standard real time calibration technique for the modulation amplitude of PEM in ellipsometry by a MHIR technique. However, in an etching/deposition process, a preliminary study is necessary under the chemistry of etching/deposition process, instead of using the MHIR, we introduce a correction factor to calibrate the modulation amplitude. This correction technique provides us a pair of dependable ellipsometric parameters for monitoring the etching process. After comparing the measured value of Ψ and Δ under etching, we are confident to propose that one should study the traces of Ψ and Δ verses the thickness for controlling instead of calculating the thickness in real time. In the appendix B, in addition to the thick SiO_2 , we also simulate a thin SiO_2 for gate oxide, which will not have a drastic change before the endpoint, but its periodic property can be used for monitoring. Since the Ψ and Δ distribution can be studied before the monitoring process, one can also monitor the patterned sample with enough database for reference.

A standard SiO_2/Si thin film is chosen to illustrate which harmonic ratio should be used to investigate frequency response in this calibration technique. As the signal

to noise ratio can be influenced by a weak signal, two experimental setups (a reflection style and a transmission style) are utilized to confirm that there is no frequency response problem by using the DAQ system. Since the harmonic intensities are measured at the same time, the error caused by the intensity fluctuation can be avoided by the simultaneous intensity ratio technique. Consequently, using the multiple harmonic intensity ratios can not only achieve the real time measurement, but also compensate the intensity fluctuation to monitor the system variation. Fig. 4.14 shows us the real time calibration of smooth varied modulation amplitude can be compensated from fluctuated intensities. The thickness of the SiO₂ layer was measured to be 364 Å by a commercial ellipsometer (J. A. Woollam M44), at an incident angle of 75°, which corresponds to the ellipsometric parameters of $\Psi = 18.36^\circ$ and $\Delta = 75.50^\circ$, measured at $\lambda = 6328 \text{ \AA}$. The consistency of measurement is clearly improved after calibration; however, there is a 3.28° difference in Δ , which is attributed to the static phase retardation of PEM itself [12]. Beside the reflection style, the digitized oscilloscope waveform measured in the transmission style also confirms our measurements. Any other system errors are still under study.

4.6 References

- [1] S. N. Japerson and S. E. Schnatterly, Rev. Sci. Instrum. **40**, 761 (1969).
- [2] H. L. Maynard and N. Layadi, Thin Solid Films **313-314**, 398 (1998).
- [3] O. Acher, E. Bigan and B. Drevillion, Rev. Sci. Instrum. **60**, 65 (1989).
- [4] Y. F. Chao, C. K. Wang, and S. Liu, Jpn. J. Appl. Phys. **38**, 6919 (1999).
- [5] M. W. Wang and Y. F. Chao, Jpn. J. Appl. Phys. **41**, 3981 (2002).
- [6] T. Oakberg, PEM-90 Application Note, HINDS Instruments, Inc., Hillsboro, U. S. A., (1991).
- [7] T. C. Oakberg, J. Trunk, and J. C. Sutherland, SPIE Proceedings **4133**, 101, August (2000).

- [8] Y. F. Chao, SPIE Proceedings, **4833**, 317 (2002).
- [9] S. A. Henck, J. Vac. Sci. Technol. A **10**, 934 (1992).
- [10] H. L. Maynard, N. Layadi, and J. T. C. Lee, J. Vac. Sci. Technol. B. **15**, 109 (1997).
- [11] Y. F. Chao and C. K. Wang, Jpn. J. Appl. Phys. **37**, 3558 (1998).
- [12] Y. F. Chao, A. Lin, and M. W. Wang, SPIE Proceedings **4595**, 43 (2001).



Table 4.1 The measured modulation amplitudes almost shifted from the displayed value by 0.02λ in reflection setup.

Displayed $\Delta_o(\lambda)$	0.368	0.373	0.378	0.383	0.388	0.393	0.398
Odd-ratio $\Delta_o(\lambda)$	0.3875	0.3918	0.3972	0.4019	0.4075	0.4125	0.4177
Standard deviation	0.0002	0.0004	0.0006	0.0009	0.0003	0.0010	0.0011
Even-ratio $\Delta_o(\lambda)$	0.3901	0.3940	0.3990	0.4032	0.4087	0.4131	0.4182
Standard deviation	0.0004	0.0005	0.0005	0.0015	0.0006	0.0014	0.0015
Displayed $\Delta_o(\lambda)$	0.450	0.500	0.550				
Odd-ratio $\Delta_o(\lambda)$	0.4689	0.5172	0.5692				
Standard deviation	0.0010	0.0002	0.0003				
Even-ratio $\Delta_o(\lambda)$	0.4619	0.5151	0.5679				
Standard deviation	0.0018	0.0003	0.0005				

Table 4.2 The measured modulation amplitudes almost shifted from the displayed value by 0.02λ in transmission setup.

Displayed $\Delta_o(\lambda)$	0.368	0.373	0.378	0.383	0.388	0.393	0.398
Odd-ratio $\Delta_o(\lambda)$	0.3890	0.3956	0.4010	0.4080	0.4118	0.4156	0.4226
Standard deviation	0.0125	0.0158	0.0178	0.0149	0.0170	0.0188	0.0170
Even-ratio $\Delta_o(\lambda)$	0.3880	0.3930	0.3978	0.4025	0.4076	0.4121	0.4174
Standard deviation	0.0003	0.0004	0.0005	0.0007	0.0005	0.0019	0.0017
Displayed $\Delta_o(\lambda)$	0.450	0.500	0.550				
Odd-ratio $\Delta_o(\lambda)$	0.4799	0.5182	0.5553				
Standard deviation	0.0196	0.0251	0.0153				
Even-ratio $\Delta_o(\lambda)$	0.4703	0.5192	0.5695				
Standard deviation	0.0009	0.0004	0.0007				

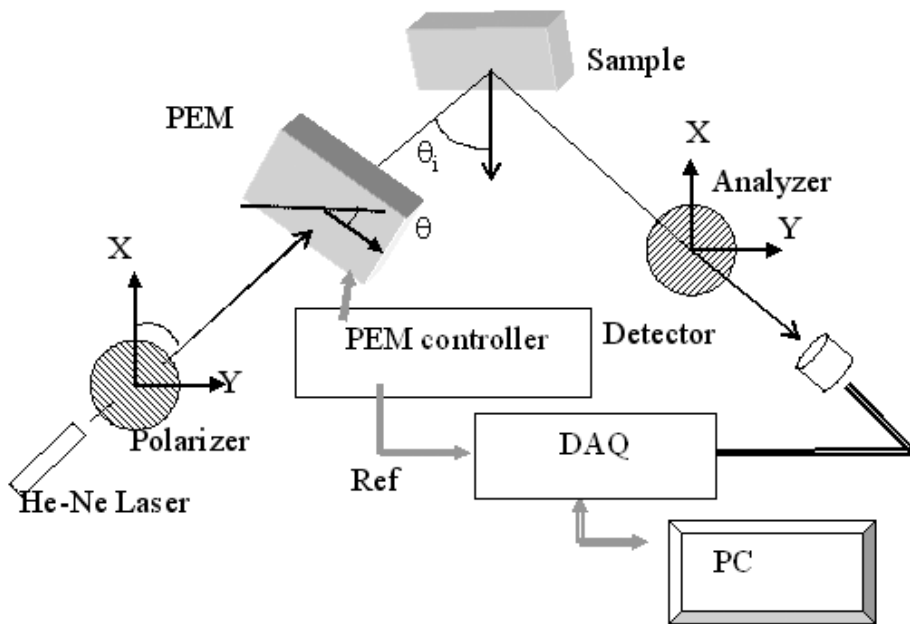


Fig. 4.1 Schematic setup of photoelastic modulation ellipsometer.

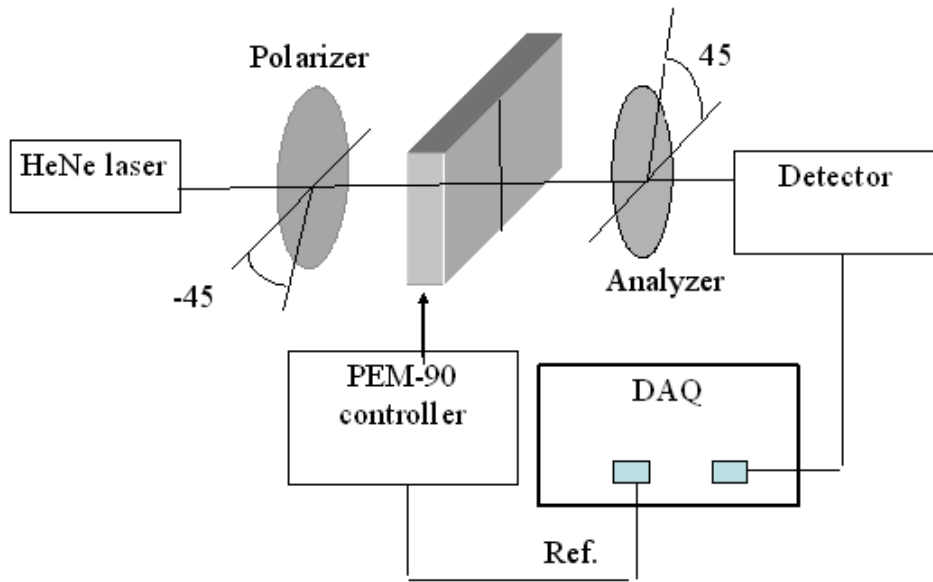


Fig. 4.2 Schematic setup of photoelastic modulation polarimeter.

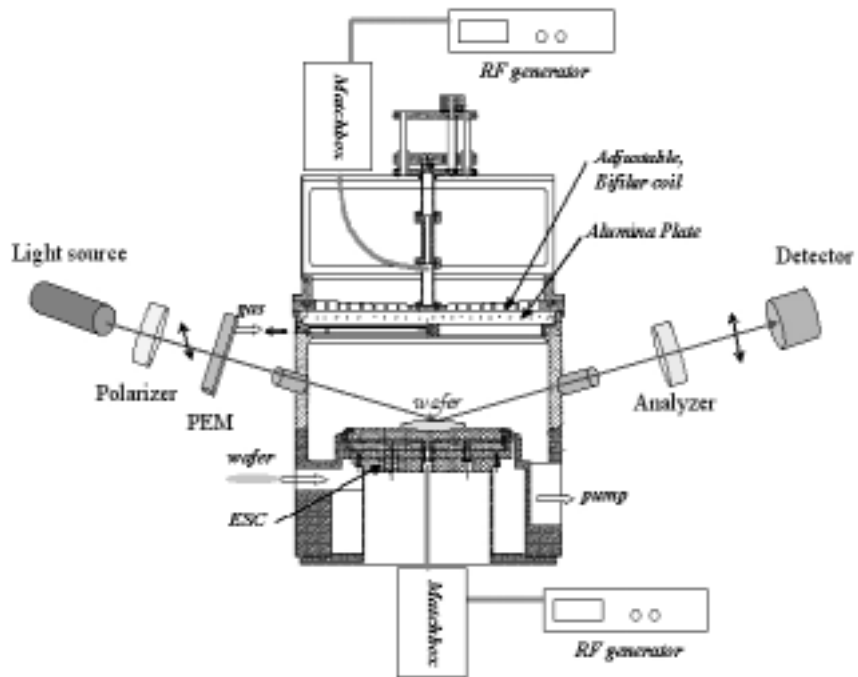


Fig. 4.3 Schematic setup of the IPC etcher with PEM ellipsometer

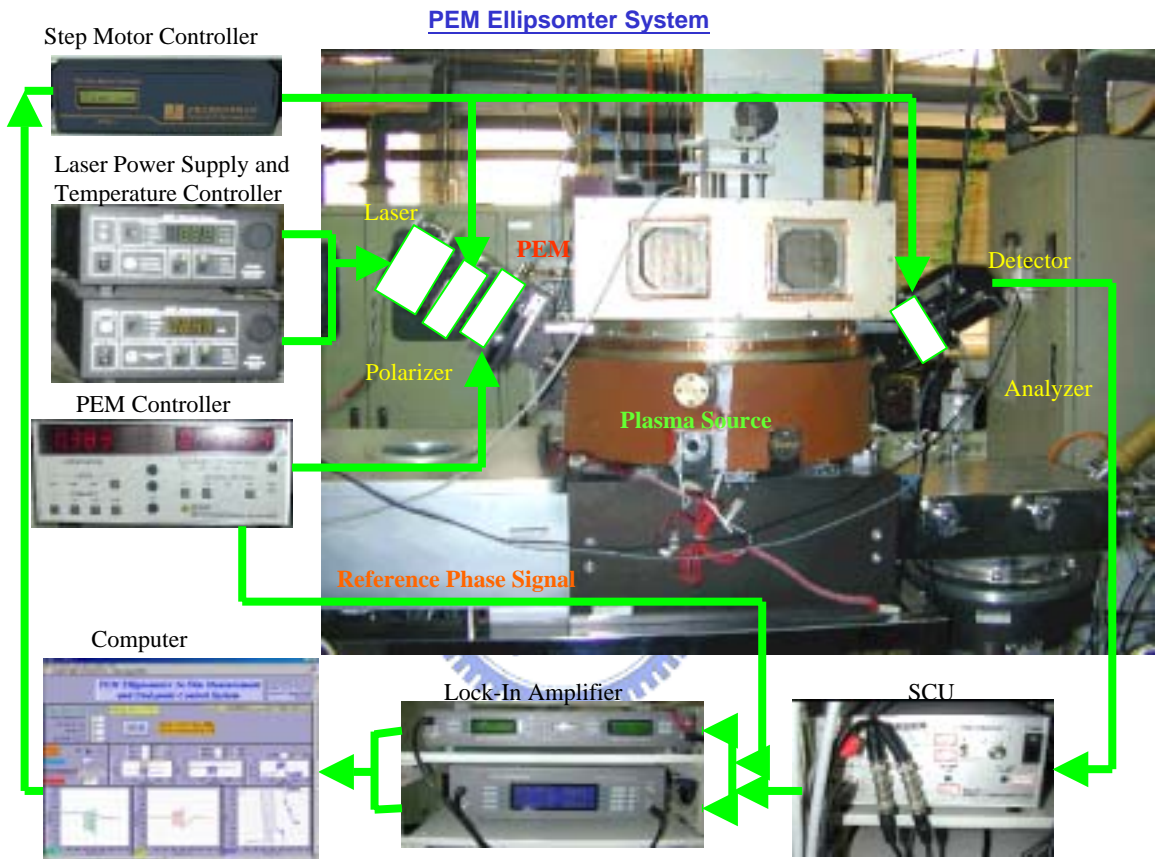


Fig. 4.4 The configuration of the PEM ellipsometer for IPC etcher.

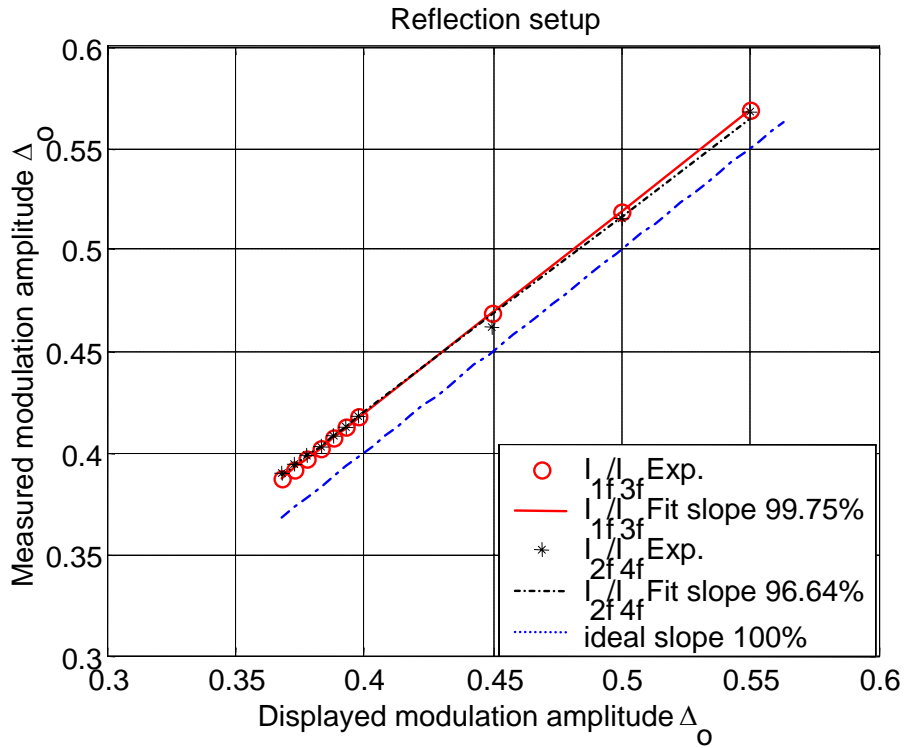


Fig. 4.5 The modulation amplitude are determined by the harmonic intensities ratios under varies displayed Δ_0 in a reflection setup. Circles and asterisks are the measured data for (I_{1f}/I_{3f}) and (I_{2f}/I_{4f}), respectively. The lines are their polynomial fit: the slope of I_{1f}/I_{3f} is 99.75%, and I_{2f}/I_{4f} is 96.64%. An ideal line is plotted, i.e. the measured data equals to the displayed value.

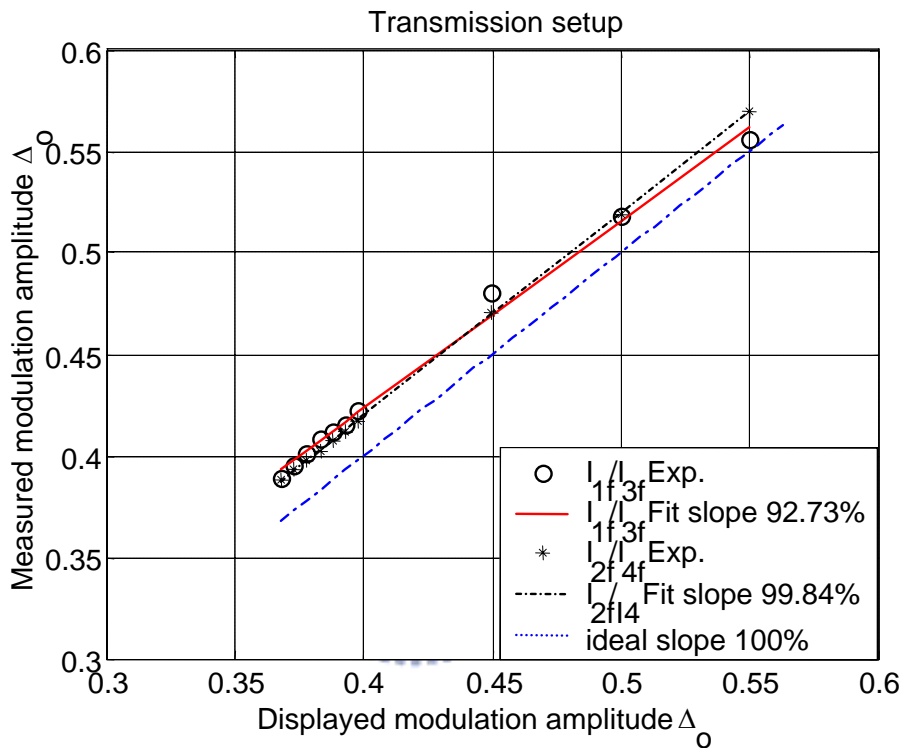


Fig. 4.6 The modulation amplitude are determined by the harmonic intensities ratios under varies displayed Δ_0 in a transmission setup. Circles and asterisks are the measured data for (I_{1f}/I_{3f}) and (I_{2f}/I_{4f}) , respectively. The lines are their polynomial fit: the slope of I_{1f}/I_{3f} is 92.73% and I_{2f}/I_{4f} is 99.84%. An ideal line is plotted, i.e. the measured data equals to the displayed value.

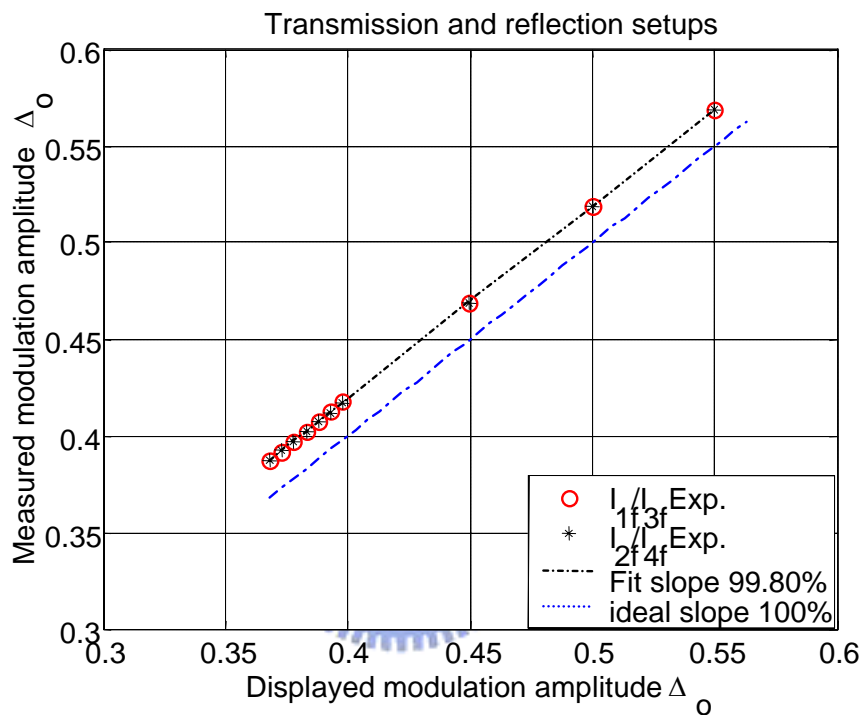


Fig. 4.7 The modulation amplitude are determined by the harmonic intensities ratios under varies displayed Δ_o : reflection (circles, I_{1f}/I_{3f}) and transmission (asterisks, I_{2f}/I_{4f}). Line is the polynomial fit, whose slope is 99.80%. An ideal line is plotted, i.e. the measured data equals to the displayed value.

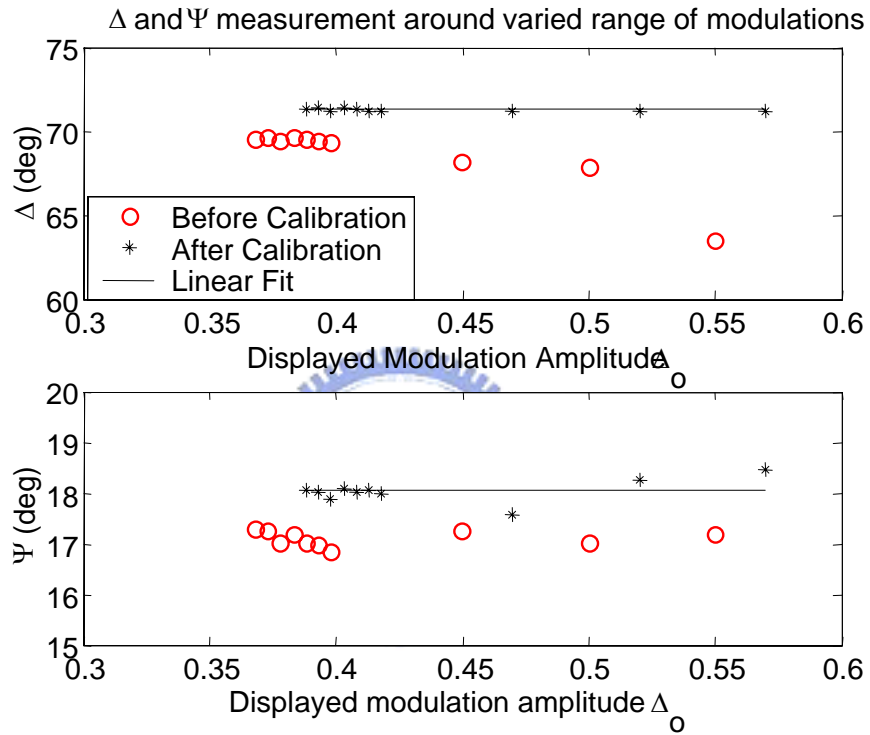


Fig. 4.8 The measured ellipsometric parameters Ψ and Δ of SiO_2/Si : before (circles) and after (asterisks) calibration under varies modulation amplitude. The line is the polynomial fit of the measured data after calibration.

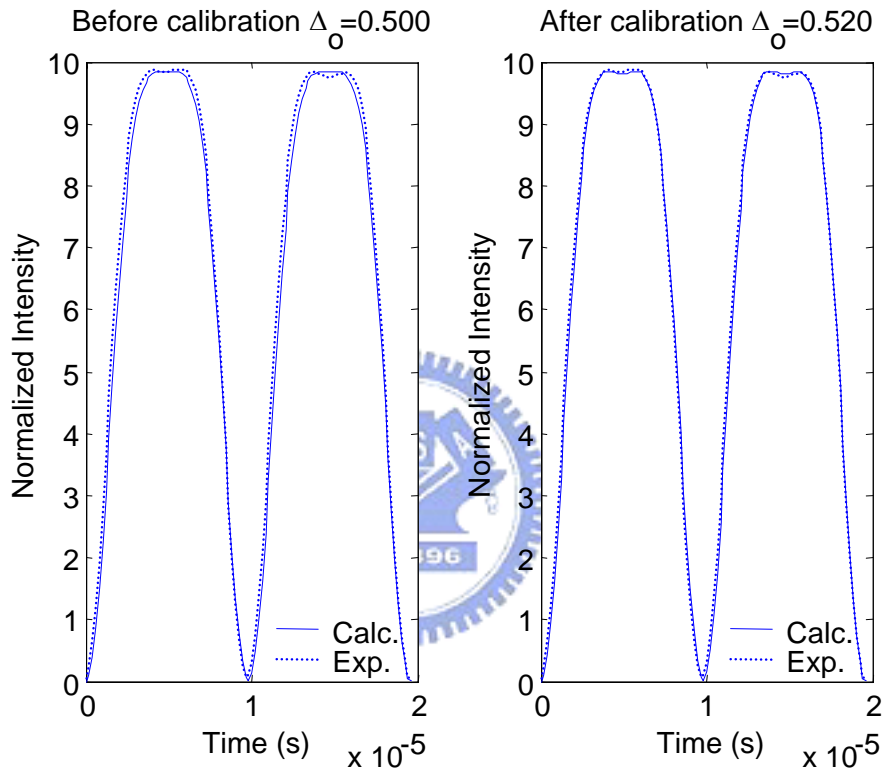


Fig. 4.9 The digitized oscilloscope waveform of a half-wave retardation.

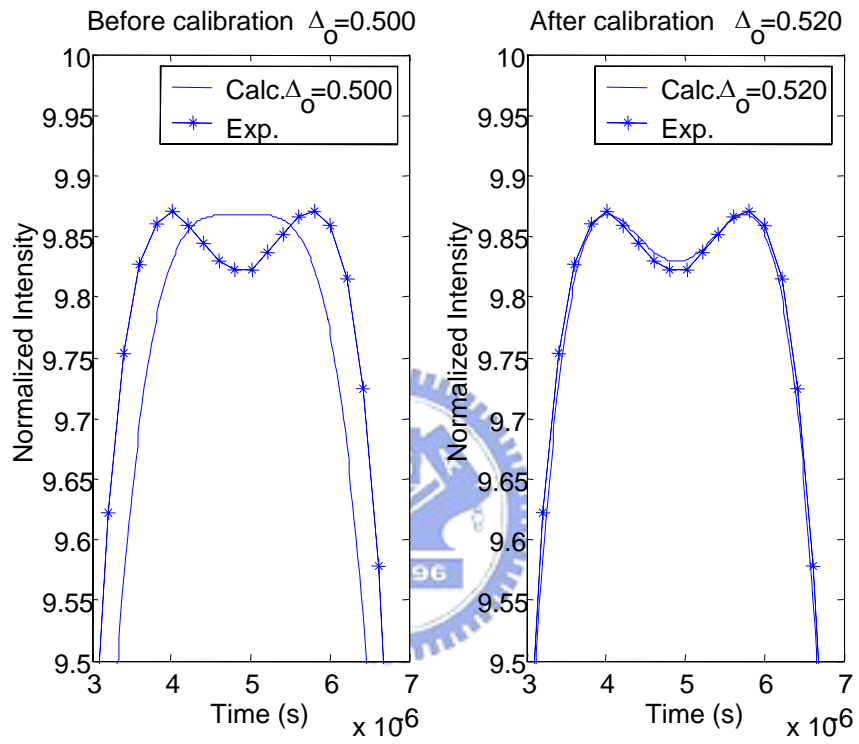


Fig. 4.10 The zooming in of Fig. 4.9.

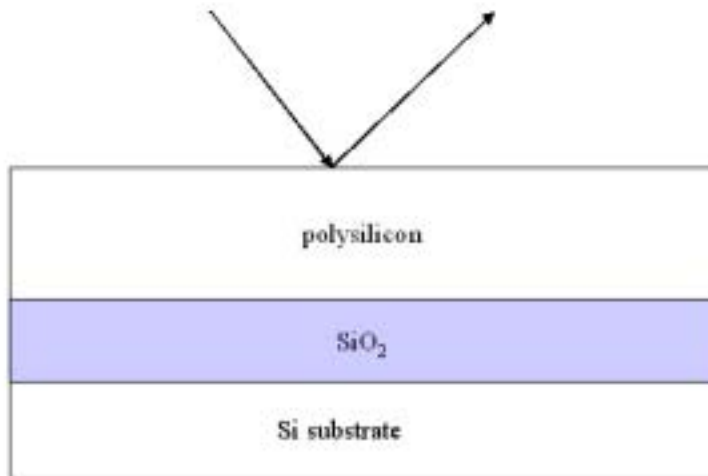


Fig. 4.11 Model of a double-layer wafer for etching.

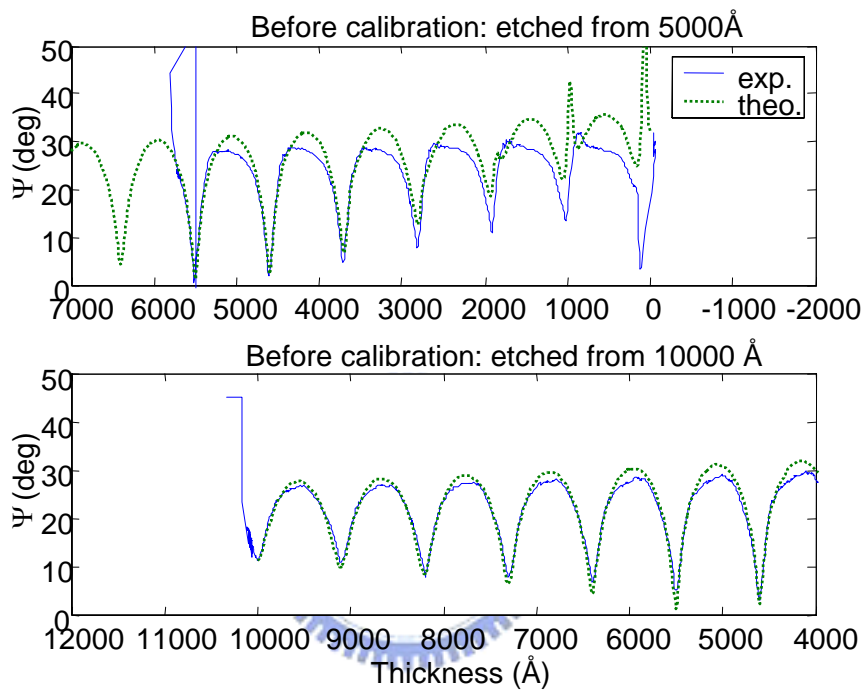


Fig. 4.12 The distribution Ψ under etching: Upper one is the film etched from around 5000 Å of poly-silicon and lower one is the one etched with 10000 Å. (dotted line) is the theoretical calculated value; (solid line) measured value.

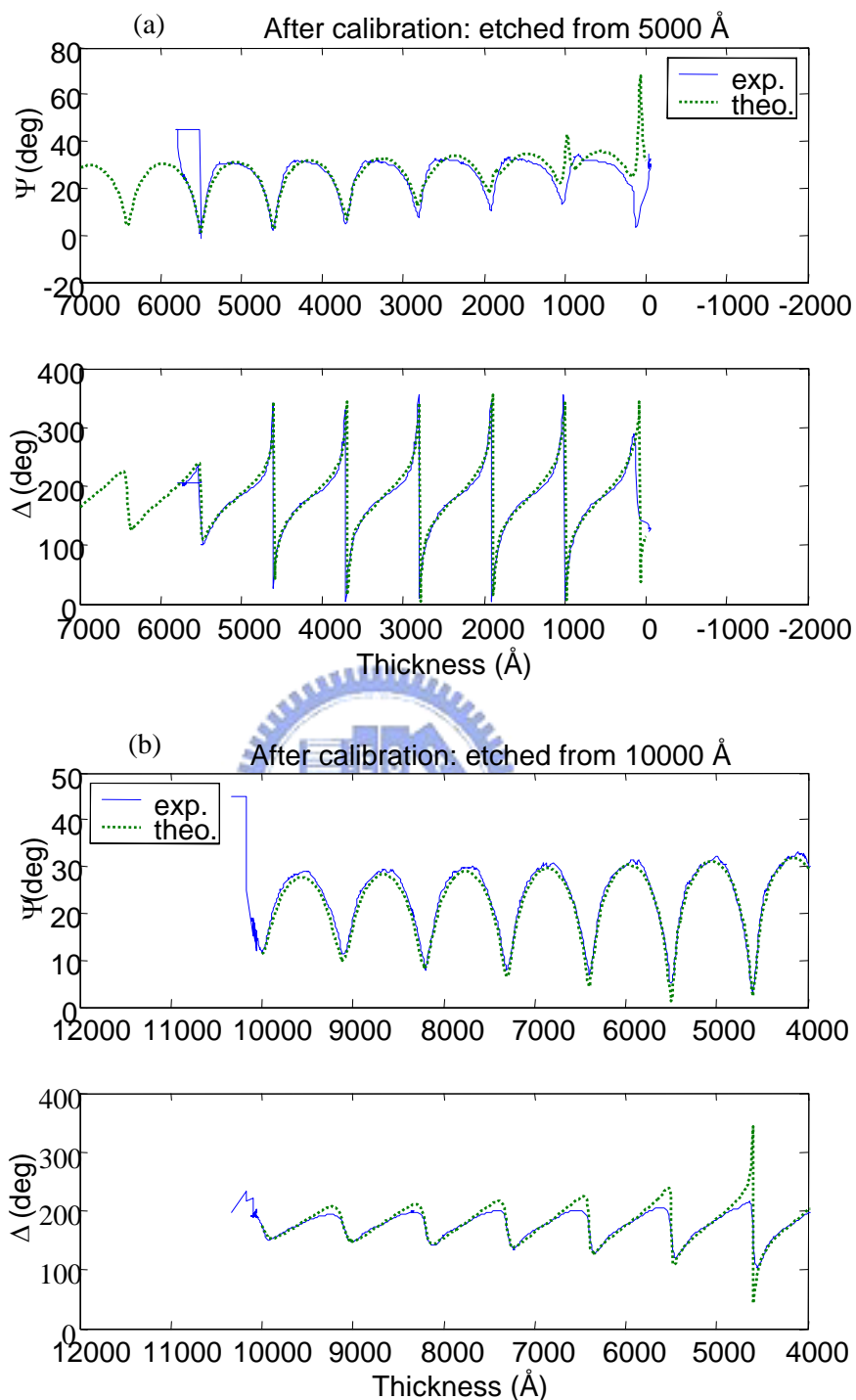


Fig. 4.13 The distribution of Ψ and Δ for film (a) etched from 5000 Å; (b) etched from 10000 Å. (dotted line) measured value x correction factor; (solid line) theoretical value.

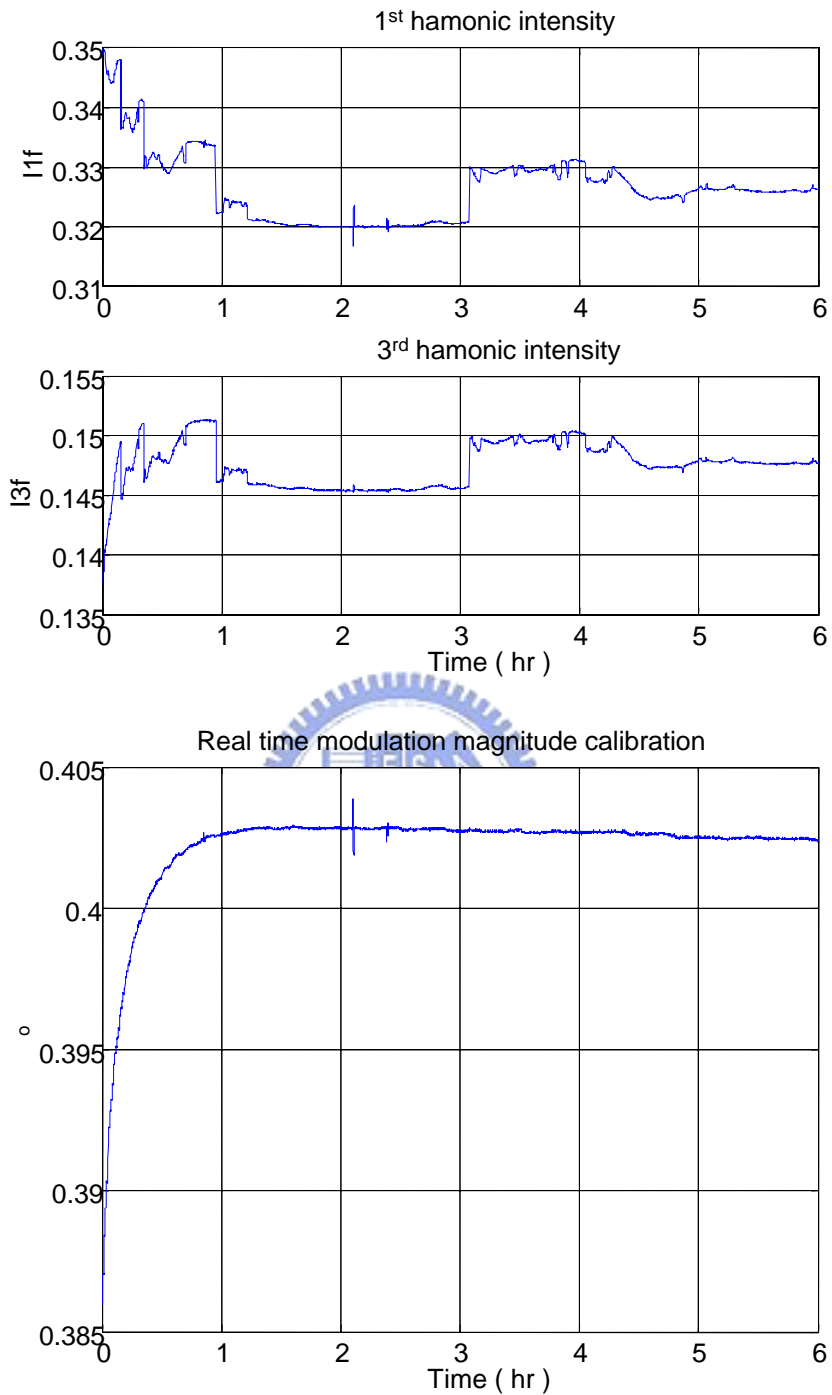


Fig. 4.14 The real time calibration of modulation magnitude of PEM: fluctuated intensities of 1st and 3rd harmonics (upper), the monitoring of smooth varied modulation magnitude (lower).

Chapter 5

***In situ* / real time multi-wavelength photoelastic modulation ellipsometry**

The modulation amplitude of a phase modulator is calibrated under a fixed incident angle in multi-wavelength photoelastic modulation (PEM) ellipsometry. In addition to its modulation amplitude, we also calibrated its static phase retardation at 632.8 nm. The ellipsometric parameters of a sample were measured by a multiple harmonic intensity ratio technique and proved that ellipsometric parameters can be obtained under various modulation amplitudes. Since the physical size of PEM is constant, we calibrated the modulation amplitude at multiple wavelengths by setting the Δ_0 value at 0.383 for 568.2 nm.

5.1 Introduction

Following the study of the alignment technique for PEM ellipsometry at a fixed incident angle [1], we calibrate, in this work, the phase modulation amplitude of PEM with the static phase retardation for *in situ* / real time multi-wavelength ellipsometry. This calibration technique is achieved by using the multiple harmonic intensity ratios (MHIR), which are obtained from the Fourier analysis of a data acquisition system (DAQ) [2]. In this technique, four harmonics are used, which are not available in the conventional lock-in amplifier; the advantage of using the DAQ is clearly demonstrated. In the theoretical analysis, the MHIR (1f/3f and 2f/4f) proved to be independent of the sample's characteristics and the azimuth positions of the optical components. Furthermore, one can identify which intensity ratio (1f/3f or 2f/4f) should be used for higher signal to noise ratio S/N by avoiding the weak signals. By comparing the digitized oscilloscope waveform of half-wave retardation, we found a 4 % offset in the display.

Other than using the modulation amplitude at $J_0(\delta_0) = 0$ for various wavelengths [3], we proved that the ellipsometric parameters can be measured under any phase modulation

amplitude. By setting the phase modulation amplitude at 0.383 for 568.2 nm, we determined the modulation amplitude at other wavelengths by the multiple harmonic intensity ratio technique; the results are well fitted to the invariant relation of the product of modulation amplitude and the wavelength, i.e. the physical thickness of the PEM cell. These calibrations provide enough information for constructing an *in situ* / real time spectroscopic ellipsometry.

5.2. Theoretical background

The basic setup of the PEM ellipsometry is shown in Fig. 5.1. If the azimuth angle of the initial linear polarized light is set at -45° , the measured intensity can be simplified as

$$I(A) = 0.5I_0[\sin^2 A + \tan^2 \Psi \cos^2 A - \tan \Psi \sin 2A (\cos \Delta \cos \Delta_p + \sin \Delta \sin \Delta_p)]. \quad (5.1)$$

Since the phase retardation of PEM is modulated with the static phase retardation (Δ_i) as $\Delta_p = \Delta_i + \delta_o \sin \omega t$, one can substitute the Fourier expansions of the harmonic functions into equation (5.1), and obtain the following relations between the measured intensity and its corresponding harmonic component:

$$\begin{aligned} I_{dc}(A) &= 0.5I_0[\sin^2 A + \tan^2 \Psi \cos^2 A - \tan \Psi \cos(\Delta - \Delta_i)J_0(\delta_o) \sin 2A], \\ I_{(2m-1)f}(A) &= -I_0[\tan \Psi \sin(\Delta - \Delta_i)J_{(2m-1)}(\delta_o) \sin 2A] \sin(2m-1)\omega t; \quad m = 1, 2, \dots \\ I_{2nf}(A) &= -I_0[\tan \Psi \cos(\Delta - \Delta_i)J_{2n}(\delta_o) \sin 2A] \cos 2n\omega t; \quad n = 1, 2, \dots \end{aligned} \quad (5.2)$$

It is very interesting to notice that the even/odd harmonics are related by the similar physical parameters except for the orders of its Bessel function. By using the intensity ratio technique, we can determine the modulated amplitude of PEM but avoid the effect of its physical setup, i.e.

$$\frac{I_{1f}}{I_{3f}} = \frac{J_1(\delta_o)}{J_3(\delta_o)}, \quad \frac{I_{2f}}{I_{4f}} = \frac{J_2(\delta_o)}{J_4(\delta_o)}. \quad (5.3)$$

It is obvious that these ratios are independent of the azimuth position of the analyzer and the physical parameters of the examined sample. Furthermore, this multiple harmonic intensity ratio technique can also be used to determine the ellipsometric parameters Ψ and Δ . That is by setting $A = \pm 45^\circ$, in the following expressions

$$\sin 2\Psi = \frac{\sqrt{\left(\frac{I_{1f}(45^\circ)}{J_1(\delta_o)}\right)^2 + \left(\frac{I_{2f}(45^\circ)}{J_2(\delta_o)}\right)^2}}{I_{dc}(45^\circ) + I_{dc}(-45^\circ)},$$

$$\tan(\Delta - \Delta_i) = \frac{I_{1f}(45^\circ)J_2(\delta_o)}{I_{2f}(45^\circ)J_1(\delta_o)}, \quad (5.4)$$

one can obtain Ψ and Δ independently. The static phase retardation (Δ_i) of PEM is embedded with the ellipsometric parameter of Δ , which can be confirmed by transmission ellipsometry.

The temporal intensity distribution of the P-PEM-A setup can be written as

$$I(t) = I_o[1 - \cos(\Delta_i + \delta_o \sin \omega t)], \quad (5.5)$$

if $P = 45^\circ$ and $A = -45^\circ$. This waveform can be compared with the digitized oscilloscope waveform obtained by the DAQ system. The Fourier expansion of the intensity at $P = 45^\circ$, namely the multiple harmonics, can be expressed as

$$I_{mf}(A) = -I_o[\sin \Delta_i J_m(\delta_o) \sin 2A] \sin m\omega t \quad m = 1, 3$$

$$I_{nf}(A) = I_o[\cos \Delta_i J_n(\delta_o) \sin 2A] \cos n\omega t; \quad n = 2, 4. \quad (5.6)$$

The static phase retardation can be obtained by taking multiple harmonic ratios. According to eq. (5.4), one can measure the ellipsometric parameters at any modulation amplitude. Since in an *in situ*/real time ellipsometric system, all the physical settings, such as azimuth of polarizer, optic axis of PEM, incident angle and the modulation amplitude of PEM should be fixed. Since the physical path of PEM is invariant, the modulation amplitude should be inversely proportion to the wavelength; i.e. $\Delta_o \lambda_o = \text{constant}$. For spectroscopic measurement, the modulation amplitude should be set at a particular wavelength, the corresponding modulation of different wavelengths should be calculated instead of resetting the system.

5.3. Experimental details

A data acquisition system (NI PCI-6111) was used in the PEM (Hinds PEM90/ CF50) ellipsometry; for comparison, we chose a SiO₂/Si thin film of 364 Å thickness at the incident angle of 70°, whose Δ was closer to 90° as with the testing sample. We systematically aligned

all the azimuth positions by a fixed incident angle alignment technique; then set the strain axis of PEM at 0° , with P and A at -45° and 45° , respectively. The amplitude of modulation was varied from 0.368λ to 0.550λ with closer steps around 0.383λ , under the following wavelengths of a KrAr tunable laser: 647.1 nm, 568.2 nm, 520.8 nm, 514.5 and 488.0 nm. In addition to the DC component, four more harmonic intensities were obtained. After deducing the modulation amplitudes by using the intensity ratios of I_{1f}/I_{3f} (odd-ratio) and I_{2f}/I_{4f} (even-ratio), we then compared it with the display provided by the vendor. This intensity ratio technique was also employed to measure the modulation amplitude at various wavelengths by setting the modulation amplitude at 0.383λ for 568.2 nm. By studying the static retardation, a transmission setup was measured with a HeNe laser wavelength of 632.8 nm; the digitized oscilloscope waveforms of half-wave retardation were recorded and analyzed.

In real time measurement, the Fourier analysis of the signal is then carried out by 100 ms in LabVIEW instrumentation program to monitor system condition. On the other hand, post-waveform analysis can be utilized to acquire signal waveform in the beginning; after acquiring signal waveform by data acquisition card (DAQ), computer program (MatLab) was engaged by Fast Fourier Transform (FFT) to analyze spectrums. By taking only two periods of signal waveform to compute the DC component and four more harmonic intensities, we could reduce our measurement time resolution to $40 \mu\text{s}$. The intensity ratios of I_{1f}/I_{3f} (odd-ratio) and I_{2f}/I_{4f} (even-ratio) could be used to simultaneously calibrate the modulation amplitudes at two wavelengths, 632.8 nm and 488.0 nm, by setting the modulation amplitude at 0.383λ for 568.2 nm. Consequently, two wavelength real time PEM ellipsometry was employed to measure ellipsometric parameters Ψ and Δ with a rapid rotating chopper to switch two laser light sources, as shown in Fig. 5.10.

5.4. Results and discussion

The modulation amplitudes of PEM were obtained from the multiple harmonic intensity ratios, as shown in Fig. 5.2; the modulation amplitudes are parallel shifted from the displayed value

by 0.02λ and the slope of I_{1f}/I_{3f} is almost equal to 1, since $\cos\Delta < \sin\Delta$ of a SiO₂ thin film at the incident angle of 70° . To avoid the effect of weak signal, we used the odd intensity ratio to measure the sample under reflection. By comparing the modulation amplitudes at different wavelengths, we found that the shifted values are the same, such as shown in Fig. 5.3. The modulation amplitudes were also measured under various azimuth positions of the analyzer, and just as expected from equation (5.3), the modulation amplitude determined by this intensity ratio technique was independent of the analyzer's azimuth position, as shown in Fig. 5.4. In the transmission setup, with $P = -45^\circ$ and $A = 45^\circ$, the digitized oscilloscope waveform of half-wave retardation were compared with the theoretical waveform of 0.50λ and 0.52λ retardation, respectively, such as shown in Fig. 5.5. However, a clear asymmetry occurred, as $P = 45^\circ$ and $A = -45^\circ$; this is shown in Fig. 5.6. This phenomenon can be explained by the existence of static retardation in PEM [4]. After considering the static retardation 4.22° at 632.8 nm, the ellipsometric parameters measured under various modulation amplitudes are shown in Fig. 5.7 and Table 5.1; we also find that the measured ellipsometric parameters at multiple wavelengths were well fitted to its calculated values, as shown in Figs. 5.8 and Table 5.2. Values of static retardations other than at 632.8 nm are calculated by neglecting its dispersion. The incident angle deduced from the measurement is $69.92 \pm 0.02^\circ$, which is also similar to what we measured in chapter 6. By taking the modulation amplitude at 0.383λ for 568.2 nm, we calculated the corresponding modulation amplitude Δ_0 (i.e. $\delta_0 / 2\pi$) for other wavelengths, and the measured values are well fitted to our expectation, as shown in Fig. 5.9 and Table 5.3.

For real time monitoring by single wavelength at 632.8 nm, the measured intensity was chopped in about 0.4 sec to demonstrate the 0.1 sec time consumption for computing ellipsometric parameters Ψ and Δ in Fig. 5.11. During the plasma etching process, Fig. 5.12 shows the monitoring of real time traces of Ψ and Δ and calculated thickness of polysilicon. After utilizing post-waveform analysis, the modulation amplitude Δ_0 alternated in 1 ms

between two wavelengths, 632.8 nm and 488.0 nm, can be calibrated simultaneously in 40 μ s in Fig. 5.13. Two real time ellipsometric parameters Ψ and Δ of a standard SiO₂ thin film of 364 Å thickness at the incident angle of 70° under two wavelengths are also closed to its multi-wavelength values, as shown in Fig. 5.14. However, the conflicting tips are caused at short intervals where two wavelengths are mixed or blocked in the acquired waveform, such as shown in Fig. 5.15. The inconsistency of the waveform can be reduced by well alignment among of laser beam beams and chopper fan.

5.5. Summary

. A standard calibration process is proposed to calibrate the modulation amplitude of PEM, which can be carried out without changing the operation setup. The main purpose of our research is trying to establish multiple wavelength ellipsometry for *in situ* / real time measurements; the modulation amplitude has to be set as a constant for a particular wavelength in the process of measurement. Since the physical path of PEM is invariant, the modulation amplitude should be inversely proportion to the wavelength. After considering the static retardation and taking the modulation amplitude at 0.383λ for 568.2 nm, we calculated the corresponding modulation amplitude for other wavelengths, and the measured values are well fitted to our expectation. To real time monitor etching processing for the end prediction, the instrumentation program dedicated to FFT computation can be employed for on line control system. Nevertheless, waveform measurement can be utilized to diagnose the sample dynamic behavior less than millisecond scale, for example, the dynamic response of etching system or the modulation of liquid crystal device. After this calibration, we believe there is enough information for the construction of an *in situ* / real time spectroscopic ellipsometry.

5.6 References

- [1] M. W. Wang and Y. F. Chao, Jpn. J. Appl. Phys. **41**, 3981 (2002).
- [2] M. W, Wang, Y. F. chao, K. C. Leou, F. H. Tsai, T. L. Lin, S. S. Chen, and Y. W. Liu, Jpn. J. Appl. Phys. **43**, 827 (2004).

[3] O. Acher, E. Bigan, and B. Drevillon, Rev. Sci. Instrum, **60**, 65 (1989).

[4] C.K. Wang and Y. F. Chao, Jpn. J. Appl. Phys. **38**, 941 (1999).



Table 5.1 The ellipsometric parameters versus the modulation amplitudes: A SiO₂ thin film is measured at the incident angle of 70° for 632.8 nm after considering the static retardation.

Displayed Δ_0 (λ)	0.368	0.373	0.378	0.383	0.388	0.393	0.398
Δ (deg)	75.51	75.56	75.39	75.60	75.54	75.48	75.43
Ψ (deg)	18.05	18.03	17.87	18.10	18.02	18.06	17.98
Thickness (Å°)	361.35	360.60	360.92	360.84	360.73	361.79	361.56
Displayed Δ_0 (λ)	0.450	0.500	0.550	Average	Woollam M44		
Δ (deg)	75.48	75.49	75.48	75.49±0.03	75.50		
Ψ (deg)	17.56	18.26	18.45	18.09±0.08	18.36		
Thickness (Å°)	356.89	363.63	365.60	361±1	364±2		

Table 5.2. The measured ellipsometric parameters of a standard SiO₂ thin film for various wavelengths after considering the static retardation.

Wavelengths (nm)	(deg)	(deg)	$\Gamma_1 (4.22*632.8/\text{wavelength})$ (deg)
488.0	24.28	101.39	5.47
514.5	22.30	102.85	5.19
520.8	21.95	103.28	5.13
568.2	20.30	104.81	4.70
647.1	18.06	108.01	4.13



Table 5.3 The modulation amplitude calculated for other wavelengths and the measured values by taking the modulation amplitude at 0.383λ for 568.2 nm

Wavelengths (nm)	Calculated $\Delta_o(\lambda)$	Measured $\Delta_o(\lambda)$
488.0	0.452	0.459
514.5	0.429	0.427
520.8	0.423	0.418
568.2	0.388	0.389
647.1	0.341	0.338

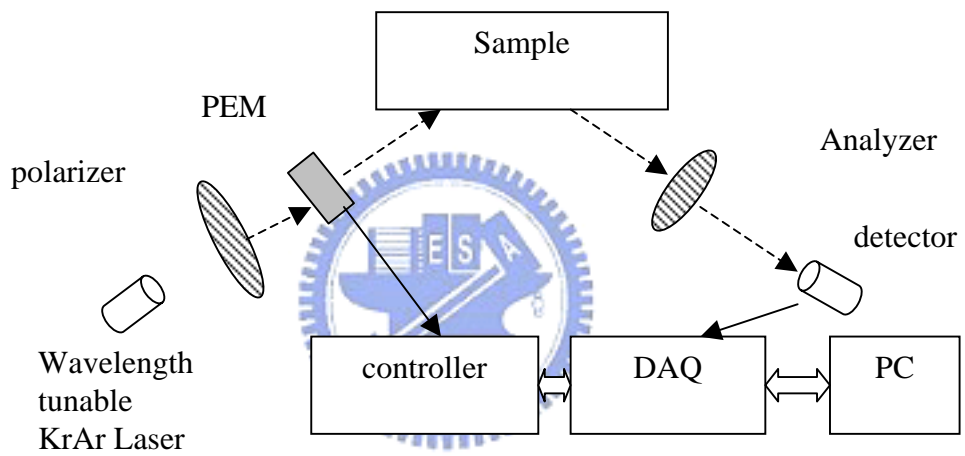


Fig. 5.1 The schematic setup of PEM ellipsometry.

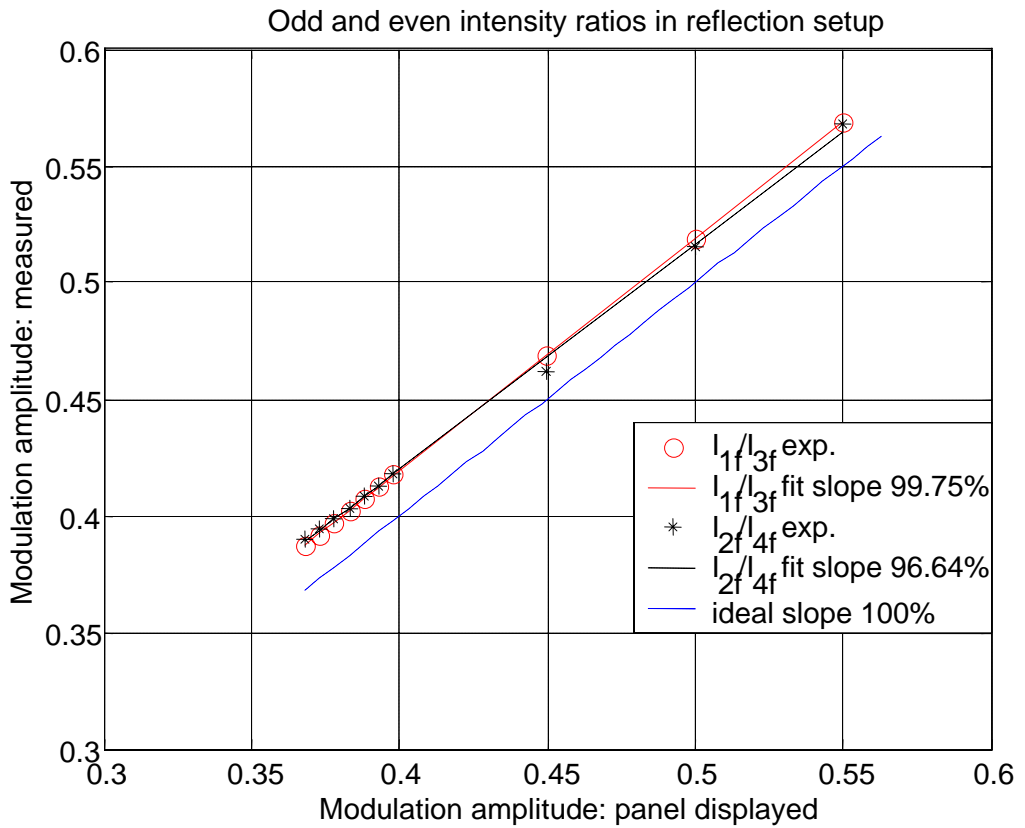


Fig. 5.2 The calibration of modulation amplitude in the reflection setup: both odd (o) and even (*) intensity ratios are measured, the ideal line is when measured values = displayed values.

The shifted modulation amplitudes under different wavelengths

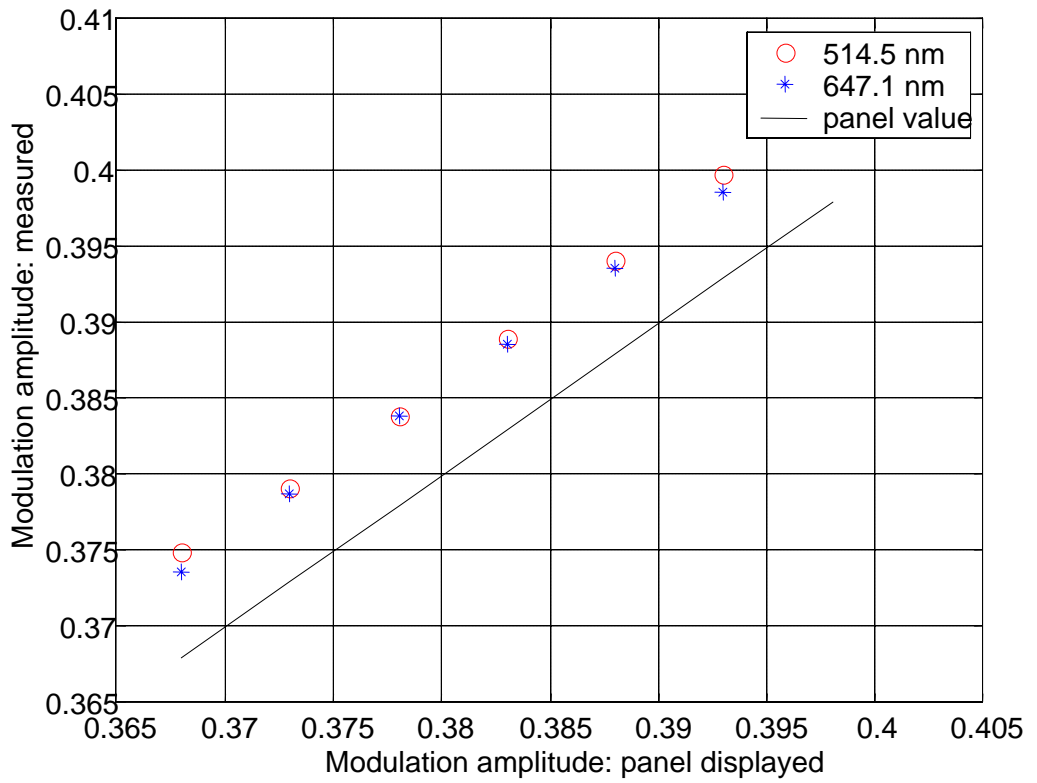


Fig. 5.3 The calibration of modulation amplitude under different wavelengths: 514.5 nm (o), 647.1 nm (*) and panel displayed values (line).

Measured modulation amplitude by 1f/13f reflected from SiO₂

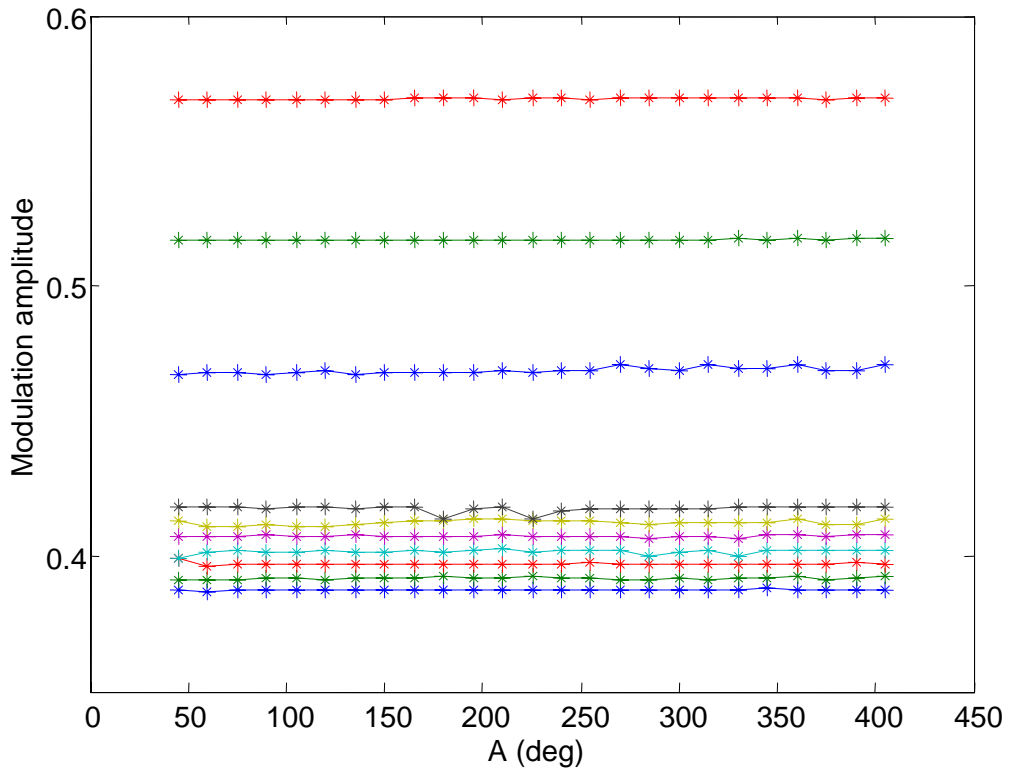


Fig. 5.4 The modulation amplitude distribution versus azimuth position of analyzer: The intensity ratios of 1f/3f are measured in the reflection setup. A SiO₂ thin film of 364 Å is measured at the incident angle of 70°.

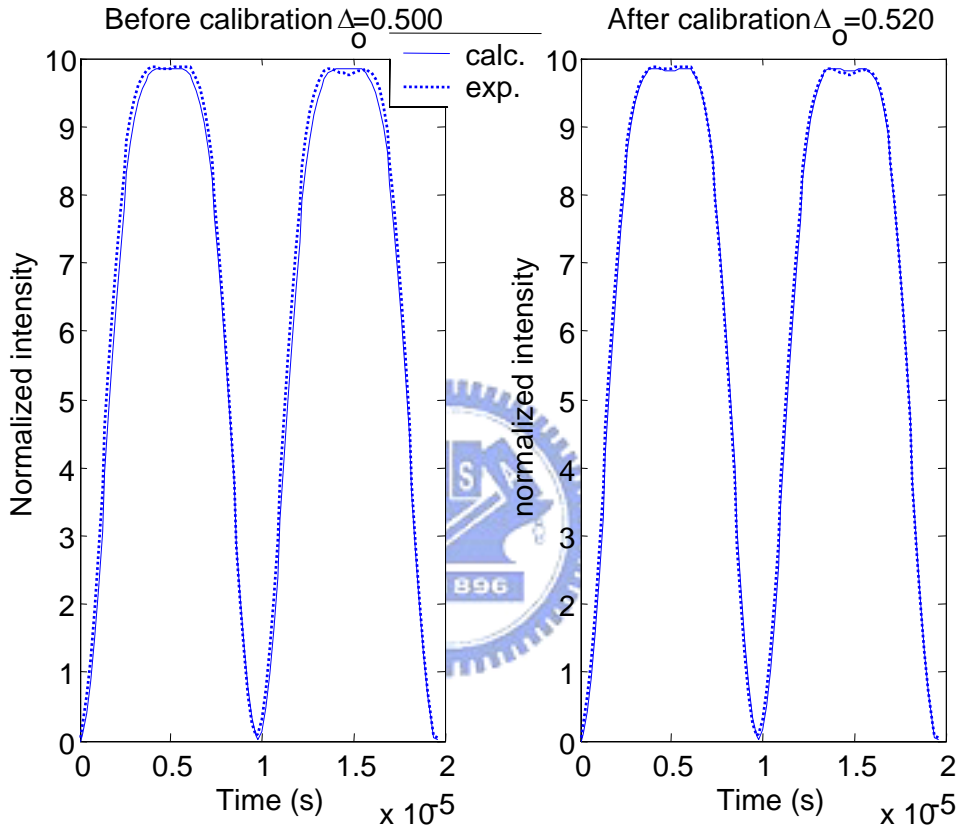


Fig. 5.5 The digitized oscilloscope waveform of half-wave retardation in the transmission setup: $P = -45^\circ$ and $A = 45^\circ$; the solid line are the calculated waveform of 0.50λ (right) and 0.52λ (left).

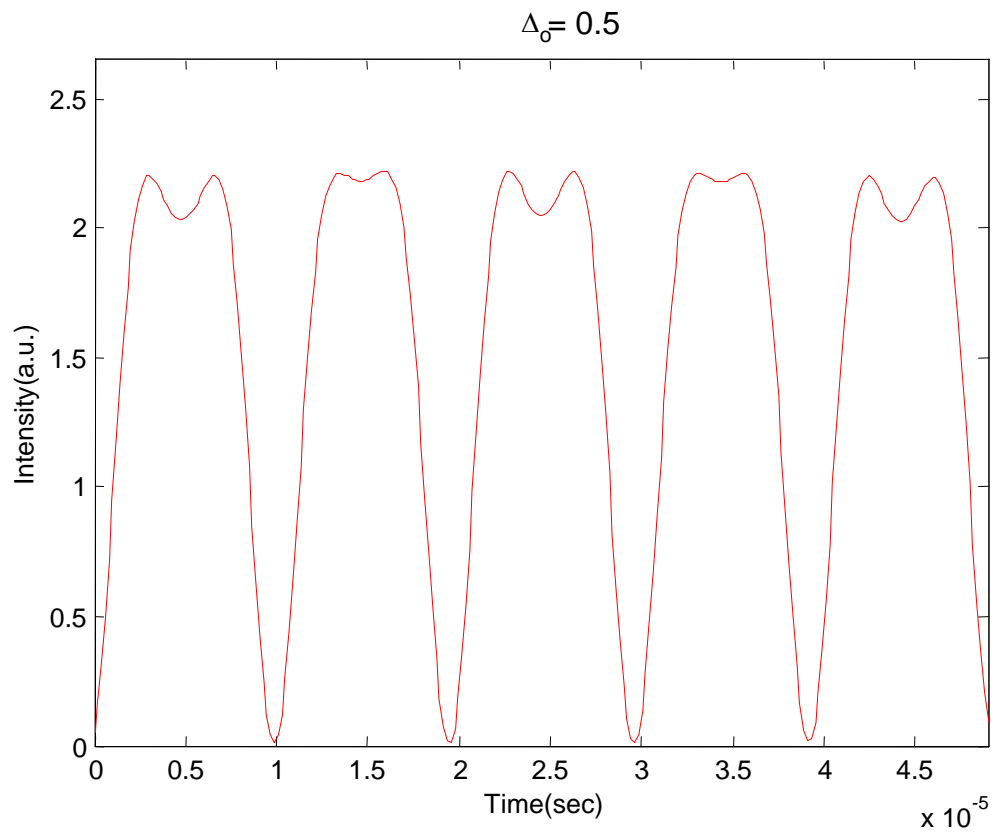


Fig. 5.6 The digitized oscilloscope retardation waveform of half-wave retardation at $P = 45^\circ$ and $A = -45^\circ$

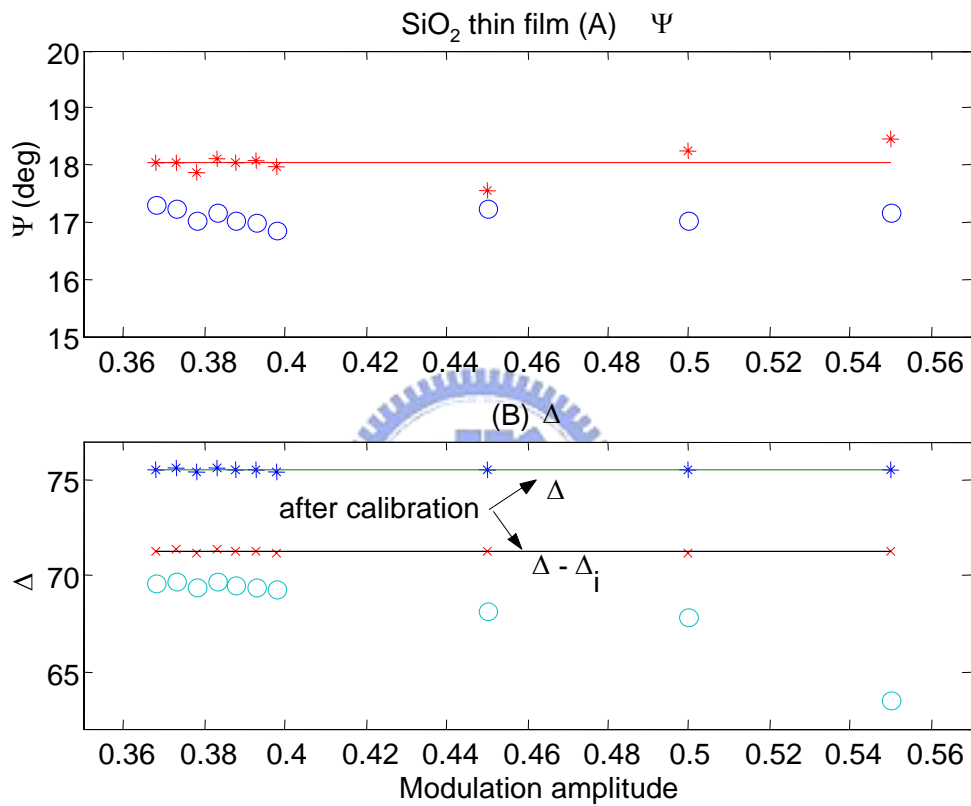


Fig. 5.7 The ellipsometric parameters versus the modulation amplitudes: A SiO₂ thin film of 364 Å is measured at the incident angle of 70° and $\lambda=632.8$ nm.

(A) Ψ : before calibration (o) ; after calibration (*)

(B) Δ : before calibration (o) ; after calibration (x) ; after introduce the static phase (*).

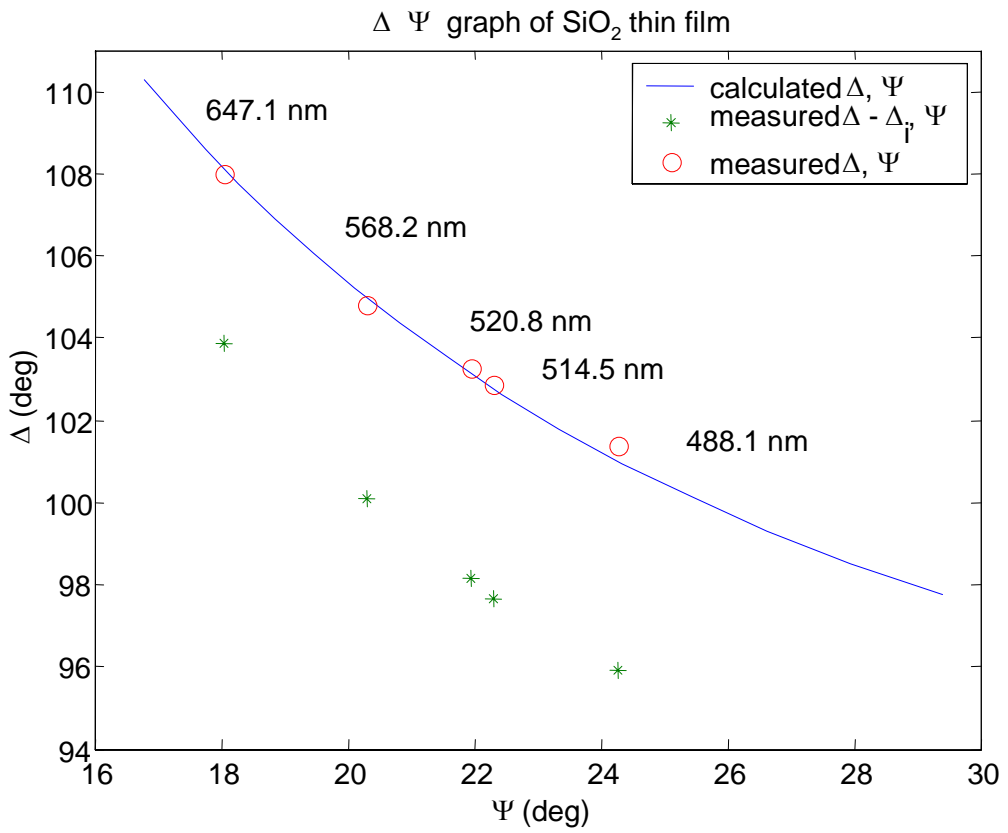


Fig. 5.8 Ψ and Δ graph of SiO₂ thin film at the incident angle of 70° with the discrete wavelengths of a KrAr tunable laser.

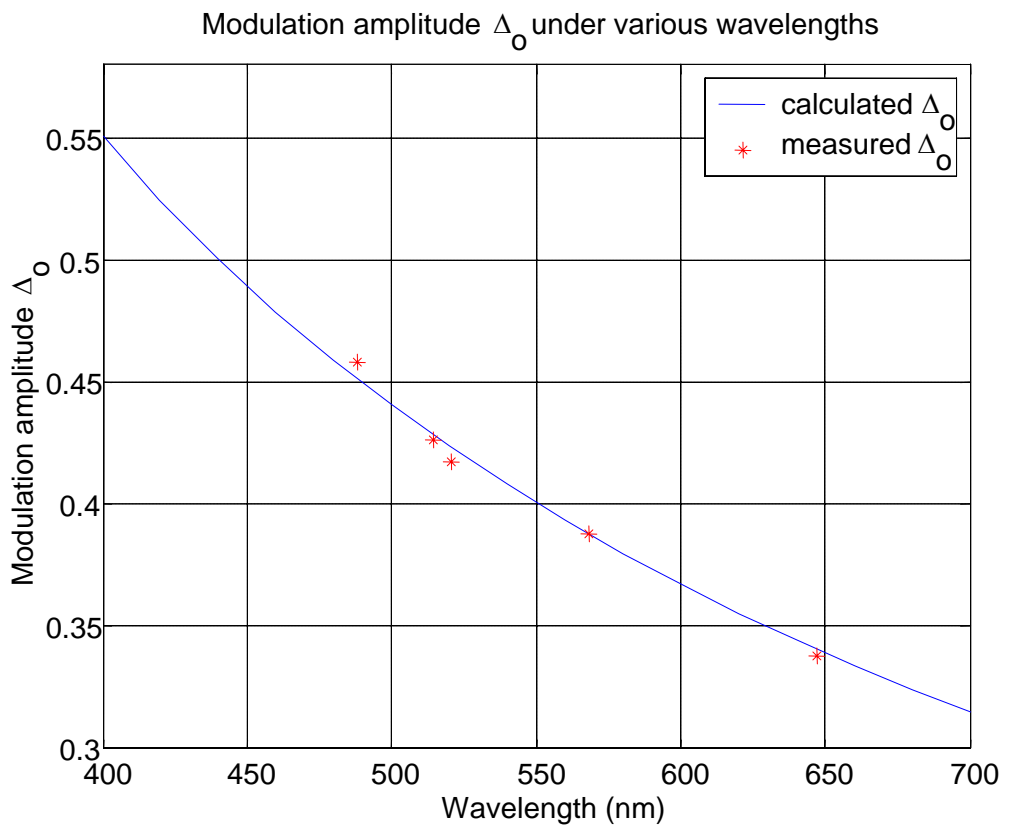


Fig. 5.9 The modulation amplitude of PEM versus wavelengths, by setting $\Delta_o = 0.383$ at $\lambda = 568.2$ nm.

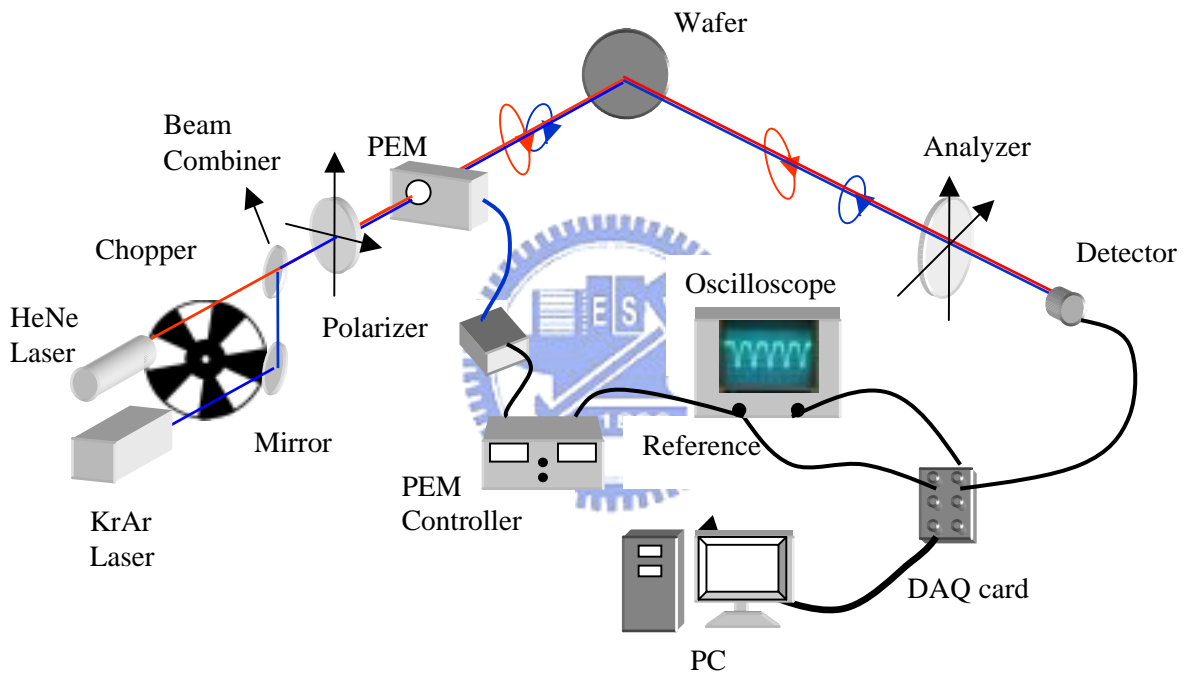


Fig. 5.10 Two wavelength real time PEM ellipsometry was employed with a rapid rotating chopper to switch two laser light sources.

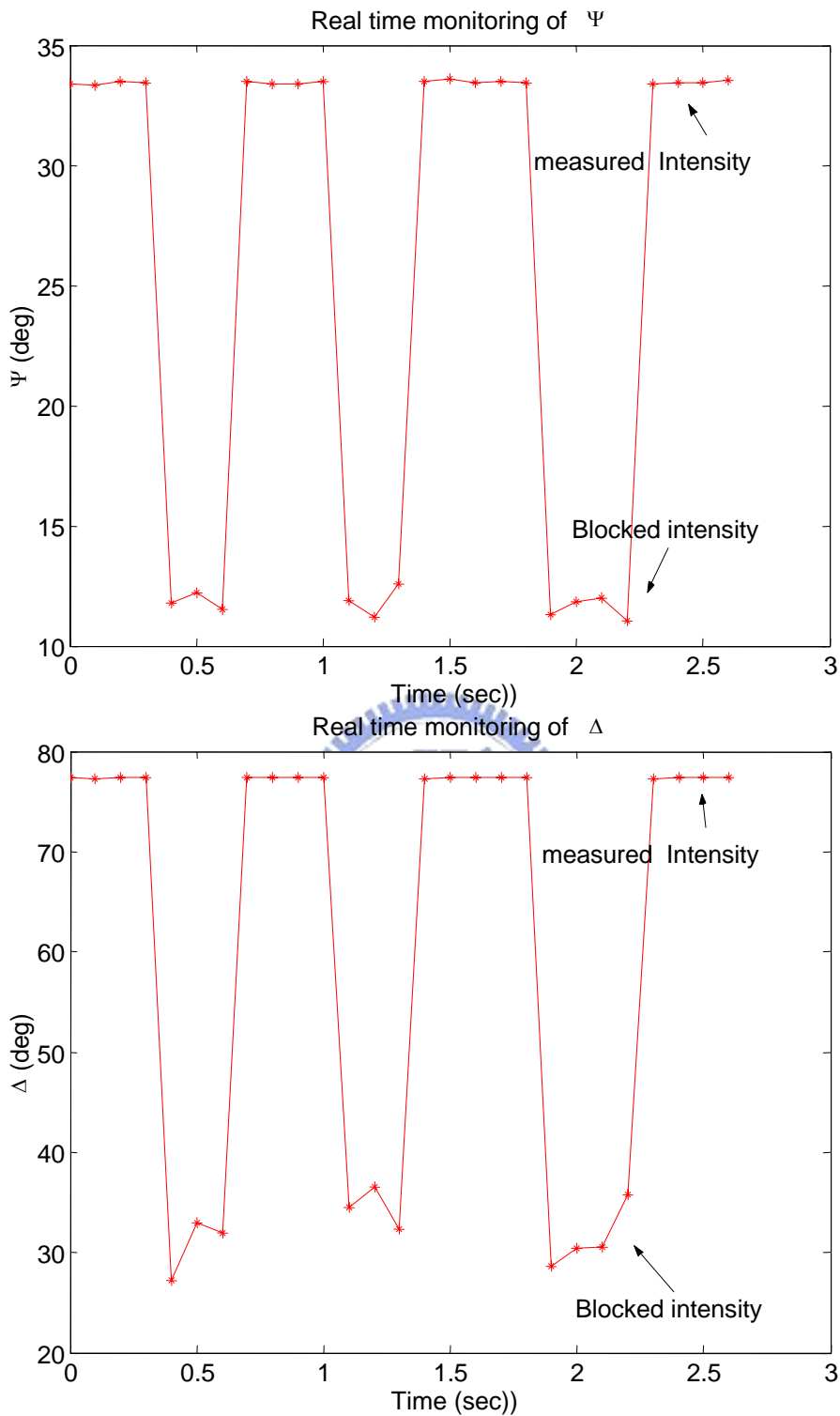


Fig. 5.11 The measured intensity was chopped in about 0.4 sec to demonstrate the 0.1 sec time consumption to sketch sample condition for real time monitoring by single wavelength at 632.8 nm.

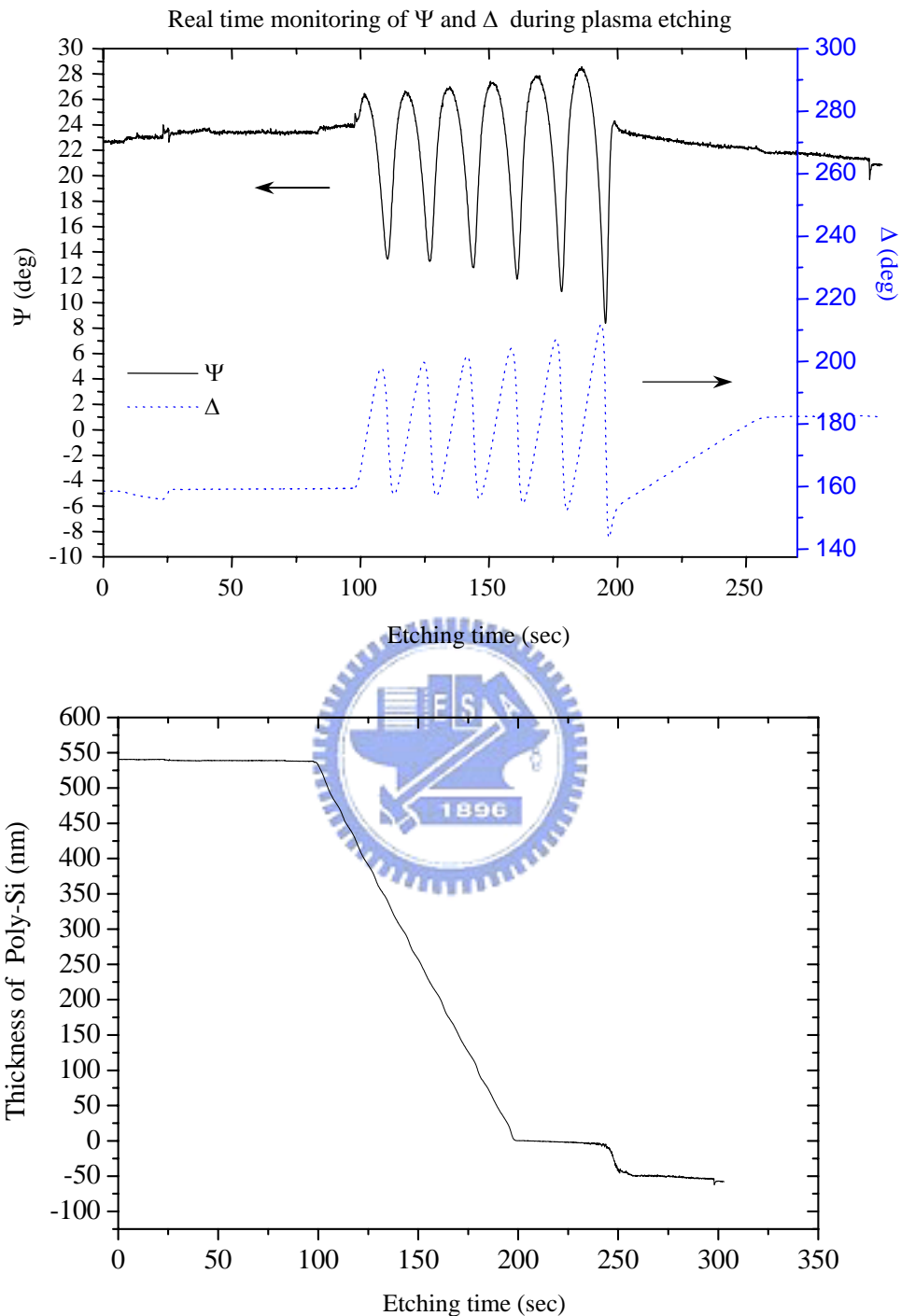


Fig. 5.12 Real time monitoring of polysilicon etching process: the traces of Ψ and Δ (upper), the calculated polysilicon thickness (lower)

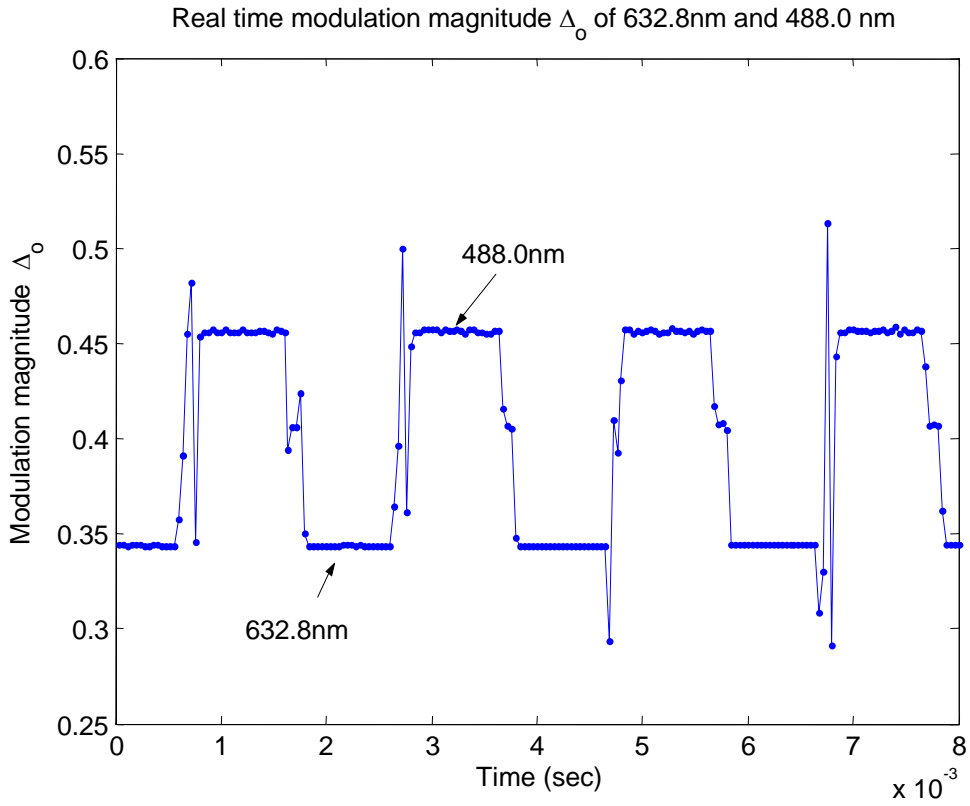


Fig. 5.13 The modulation amplitude Δ_o alternated in 1 ms between two wavelengths, 632.8 nm and 488.0 nm, calibrated simultaneously in 40 μ s.

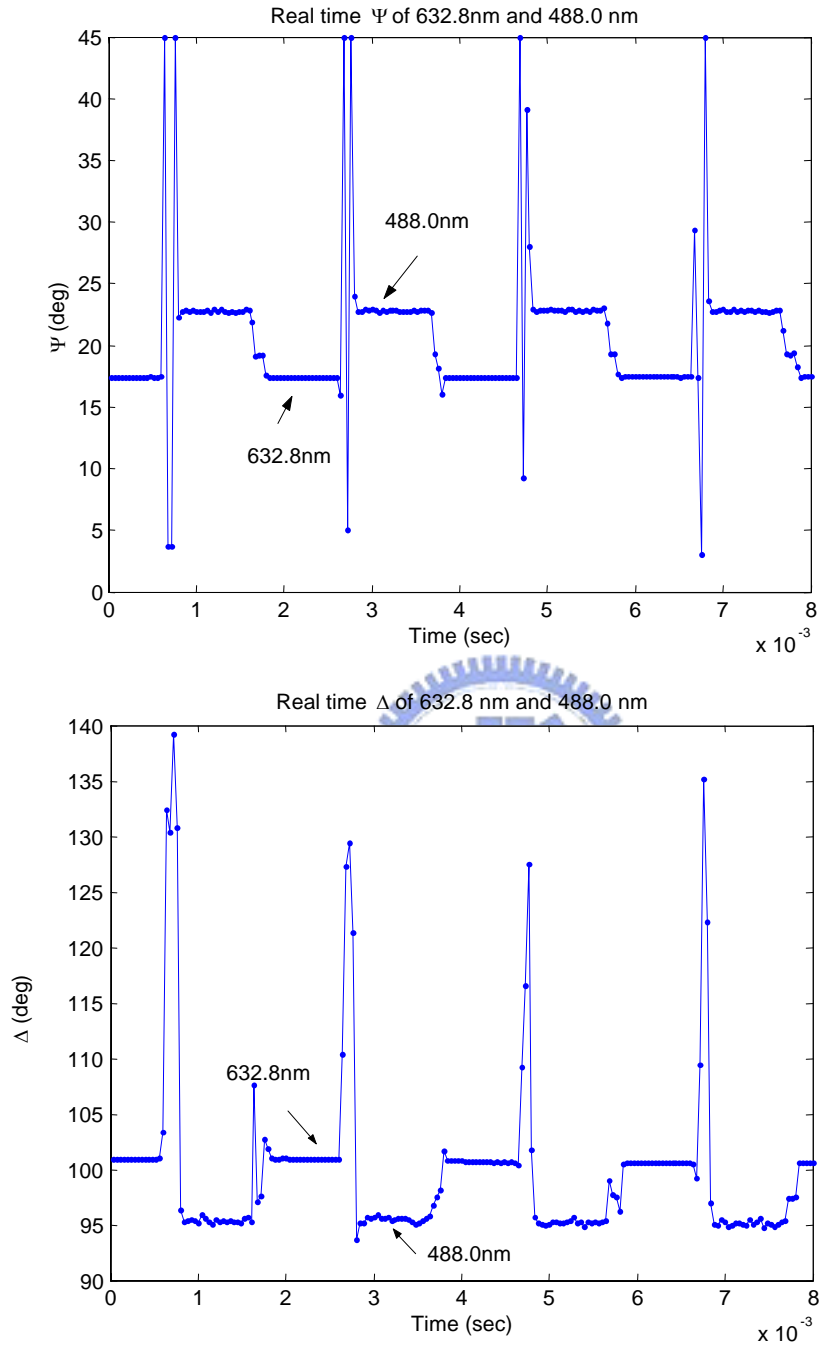


Fig. 5.14 Two real time obtained ellipsometric parameters Ψ and Δ of a standard SiO₂ thin film of 364 Å thickness at the incident angle of 70° under two wavelengths, 632.8 nm and 488.0 nm.

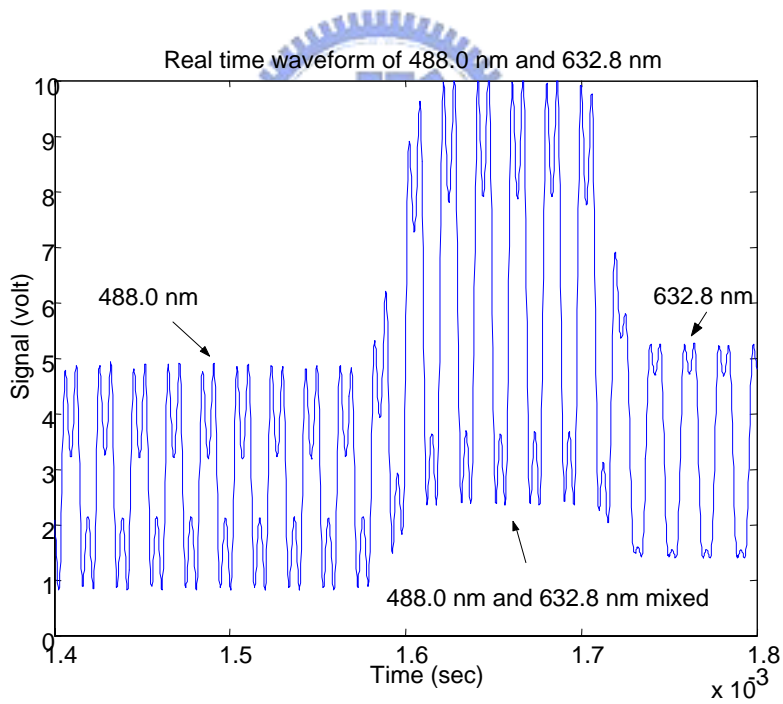
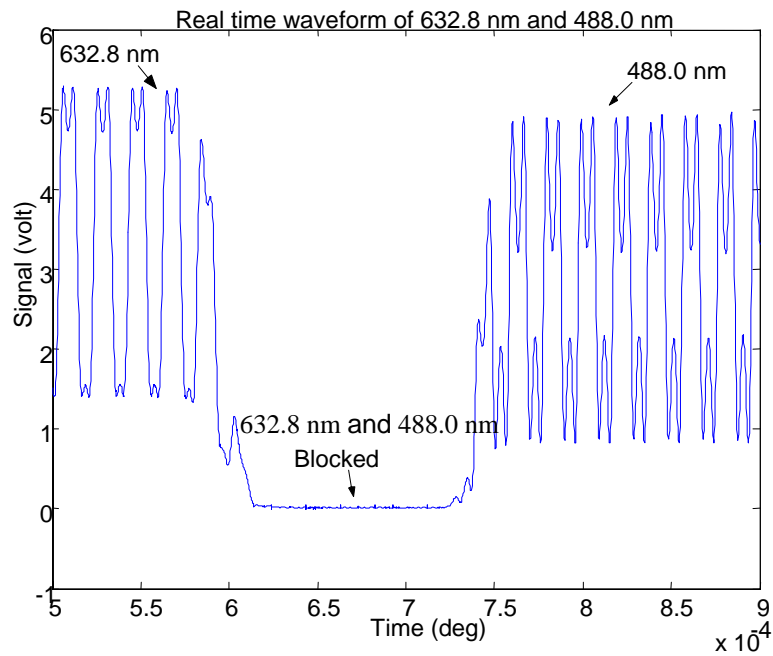


Fig. 5.15 the short intervals where two wavelengths are blocked (upper) or mixed (lower) in the acquired signal waveform.

Chapter 6

An error evaluation technique for the angle of incidence in a rotating element ellipsometer using a quartz crystal

The error in the angle of incidence for a rotating element ellipsometer is evaluated using a uniaxial quartz crystal. At a fixed angle of incidence, with respect to the surface of reflection, the ratio of reflectance in the parallel to that in the perpendicular electromagnetic field are measured by rotating the quartz crystal for a full cycle. We determine the deviation in the angle of incidence by fitting the reflectance ratio to its calculated value.

6.1 Introduction

The reflection technique has been widely used to determine the refractive indices of materials, even in powder form [1-4]. It was proved [4] that the ratio of reflectance in the parallel (R_p) to that in the perpendicular (R_s) electromagnetic field is insensitive to the condition of the surface. The ellipsometric parameter $\tan\Psi$ is the square root of the reflectance ratio [5]; it can be easily obtained using the ellipsometric measurements. Ellipsometry is a powerful technique for determining the optical properties of materials, such as isotropic multilayer thin films [5] and anisotropic crystals [6]. The rotating-element ellipsometry [7] is now known to be more competitive than the conventional null ellipsometry for automation. It has been known [8] that the beam deviation in the rotating-element ellipsometry can cause serious errors in the angle of incidence (AI), which is one of the crucial angles in ellipsometric measurements. Although both groups of McCrackin [9] and Chao [10] can systematically align the azimuth angles of the polarizer and analyzer to the incident plane in an ellipsometric system with high degree of accuracy, none of them have dealt with AI deviation. Because the analytical Fresnel reflection coefficients for uniaxial crystals have been developed [11] explicitly, it is possible to calculate the ellipsometric parameter Ψ as a function of the azimuth angle for a known uniaxial

crystal at a given incident angle. For aligning an incident angle in a PSA ellipsometry [12], we measure the ellipsometric parameter Ψ of a quartz crystal by rotating it around its normal line for a full cycle. A deviation in AI can be clearly observed by comparing the improved values of Ψ with its calculated values. This AI deviation can be determined by fitting the measured parameter to its calculated value. Because of this evaluation, we are able to use a dichroic sheet polarizer to substitute a prism polarizer. Taking the AI deviation into consideration, the deduced refractive index of glass (BK7) is comparable to that specified in the catalog.

According to our analysis, only a uniaxial crystal with small differences between the ordinary (n_o) and extraordinary (n_e) refractive indices can resolve the small error of AI, as illustrated numerically in this article. We also applied this technique to measure the angle between the normal to the cleavage plane and optic axis of a Yttrium Orthovanadate (YVO4) crystal to explore the feasibility of this PSA system.

6.2 The reflectance ratio of a uniaxial crystal

The reflected χ_r and incident χ_i polarization states are related by [6]

$$\chi_r = \frac{\left(\frac{r_{sp}}{r_{ss}}\right) + \chi_i}{\left(\frac{r_{pp}}{r_{ss}}\right) + \left(\frac{r_{ps}}{r_{ss}}\right) \cdot \chi_i}, \quad (6.1)$$

where r_{xy} is the Fresnel reflection coefficient for the parallel (p, i.e. x) and perpendicular(s, i.e. y) polarizations. According to reference 11, we summarize the analytical expressions of these Fresnel reflection coefficients for uniaxial crystals in the appendix C. The complex pseudorefectance ratio was defined [6] as $\langle \rho \rangle = \chi_i / \chi_r$ for anisotropic media, while in general ρ is defined as [5]

$$\rho = \tan \Psi e^{i\Delta},$$

thus

$$\tan^2 \Psi = \left| \frac{\chi_i}{\chi_r} \right|^2. \quad (6.2)$$

Since the cross terms vanish in an isotropic medium, $\tan\Psi$ [5] equals $|r_{pp}/r_{ss}|$, which is the conventional expression for the ellipsometric parameter. The reflection geometry for a uniaxial crystal is shown in Fig. 6.1. A simple model for anisotropic crystals was proposed by Aspnes [13]: the measured ellipsometric parameters for a particular θ_a equal those of the effective isotropic sample whose refractive index is given by its dielectric tensor projection onto the sample surface along the incident direction. This implies that

$$\tan^2 \Psi = \frac{I_{rp}}{I_{rs}}, \quad (6.3)$$

where I_{rp} represents the reflected intensity parallel to the incident plane and I_{rs} represents the reflected intensity perpendicular to the incident plane, for $P = 45^\circ$, i.e. $\chi_i = 1$. According to equation (6.3), one can obtain $\tan\Psi$ simply by measuring the reflected intensities I_{rp} and I_{rs} . If the optical axis of a nonabsorbent uniaxial crystal is parallel to the reflection surface, i.e. $\theta_c = 90^\circ$, then the ellipsometric parameter Ψ can be characterized by a twofold symmetry with respect to θ_a , the azimuth angle. Since we were only interested in determining the AI in a PSA ellipsometry, we simulated the ellipsometric parameter function $\Psi(\theta_a)$ for a uniaxial crystal with n_o and n_e as its ordinary and extraordinary refractive indices, respectively. Furthermore, we assume the optical axis of the sample crystal is parallel to the reflection surface so as to obtain the twofold symmetry for comparison.

Two types of crystals are simulated to examine their resolving power in AI. The difference of one crystal's ordinary and extraordinary refractive indices is about one order of magnitude lower than that of the other crystal. The function $\Psi(\theta_a)$ is simulated for $\chi_i = 1$, i.e. $P = 45^\circ$, and optimized [12] by $\chi_i = -1$, i.e. $P = -45^\circ$, to eliminate the error caused by the misalignment of the polarizer, according to equation (6.3), one can obtain

$$\tan \Psi = \left[\frac{I_{rp}}{I_{rs}} \Big|_{P=45^\circ} \frac{I_{rp}}{I_{rs}} \Big|_{P=-45^\circ} \right]^{1/4}. \quad (6.4)$$

The incident angle θ_i is set to be 45° and 44.94° for quartz crystal ($n_o=1.544$ and $n_e=1.553$) and 45° and 44.5° for yttrium orthovanadate Crystal (YVO₄, $n_o = 1.9929$, $n_e = 2.2154$), as shown in Fig. 6.2a and Fig. 6.2b, respectively. These two figures indicate that the resolving power of quartz crystal is about one order of magnitude higher than that of YVO₄ crystal. The resolving power is even higher when the AI is at Brewster angle (the numerical simulated curves for $\theta_i= 57^\circ$ are shown in Fig 6.3). But, the reflectance of the parallel electromagnetic field is too low to be practical for measuring in this intensity ratio technique, especially for a nonabsorbent.

6.3 Experimental Procedures

Figure 6.4 depicts the experimental setup. The light (L: HeNe laser) passes through a polarizer (P: dichroic sheet polarizer of extinction ratio 10^{-4}) whose azimuth angle is set to be 45° with respect to the incident plane of the sample. The AI (θ_i) is taken to be 45° . The analyzer (A) is mounted on a stepping motor controlled rotator. The samples (quartz crystal, surface flatness $\lambda/4$; BK7 glass, surface flatness $\lambda/4$; and YVO₄ crystal-CASIX, surface flatness 2λ) are mounted on a rotatable holder and measured at 10° intervals. All intensities are measured using a power meter (D) (Newport 818-SL), digitized by a multimeter (Keithley 195A), and stored in a PC for calculating the ellipsometric parameters. The reflectance ratios are obtained by the ratio of intensity at $A= 0^\circ$ to that at $A=90^\circ$. Prior to the measurements, all the azimuth angles of the polarizer and the analyzer are systematically aligned according to reference 10 using an optical flat thick platinum plate. Moreover, the reference zeros of the polarizer and analyzer are confirmed using the technique of reference 12.

6.4 Results

In parallel to our experiment, we numerically analyze the improved value of Ψ , using equation (6.4) incorporated with the analytical solution of reflection coefficients for uniaxial crystals. The improved Ψ is found to be free from the

misalignment of polarizer and only off 0.002° if there is a 0.5° misalignment in the analyzer. However, the azimuthal deviations of the polarizer and analyzer with respect to the incident plane can be as low as 0.005° in the PSA ellipsometric system [12]. Comparing the measured Ψ of quartz crystal with its calculated value, as shown in Fig. 6.5a, we conclude that the systematic error is mainly caused by the deviation of AI. The deviation is found to be $-0.06 \pm 0.01^\circ$ by fitting the experimental data to the calculated values. Furthermore, the azimuth angle θ_a of the optical axis is found to be $1.78 \pm 0.01^\circ$ to the incident plane, as shown in Fig. 6.5b, the standard deviation between the measured value and calculated value is 0.02° after the adjustment of azimuth angle. The refractive index of BK7 deduced [5] from $\tan\Psi$ (Fig. 6.6) is 1.517 ± 0.002 at an incident angle of 44.94° ; and is 1.521 ± 0.002 at an incident angle of 45° . Since the refractive index of BK7 is 1.515 (Schott: optical glass no. 1000), this error evaluation can improve the measurement of glass. Using the specified value of $n_o = 1.9929$, $n_e = 2.2154$ for YVO4 crystal at $\theta_i = 44.94^\circ$, we obtained the angle (θ_c) between the normal to the cleavage plane and the optic axis to be 136.01° and the angle θ_a (Fig. 1) to be $7.24 \pm 0.01^\circ$, as shown in Fig. 6.7, while θ_c was specified as 135° from CASIX.

6.5 Concluding remarks

The small difference between the ordinary and extraordinary refractive indices of the quartz crystal allows us to resolve the deviation in the incident angle for the rotating-element ellipsometry. The other two primary errors in a rotating PSA ellipsometric system, the azimuthal misalignment and degradedness of polarizers, can be reduced by intensity ratio technique [12]. Since all three primary errors in a rotating PSA ellipsometry can be reduced, we can substitute a prism polarizer with a low cost dichroic sheet polarizer without losing its accuracy in a PSA ellipsometric system. In addition to determining the deviation of incident angle in a rotating element ellipsometry, the following three parameters can be obtained by fitting the

measured $\tan\Psi$ to the analytic solution of uniaxial crystals: the absolute value of n_o , n_e and directions of optical axis (θ_a and θ_c) in the laboratory frame. Since the resolving power of the system can be increased as the incident angle moves closer to the Brewster angle (the reflected intensity at 50° will be about 0.4% of the incident intensity), the system can be improved by using a sensitive detector or a higher power light source. It is our interest to extend the system to measure a material, which consists of both linear and circular birefringence.

6.6 References

- [1] J. R. Beattie, *Philos. Mag.* **46**, 235 (1955).
- [2] E. A. Taft and H. R. Philipp, *Phys. Rev. A* **138**, 197 (1965).
- [3] V. P. Tomaselli, R. Rivera, D. C. Edeward, and K. D. Möller, *Appl. Opt.* **20**, 3961 (1981).
- [4] B. J. Stagg and T. T. Charalampopoulos, *Appl. Opt.* **30**, 4113 (1991).
- [5] R. M. A. Azzam and N. M. Bashara, *Ellipsometry and Polarized light* (Amsterdam: North-Holland, 1992)
- [6] M. I. Alonso and M. Garriga, *Appl. Phys. Lett.* **67**, 596 (1995).
- [7] R. W. Collins, *Rev. Sci. Instrum.* **61**, 2029 (1990).
- [8] J. R. Zeidler, R. B. Kohles, and N. M. Bashara, *Appl. Opt.* **13**, 1938 (1974).
- [9] F. L. McCrankin, E. Passaglia, R. R. Stromberg, and H. L. Steinberg, *J. Res. Natl. Bur. Stand. A.* **67**, 363 (1963).
- [10] Y. F. Chao, C. S. Wei, W. C. Lee, S. C. Lin, and T. S. Chao, *Jpn. J. Appl. Phys.* **34**, 5016 (1995).
- [11] J. Lekner, *J. Phys.: Condens. Matter* **3**, 6121 (1991).
- [12] Y. F. Chao, W. C. Lee, C. S. Hung, and J. J. Lin, *J. Phys. D: Appl. Phys.* **31**, 1968 (1998).
- [13] D. E. Aspnes, *J. Opt. Soc. Am.* **70**, 1275 (1980).

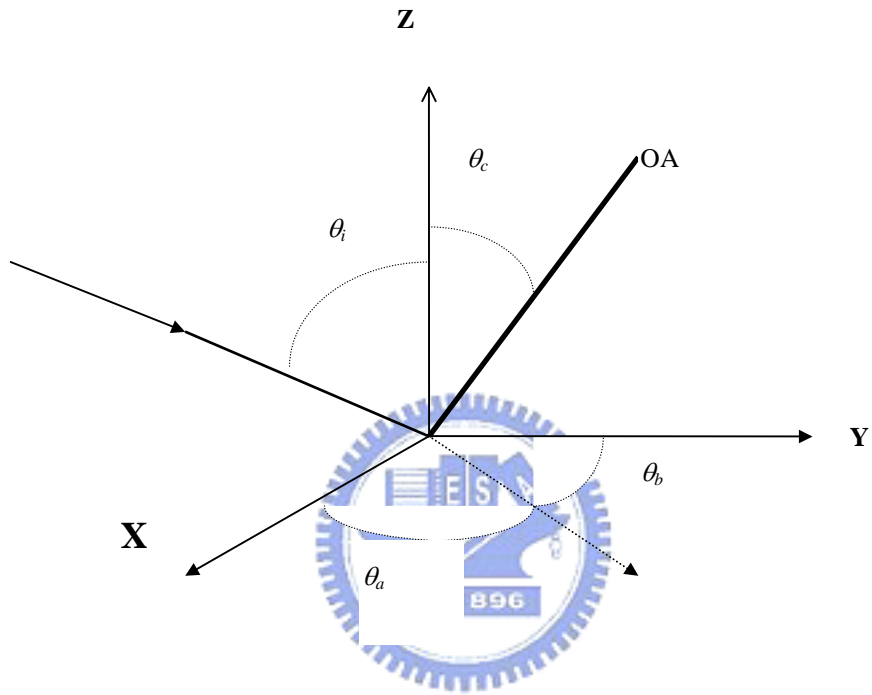


Fig. 6.1. The reflection geometry: θ_i is the incident angle, xy plane is the reflecting face of the crystal, zx plane is the incident plane, the z axis is the normal line. OA is the optical axis of the crystal.

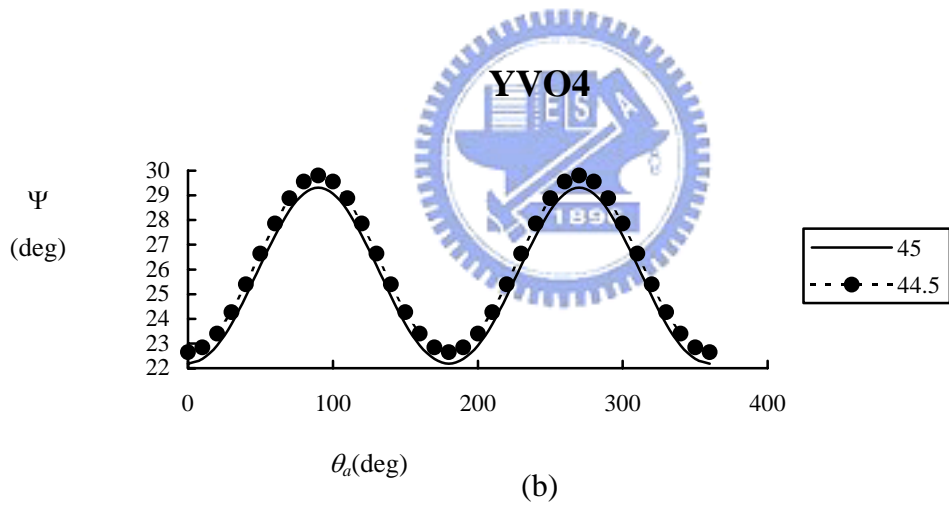
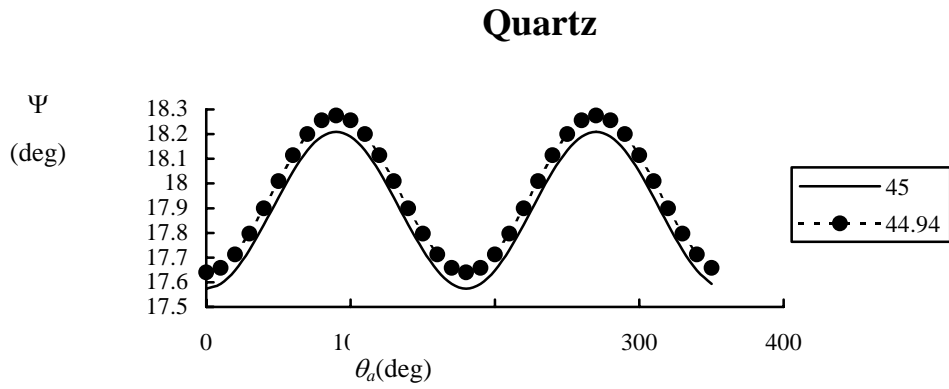


Fig. 6.2. The numerically simulated Ψ as a function of azimuth angle of θ_a while $\theta_c=90^\circ$: (a) quartz crystal: $n_o=1.544$, $n_e=1.553$ at the incident angle of 45° (line), and 44.94° (dot); (b) yttrium orthovanadate crystal: $n_o=1.9929$, $n_e=2.2154$ at the incident angle of 45° (line), and 44.5° (dot).

Quartz: near principl angle

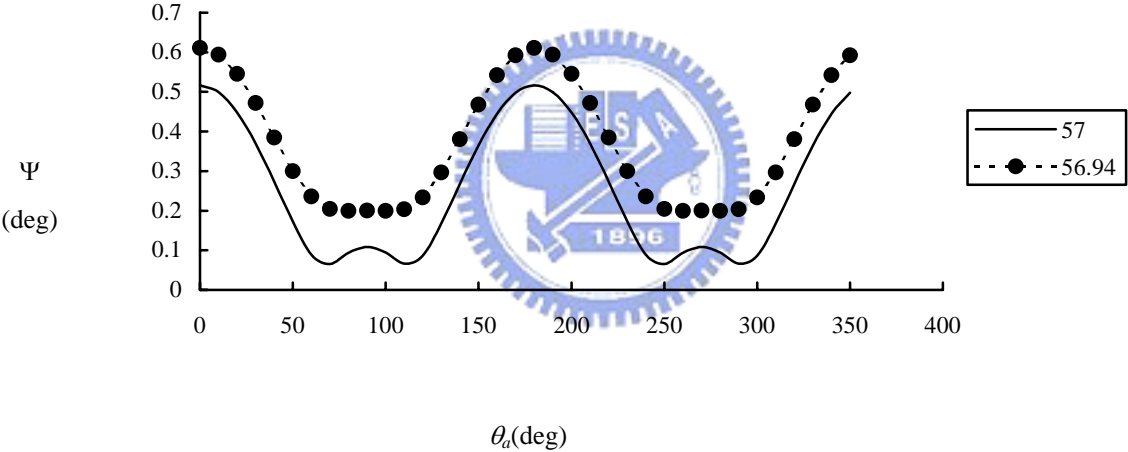


Fig. 6.3. The numerically simulated ψ as a function of azimuth angle of θ_a while $\theta_c = 90^\circ$, quartz crystal of $n_o = 1.544$, $n_e = 1.553$ at the incident angle of 57° (line), and 56.94° (dot), respectively.

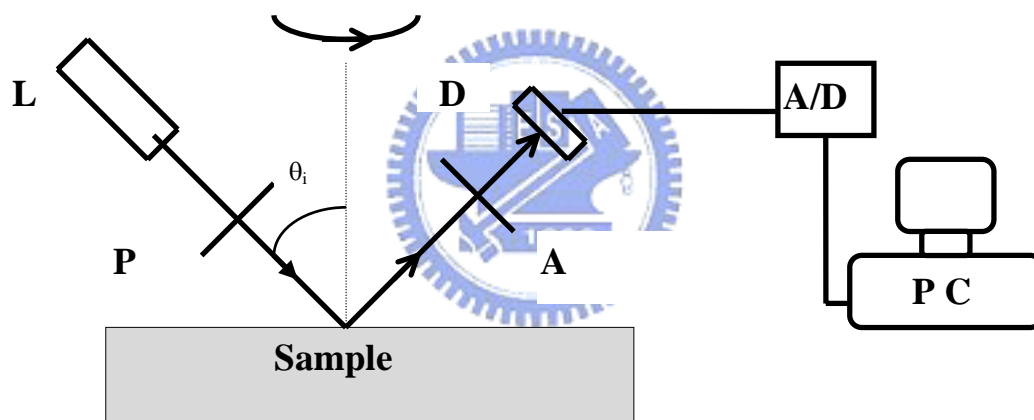
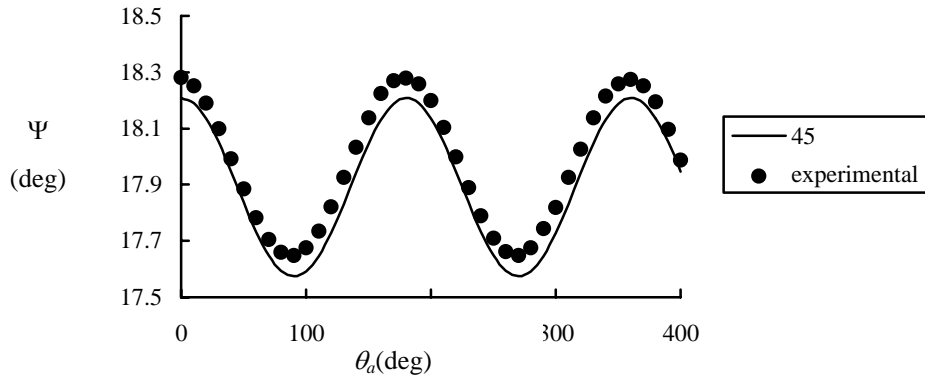
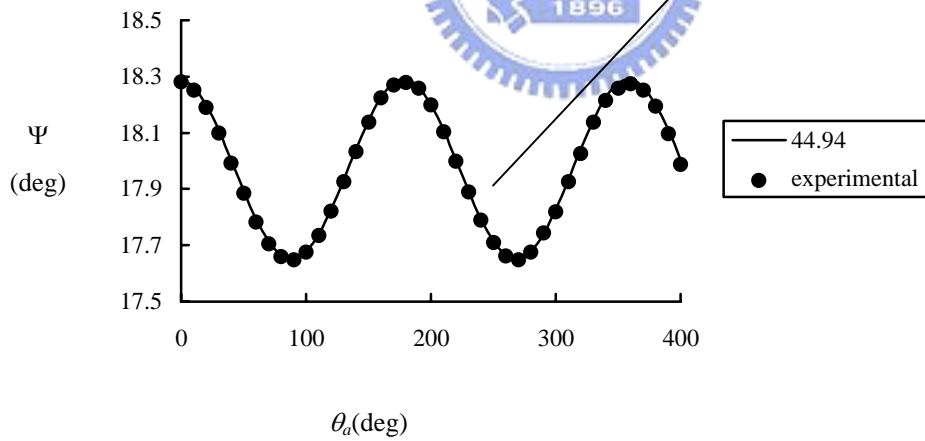
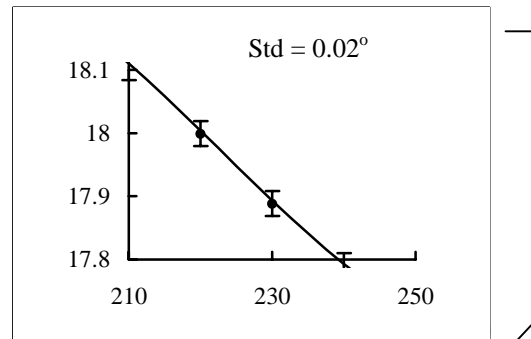


Fig. 6.4. A schematic set-up of the PSA ellipsometer: L, light source (He-Ne laser); P, polarizer; A, analyzer; D, detector.



(a)



(b)

Fig. 6.5. Ψ versus θ_a : Quartz

$\theta_c=90^\circ$, $n_o=1.544$, $n_e=1.553$: (a) $\theta_i = 45^\circ$ (line: calculated \bullet : measured) and $\theta_a = 0^\circ$; (b) $\theta_i = 44.94^\circ$ (line: calculated \bullet : measured) and $\theta_a = -1.78^\circ$. Subplot: portion of the main plot, “ I ” is the standard deviation of the measured value to its calculated value.

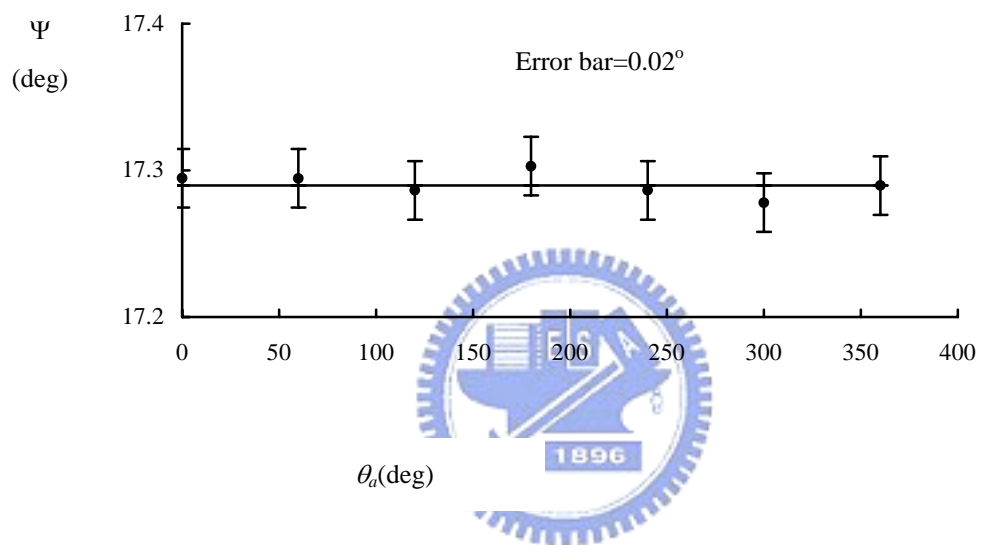


Fig. 6.6. Ψ verses θ_a : BK7

The standard deviation is 0.02° . The line indicates the mean value which is 17.29° .

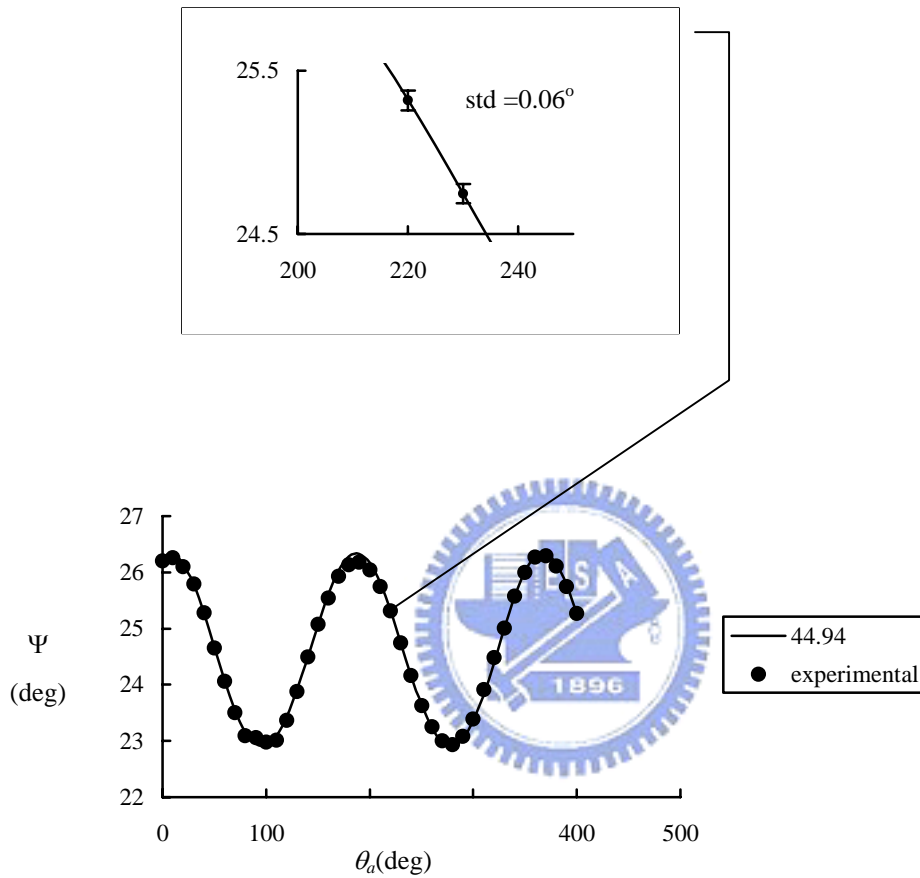


Fig. 6.7 Ψ verses θ_a : YVO4

$\theta_c = 136.01^\circ$ for YVO4 with $n_o = 1.9929$ and $n_e = 2.2154$, $\theta_i = 44.94^\circ$ (line: calculated \bullet : measured) and $\theta_a = 7.24^\circ$. Subplot: portion of the main plot, "I" is the standard deviation of the measured value to its calculated value.



Chapter 7

Conclusion

Multi-wavelength photoelastic modulation (PEM) ellipsometry, based on phase modulation, have been presented. From the spectroscopic point of view, they can cover visible range. Like other ellipsometric techniques, PEM ellipsometry is non invasive and can be used in any ambient atmosphere. Nevertheless, the main characteristic of PEM ellipsometry is the fast, whose measuring speed is provided by a photoelastic modulator (50kHz). This leads that PEM ellipsometry superior to the low frequency ellipsometric techniques (100Hz), such as the rotating element ellipsometry at the tens of millisecond scale. Furthermore, PEM ellipsometry can be easily combined with other low frequencies of modulations leading to double modulation techniques. For reducing the error of DC signal, one can combined with mechanical rotating chopper or modulated diode laser light source

We have developed *in situ* alignment techniques to align all of the optical components (namely P, PEM and A) to the reflective surface of a specimen in a PEM ellipsometer at fixed incident angle. In addition to the azimuths of polarizer and analyzer, the strain axis of PEM can also be determined at the same incident angle by intensity ratio technique. This intensity ratio technique not only can reduce the error caused by the intensity fluctuation, it also simultaneously determine the ellipsometric parameter Ψ , which can be used to determine the incident angle on-line. Just like two incident-angle-alignment technique, it requires at least two testing samples or two-wavelengths to align the system prior to any measurement at a working incident angle. This technique is particularly suitable to a pre-designed closed system, in which a multi-incident-angle technique is not possible.

We also introduce a real time calibration technique for the modulation amplitude

Δ_0 of PEM in ellipsometry by a Multiple Harmonic Intensity Ratio (MHIR) technique with a data acquisition (DAQ) system. By reflection and transmission set up, it can be verified that MHIR technique is independent of frequency. In addition to confirm our calibration by the digitized oscilloscope waveform, we also obtain a set of ellipsometric parameters Ψ and Δ under various values of modulation magnitude Δ_0 . However, in an etching/deposition process, a preliminary study is necessary under the chemistry of etching/deposition process, instead of using the MHIR, we introduce a correction factor to calibrate the modulation amplitude. This correction technique provides us a pair of dependable ellipsometric parameters for monitoring the etching process. After comparing the measured value of Ψ and Δ under etching, we are confident to propose that one should study the traces of Ψ and Δ versus the thickness for controlling instead of calculating the thickness in real time.

The main purpose of our research is trying to establish multiple wavelength ellipsometry for *in situ* / real time measurements, the modulation amplitude has to be set as a constant for a particular wavelength in the process of measurement. Since the physical path of PEM is invariant, the modulation amplitude should be inversely proportion to the wavelength. After considering the static retardation and taking the modulation amplitude at 0.383λ for 568.2 nm, we calculated the corresponding modulation amplitude for other wavelengths, and the measured values are well fitted to our expectation. To real time monitor etching processing, the instrumentation program dedicated to FFT computation can be employed for on-line control system. Nevertheless, waveform measurement can be utilized to diagnose the sample dynamic behavior less than millisecond scale, for example, the dynamic response of etching system or the modulation of liquid crystal device.

The small difference between the ordinary and extraordinary refractive indices of the quartz crystal allows us to resolve the deviation in the incident angle for the

rotating element in ellipsometry. In addition, the degradedness of polarizers can be reduced by intensity ratio technique. After these calibrations, we believe there is enough information for the construction of an *in situ* / real time spectroscopic ellipsometry. On the other hand, the capability of PEM ellipsometry to provide real time control and monitoring of semiconductor processes has been prospective. Real time applications of PEM ellipsometry, combined with two alternative wavelength, for adaptive control in etching processing can be employed by hardware Digital Signal Process (DSP). In particular, it has been shown that the ability to diagnose the interruption of etching process for end point prediction.

In conclusion, it can be anticipated that the ellipsometric techniques, based on phase modulation, will be extensively used, in the near future, for process monitoring and control, as well as probing the fundamental semiconductor growth/etching mechanisms.





Appendices

Appendix A The samples for fixed incident angle alignment

One has to choose appropriate samples for fixed incident angle alignment. Chao [1] aligned the PSA system by two incident angles; one is less than the principle angle and the other one is greater than the principle angle. The reason of this choice is because $\cos\Delta$ changes sign across the principle angle. This basic concept can be substituted by two thin films, i.e., 105 nm and 5 nm SiO_2/Si , or two different wavelengths 488nm and 647nm for one thin film (SiO_2/Si 105 nm). For expressing the concept, we plot their ellipsometric parameters in the Ψ - Δ diagram, such as shown as Fig. A.1 and Fig A.2, respectively. From the diagrams, one can immediately identify two suitable thin films or two appropriate wavelengths for the thin film of 105 nm thickness at the incident angle of 70° .

The reflected intensity ratio A and B of a typical SiO_2/Si thin film is shown in Fig. A.3. One can obtain the position and value at the intersections of A and B by a polynomial fit. Two parameters can be obtained from the intensity ratio distribution : (a) the position of intersection (α, β) , (b) the value of the intersection, $\tan^2 \Psi$. From Fig. A.3 one clearly observes that these intersections switch sides with respect to plane of incident when β changes its sign. This phenomenon provides a apparent indication to the plane of incident in the laboratory scale.





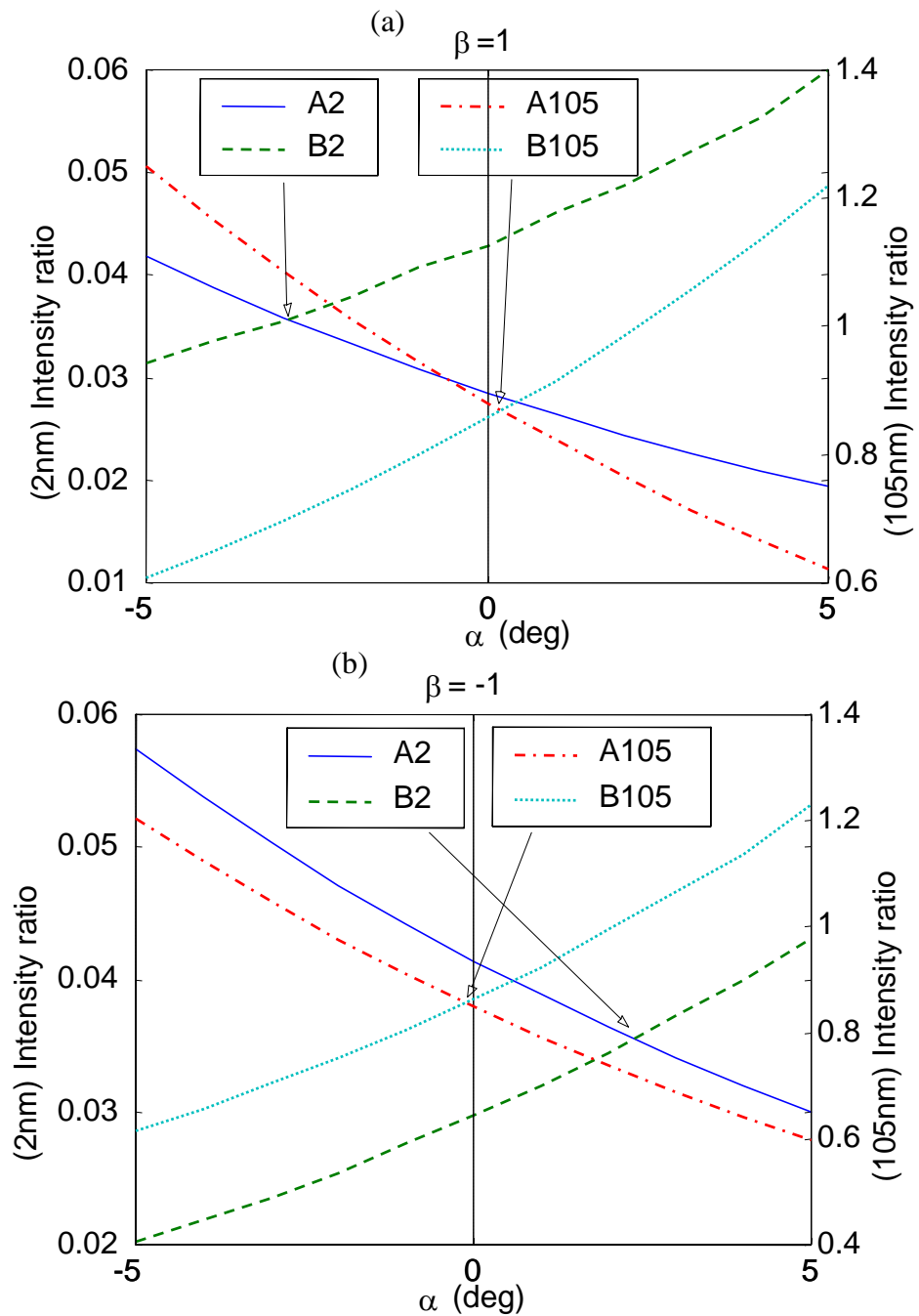


Fig. A.3 Intensity ratio of A and B plotted against angular position of polarizer (α) at a fixed angular position of analyzer (β) for the SiO_2/Si 105 nm thin film sample and native oxide 2 nm silicon sample. The intensity ratios are scaled according to different sample and denoted as (105 nm) and (2 nm), respectively.

Appendix B The analysis of etching process

To study of etching process, we are trying to build a model for monitoring the poly silicon etching process in real time; in the beginning, however, only a flat poly silicon layer on a oxide (about 1000 Å) on silicon substrate is measured. From our numerical simulation, we expect to observe a significant change in Ψ about 900 Å prior to the endpoint. This phenomenon did appear in the process of etching. In etching process, the thickness of film is determined by the measured value of $\Psi(t)$ and $\Delta(t)$ through modeling. It is known that both parameters oscillate, especially at the wavelength where the material is less absorbing. Maynard [2] suggested choosing the wavelength with high extinction coefficient for monitoring and controlling. Since certain amount prior knowledge of the film is needed for deducing the thickness of the film, the basic etching behavior can be studied before the etching. Instead of deducing the thickness of the film in real time, one can provide the traces of $\Psi(t)$ and $\Delta(t)$ with respect to the thickness of film in the process of etching and compare it with the real time recording traces of $\Psi(t)$ and $\Delta(t)$. For reference, we use two models (poly-silicon/SiO₂/silicon substrate) to illustrate the characteristic traces of $\Psi(t)$ and $\Delta(t)$: (1) the gate oxide region, where the thickness of SiO₂ less than 100 Å, such as shown in Fig. B.1; (2) the field oxide region, where the thickness of SiO₂ more than 500 Å, such as shown in Fig. B.2. The oscillation of $\Psi(t)$ and $\Delta(t)$ give the information of how thick the film has been etched for both cases.

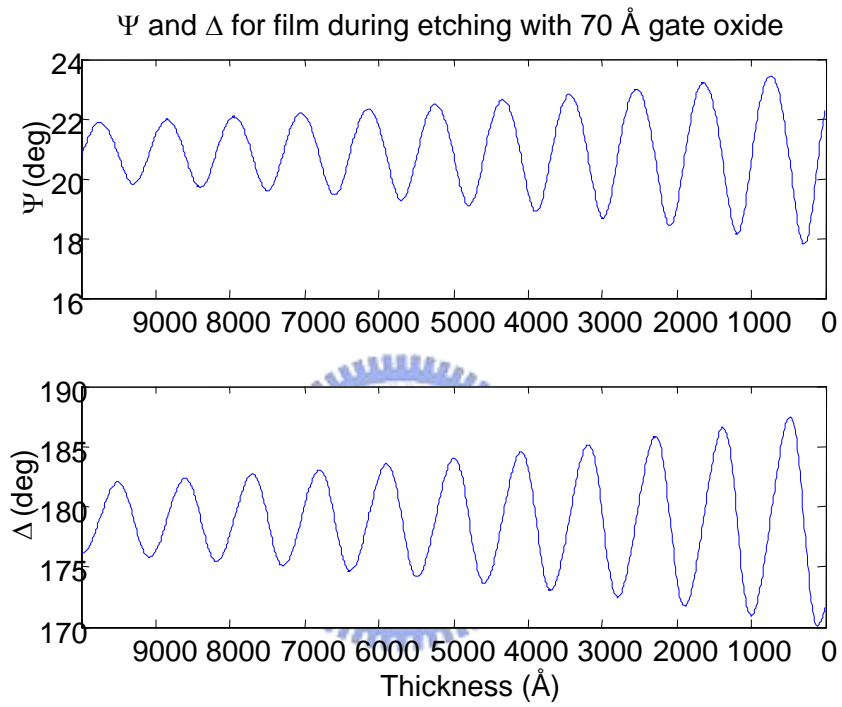


Fig. B.1 The distribution of Ψ and Δ for film under etching with 70 Å gate oxide.

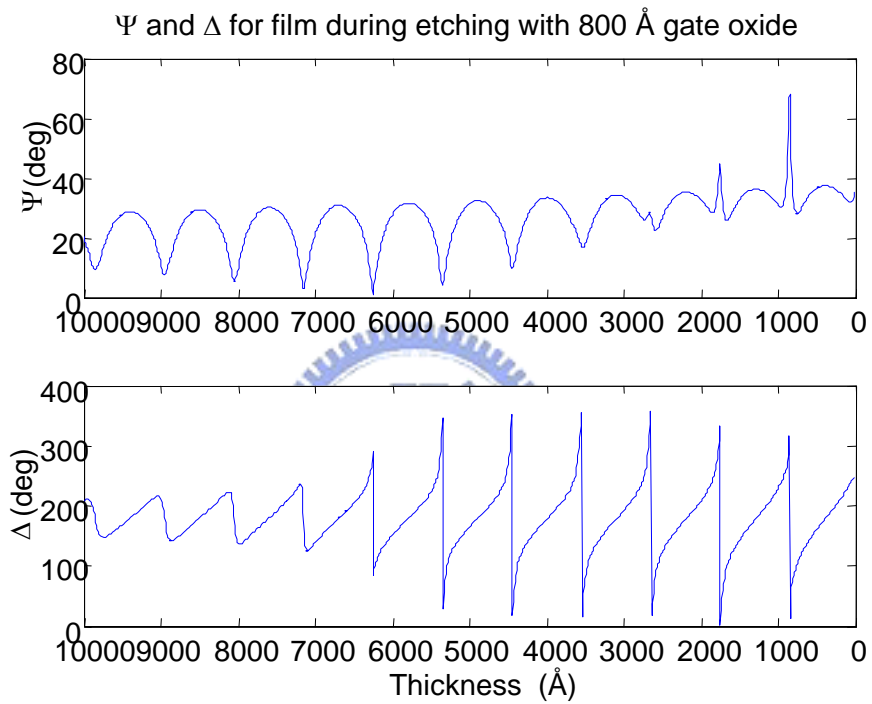


Fig. B.2 The distribution of Ψ and Δ for film under etching with 800 Å field oxide.

Appendix C Fresnel reflection coefficients of uniaxial crystals

The reflection geometry is shown in Fig. C.1. The direction of optical axis is specified by angles θ_a and θ_c relative to the laboratory xyz , if \vec{c} is the unit vector of optical axis, we can express it as

$$\vec{c} = (\alpha, \beta, \gamma),$$

where $\alpha = \cos\theta_a \sin\theta_c$, $\beta = \sin\theta_a \sin\theta_c$ and $\gamma = \cos\theta_c$. Let the incident wave vector be $K\vec{i} + q_1\vec{k}$, where $K = k n_i \sin\theta_i$, $q_1 = k n_i \cos\theta_i$, for a wave number $k = \omega / c$ at incident angle θ_i . According to reference [3], we summarized the Fresnel reflection coefficients for uniaxial crystals of ordinary refractive index $n_o = \sqrt{\varepsilon_o}$ and extraordinary refractive index $n_e = \sqrt{\varepsilon_e}$ as follows;

$$r_{ss} = [(q_1 - q_e)AE_y^e - (q_1 - q_e)BE_y^o] / D$$

$$r_{sp} = 2n_i k (AE_x^e - BE_x^o) / D$$

$$r_{pp} = 2q_i [(q_1 + q_e)E_x^o E_y^e - (q_1 + q_o)E_x^e E_y^o] / D - 1$$

$$r_{ps} = 2n_i k (q_e - q_o) E_y^o E_y^e / D$$

The ordinary and extraordinary modes have wave vector normal components q_o , and q_e related to the medium as

$$q_e = (\sqrt{d} - \alpha\gamma K \Delta\varepsilon) / (\varepsilon_o + \gamma^2 \Delta\varepsilon),$$

$$q_o = \varepsilon_o k^2 - K^2, \quad q_t = q_1 + K \tan\theta_i$$

where $\Delta\varepsilon = \varepsilon_e - \varepsilon_o$, and

$$d = \varepsilon_o [\varepsilon_e (\varepsilon_o + \gamma^2 \Delta\varepsilon) k^2 - (\varepsilon_e - \beta^2 \Delta\varepsilon) K^2];$$

the corresponding electric field vectors \mathbf{E}^o and \mathbf{E}^e noted as

$$\mathbf{E}^o = N_o (-\beta q_o, \alpha q_o - \gamma K, \beta K),$$

$$\mathbf{E}^e = N_e (\alpha q_o^2 - \gamma q_e K, \beta \varepsilon_o k^2, \gamma (\varepsilon_o k^2 - q_e^2) - \alpha q_e K),$$

where N_o , N_e are the normalization factor, respectively. For simplicity, we also state the collective parameters as follows;

$$A = (q_o + q_1 + K \tan\theta_i) E_x^o - K E_z^o$$

$$B = (q_e + q_1 + K \tan\theta_i) E_x^e - K E_z^e$$

$$D = (q_1 + q_e) A E_y^e - (q_1 + q_o) B E_y^o$$

References of appendices

- [1] Y. F. Chao, C. S. Wei, W. C. Lee, S. C. Lin, and T. S. Chao, *Jpn. J. Appl. Phys.* **34**, 5016 (1995).
- [2] H. L. Maynard, N. Layadi, and J. T. C. Lee, *J. Vac. Sci. Technol. B.* **15**, 109 (1997).
- [3] J. Lekner, *J. Phys.: Condens. Matter* **3**, 6121 (1991).



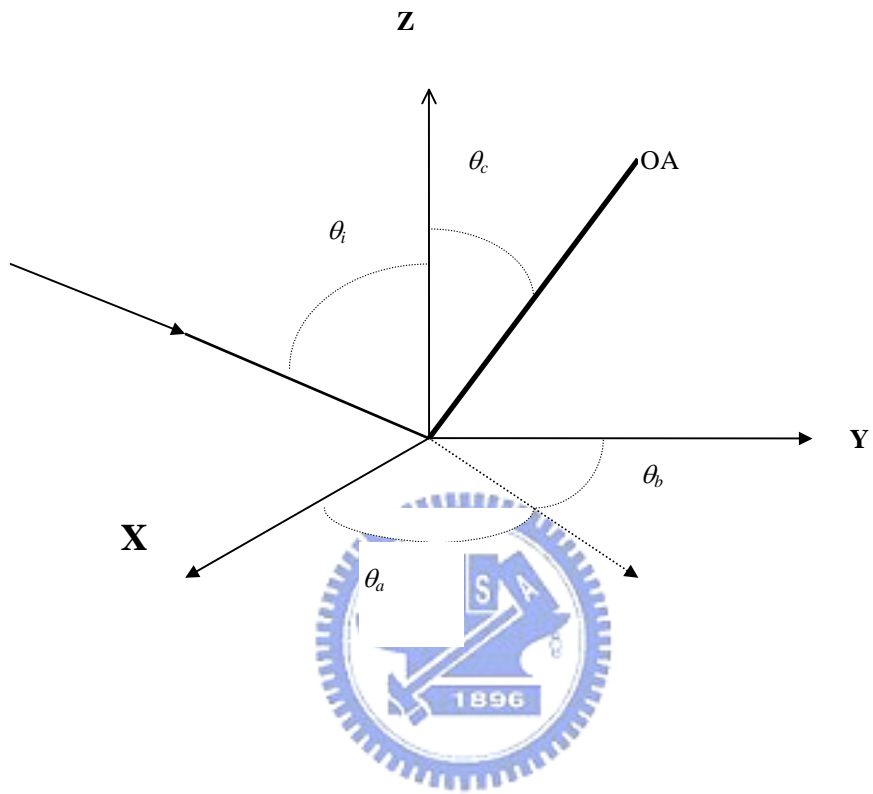


Figure C.1. The reflection geometry: θ_i is the incident angle, xy plane is the reflecting face of the crystal, zx plane is the incident plane, the z axis is the normal line. OA is the optical axis of the crystal.

簡歷 (Vita)

一、基本資料

中文姓名	王夢偉	英文姓名	Meng-Wei Wang (First Name) (Last Name)
國籍	中華民國	性別	男
聯絡地址	300 新竹市大學路 1001 號交通大學光電所偏光量測實驗室		
聯絡電話	(公).03-5731941	(宅). 0991271982	
傳真號碼	03-5716631	E-MAIL	mwwang.eo86g@nctu.edu.tw

二、主要學歷

畢 / 肄業學校	國別	主修學門系所	學位	起訖年月(西元年/月)
成功大學	R.O.C.	電機系	工學學士	1991/9 至 1995/6
交通大學	R.O.C.	光電所	工學碩士	1995/9 至 1997/6
交通大學	R.O.C.	光電所	工學博士	1997/9 至 2004/6
				___ / ___ 至 ___ / ___

三、專長

1. 偏極光量測	2. 線上校正即時監控	3. 光電信號處理	4.
----------	-------------	-----------	----

CURRICULUM VITAE

GENERAL INFORMATION

Meng-Wei Wang (王夢偉)

Addr.: Institute of Electro-Optics Engineering, National Chiao Tung University,
No. 1001 Ta Hsueh Rd., Hsinchu, Taiwan, R. O. C.

Email: mwwang.eo86g@nctu.edu.tw

Telephone: (886)-(3)-5731941

Fax: (886)-(3)-5716631

PERSONAL DATA

Academic Degree: Ph. D.

Birth Place: Taipei, Taiwan, Republic of China

Sex: Male

EDUCATION

Bachelor of Electrical Engineering, National Cheng Kung University, Tainan, Taiwan,
R. O. C. 1995.

Focus: Electronics, Electromagnetic Wave, and Computer Organization.

Master of Electro-Optical Engineering, National Chiao Tung University, Hsinchu,
Taiwan, R. O. C. 1997.

Focus: Polarization Optics, Crystal Optics, Experimental Computing.

Master Thesis: Uniaxial Crystal and Its Ellipsometric Measurement.

Ph.D. of Electro-Optical Engineering, National Chiao Tung University, Hsinchu,
Taiwan, R. O. C.. 2004.

Focus : Polarization Measurement, Error Evaluation, Instrument Calibration.

Ph. D. Thesis: Multi-wavelength Photoelastic Modulation Ellipsometry.



著作目錄 (Publication List)

所有學術性著作分成三大類：(A)期刊論文 (B)研討會論文 (C)專利

(A)期刊論文 (Journal Paper)

1. Y. F. Chao, M. W. Wang and Z. C. Ko, "An error evaluation technique for the angle of incidence in a rotating element ellipsometer using a quartz crystal," J. of Phys. D: Appl. Phys. **32** (1999) 2246-2249
2. M. W. Wang, Y. F. Chao, "Azimuth alignment in photoelastic modulator ellipsometry at a fixed incident angle," Jpn. J. Appl. Phys. **41** (2002) 3981-3986
3. M. W. Wang, Y. F. Chao, K. C. Leou, F. H. Tsai, T. L. Lin, S. S. Chen and Y. W. Liu, "Calibrations of phase modulation amplitude of photoelastic modulator," Jpn. J. Appl. Phys. **43** (2004) 827-832
4. M. W. Wang, F. H. Tsai and Y. F. Chao, "In situ calibration technique for photoelastic modulator in ellipsometry," Thin Solid film **355-356** (2004) 78-83

(B)研討會論文 (Conference Paper)

1. 王夢偉, 趙于飛 "光彈調變式橢圓儀方位角線上校正" OPT 99, 台灣光電研討會論文集(1999) 1251-1254
2. M. W. Wang and Y. F. Chao, "Azimuth alignment in photoelastic modulator ellipsometry at a fixed incident angle," OSA Annual MEETING 2000, Oct 22-26, Providence, Rhode Island, USA
3. Yu-Faye Chao, Andy Lin and M. W. Wang, "Photoelastic modulation polarimetry and its measurement of twisted nematic liquid crystal," ISPA photonics system and applications, Singapore 27-30 November 2001, SPIE proceedings, 4595, (2001) 43-51
4. 王夢偉, 蔡斐欣, 趙于飛, "光彈調變式橢圓儀之相位調變線上校正", OPT02, 2002年台灣光電科技研討會論文集 I, TD1-5 (2002) 85-87
5. 王夢偉, 劉育維, 柳克強, 趙于飛, 林滄浪, "相位調變式橢圓儀應用於電漿蝕刻製程", OPT02, 2002年台灣光電科技研討會論文集 I, TD1-7 (2002) 91-93
6. M. W. Wang, F. H. Tsai and Y. F. Chao, "In situ calibration technique for photoelastic modulator in ellipsometry," 3rd International Conference on Spectroscopic Ellipsometry, Vienna, Austria, July 6-11 (2003)
7. 柯凱元, 王夢偉, 趙于飛 "多波長光彈調變式橢圓偏光儀之即時量測", OPT2003 Proceedings I TG1-3, (2003) 267-269
8. 郭俊儀, 王夢偉, 趙于飛, 林滄浪, 柳克強 "光彈調變式橢圓儀線上監控電漿蝕刻製程", OPT2003 Proceedings II FG1-6, (2003) 464-467

(C) 專利 (Patent)

1. 趙于飛, 王夢偉, “光彈調制式橢圓偏光儀之單角入射校正法”, 中華民國發明專利 145274 有效期 2001-2020
2. 趙于飛, 王夢偉, 寇人傑 ”利用石英量測轉動式橢圓偏光儀之入射角偏差的方法”, 中華民國發明專利 180743 有效期 2003-2020

